PEOPLE'S DEMOCRATIC REPUBLIC OF ALGERIA

MINISTRY OF HIGHER EDUCATION AND SCIENTIFIC RESEARCH

UNIVERSITY OF MOHAMED BOUDIAF- M'SILA

Faculty of Technology

Department of Electrical Engineering

N°: ……...…….

Domain: Sciences and Technology

Branch: Renewable Energy

Specialty: Green Hydrogen

MASTER THESIS

Presented by: Kamel KHIARI

Haroune BAIT

With a view to obtaining the Professional Master Diploma in 3rd Cycle (LMD)

Topic

Study of an Electric Drive System Powered by Renewable Sources

Dissertation Committee:

Presented on: June 22th, 2025, in front of the jury composed of:

Mr. Fouad BERRABAH	Prof	University of M'sila	President
Mr. Toufik ROUBACHE	Prof	University of M'sila	Supervisor
Mr. Tarak BENSLIMANE	Prof	University of M'sila	Examiner
Mr. Bilal BOUDJELLAL	MCA	University of M'sila	Examiner

Academic year: 2024/2025

Thanks

All praise and thanks belong to Allah for granting us the strength and opportunity to complete this master's thesis.

We are deeply grateful to our supervisor, Pr. Toufik Roubache. His profound knowledge and commitment truly inspired us, and we deeply appreciate all the time and effort he invested in helping us shape this thesis.

Our sincere thanks also go to the distinguished members of the jury for agreeing to evaluate our work. We are grateful for your thorough review.

We would like to extend our heartfelt thanks to Dr. Hamza Bahri for his support.

We also thank all those who contributed directly or indirectly to the completion of this modest work.

Dedication

This work is lovingly dedicated to my dear parents, whose endless sacrifices, unwavering support, and boundless love have been my constant source of strength and inspiration.

To my beloved family, my sisters your encouragement and belief in me made every challenge worthwhile.

To my brothers Holo, Khaled and Smail thank you for everything. Your presence in my life is a true blessing.

To my incredible residence friends, thank you for your laughter, your understanding, and for always being there.

Kamel KHIARI

Dedication

I dedicate this to my parents, with all my love and gratitude, for everything they've given me.

To my family, for your constant encouragement and belief.

To my friends, for your invaluable support and for making life brighter. Thank you all for being a part of my journey.

Haroune BAIT

List of tables

Chapter I:

Chapter III:

APPENDIX:

List of figures

Chapter I:

Chapter II:

Chapter III:

Contents

Table of Contents

General Introduction

General introduction

Environmental degradation, global warming, atmospheric pollution, and related diseases are critical byproducts of rising living standards and growing energy demand, currently met predominantly by fossil fuels. Projections indicate global energy demand may grow by 45% by 2030, driven by population growth, disparities in wealth distribution, economic welfare, and ecosystem pressures. These factors entrench dependence on fossil fuels, exacerbating environmental challenges worldwide.

Road vehicles significantly contribute to global pollution, emitting 15% of suspended particulates, 20% of volatile organic compounds, 5% of lead, 50% of nitrogen oxides, and 70% of carbon monoxide. They also account for 20% of global energy-related CO2, the principal greenhouse gas. As millions gain access to public and personal transportation, global pollution levels rise at an alarming rate, intensifying the need for sustainable solutions [1].

The electrification of the energy economy and the rise of automotive transportation rank among the twentieth century's most significant technological revolutions, transforming lifestyles through expanded fossil fuel use. From negligible markets in 1900, electrical generation now consumes 40% of global primary energy, while transportation accounts for 30%. Coal and natural gas supply over 60% of the energy for global electricity, and refined crude oil fuels nearly all 1.5 billion vehicles on global roadways, with renewable energy contributing less than 10% to either sector.

Electricity powers commercial, industrial, and residential sectors extensively but barely contribute to transportation, while oil provides only 2% of electricity's energy input. Conversely, more than half of global oil consumption fuels transportation, primarily cars, trucks, and buses,

with aircraft using 8% and ships and locomotives 6%. This heavy reliance on oil for transport drives increased dependence on diverse global oil sources, as demand continues to grow.

The current rate of fossil fuel consumption for electricity and transportation is 100,000 times faster than their natural formation, making extraction costlier and more complex as readily exploitable reserves deplete. This rapid depletion underscores the urgency of transitioning to sustainable energy systems to meet rising global energy demands.

Renewable energy sources, such as wind, water, solar, and geothermal (WWSG), are critical for sustainable development, yet they supply less than 10% of energy for electricity and transportation. Higher costs compared to conventional energy, along with economic, financial, political, geographical, and technological barriers, hinder large-scale adoption. Initiatives like Germany's Feed-in-Tariff (FIT) programs for solar energy aim to bridge this gap, but current economic incentives often fall short, making renewables less competitive [2].

Little progress has been made in using centralized grid electricity for transportation, though history offers lessons in sustainable transport. In 1900, electric vehicles outnumbered gasoline-powered ones by more than a factor of two. These silent, less-polluting machines, favored by the urban social elite for avoiding dangerous hand-crank starters, spurred over 150 EV manufacturers worldwide, highlighting early potential for clean transportation solutions

---

Chapter I
Generality of electric drive system powered by different renewable sources

I.1 Introduction

Human beings utilize three fundamental forms of energy to sustain life: mechanical, electrical, and thermal energy. Among these, electrical energy is the most preferable as it is simple to transport, convert, and store. Industries thus compete to develop the optimal end-user solutions. The production technology of renewable energy devices is near maturity with high system efficiency being the central issue for manufacturers and consumers. The solar panel manufacturers are creating highly efficient panels, whereas power converter and semiconductor manufacturers are creating faster and low-loss switch devices. Similarly, FC manufacturers are creating long life optimized designs. Development of electrical storage technology is being driven by demands for energy storage devices of high reliability to complement renewable sources.

However, renewable energy sources are very dependent on climatic conditions and hence cannot be used for continuous operation. To get around this disadvantage, the blend of different renewable energy sources can be put to use in order to supply constant power. Through the blending of systems, which complement each other, an uninterrupted energy supply can be ensured. Thus, Hybrid Systems (HS) and their control strategies have been the subject of extensive research in the field of renewable energy. Wind, solar, and hydrogen-based power generation are a few of the most encouraging technologies of renewable energy. While photovoltaic (PV) and wind energy have achieved great advances, fuel cells are emerging as a prospective green energy source because they have the advantages of zero noise, high efficiency, and low emission of pollutants.

However, all these technologies have their limitations solar and wind are environmentally dependent, while fuel cells need a fuel supply. Combination of more than one energy source in a hybrid system avoids these limitations. A multi-source HS delivers more reliable and better-quality power than a single-source system. With more than one renewable source combined, HS can be developed to supply energy around the clock during the day. For example, PV systems may be employed to generate daytime electricity for charging batteries and giving power, and batteries and fuel cells can supply nighttime energy requirements.

Hybrid power systems received worldwide research interest in recent years. Moreover, it is easier to optimize each renewable energy source's control process within an HS for enhanced energy efficiency. Depending on optimal harvesting power from every source, hybrid systems can effectively enhance energy use and reliability by a large amount [1].

I.2 Renewable Energy sources

I.2.1 General Renewable Energy Sources

The heightened demand for environmentally friendly transport means has catalyzed development and research in hybrid electric vehicles (HEVs) to increase their energy efficiency and environmental sustainability. One of the approaches utilized in curbing the use of fossil fuels and decreasing carbon imprints is adding renewable energy sources into the powertrain of HEVs as the automotive sector evolves to greener and more eco-friendly means [3].

The incorporation of the alternative energy sources, like solar, wind, biomass and mechanical vibration, in the electric drive system of HEV is an ultimate objective. For solar roof, the car's roof

is infilled with solar panels that produce electricity that can be used to power accessories or to charge the hybrid battery. This method utilizes solar energy for electric drive as a way to reduce the consumption of gasoline. The solar roof on the Fisker Karma gave extra electrical power to drive its accessory systems, which enhanced efficiency as a whole and minimized dependence on the internal combustion engine. It's important to remember that the real-world effects of these technologies can differ depending on the environment, driving conditions, and overall vehicle design.

In order to build a more resilient and cleaner energy future, government, corporations, and individuals all over the world are investing more in and utilizing renewable energy technologies. It is anticipated that in the upcoming years, continued technological advancements and encouraging legislation will hasten this shift. Renewable energy sources for the application of electric vehicles (EVs) and electric drive systems are highly demanding in this current era [4].

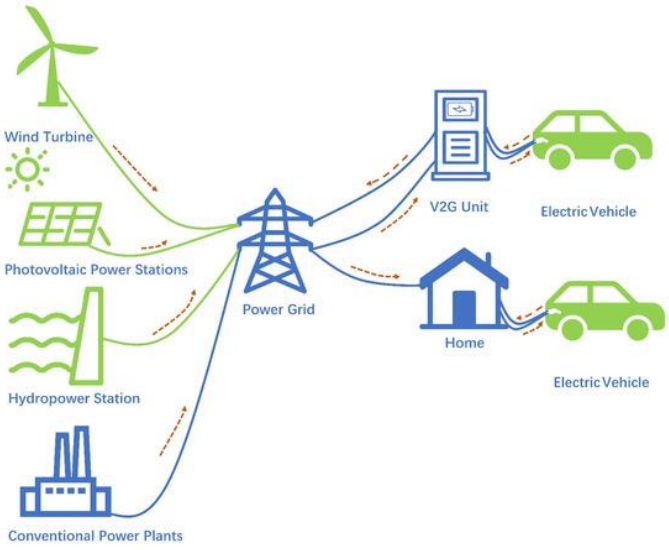

Figure 1.1: Vehicle-to-grid service diagram.

I.2.2 Solar Energy

Solar Power can be generated by converting sunlight into electricity using semiconductor materials in solar panels. On the other hand, Solar Thermal Energy can be generated by capturing solar radiation to generate heat, often used for space heating, water heating, or electricity generation. In order to generate power, solar PV systems are utilized in commercial, industrial, and residential contexts. They can be installed as solar farms' components or as rooftop panels. Semiconductor materials, usually silicon, are used to make solar PV cells. Electrons in the semiconductor material are excited when photons from sunlight strike the surface of these cells. The majority of practical applications require the conversion of the DC electricity generated by the solar cells into alternating current AC. An inverter does this by converting DC electricity to AC electricity. Batteries or other energy storage devices can be used in independent or off-grid solar systems to store extra electricity produced during sunny hours for use at a later time when sunshine isn't available, Photovoltaic cells are devices that convert sunlight or solar energy into direct current electricity. They are usually found as flat panels, and such panels are now a fairly common sight, on buildings and powering roadside equipment, to say nothing of being on calculators and similar electronic equipment. They can also come as thin films, which can be curved around a car body [5].

I.2.3 Hydrogen Energy

Hydrogen energy has rapidly emerged as a major contender in the quest of the world for clean and sustainable sources of fuel. With the increasing concern about climate change and the depleting fossil fuel reserves, hydrogen presents a hopeful and versatile option. As the universe's most common element and a highly versatile energy carrier, hydrogen possesses the revolutionary potential to revolutionize different industries, including transportation, electricity generation, and industrial processes.

The best thing about hydrogen energy is that it can generate energy without causing harmful emissions. Hydrogen, when burned or utilized in fuel cells, has only one byproduct, which is water (H_2O), so it is a very environmentally friendly and clean option. Compared to traditional fossil fuels, hydrogen combustion does not release greenhouse gases such as carbon dioxide (CO_2), nitrogen oxides (NOx), or sulfur oxides (SOx), and it does not contribute to the formation of hazardous particulate matter (PM). All these characteristics establish hydrogen energy as a critical factor in the globe's transformation toward a sustainable, low-carbon economy.

But despite all its wonderful promise, widespread adoption of hydrogen power is faced with a series of daunting challenges and limitations that must be overcome. Chief among these are the cost-effective and efficient production of hydrogen, particularly from renewable energy, and the development of safe and scalable storage technology. Current processes for hydrogen production, such as steam methane reforming, rely on fossil fuels, which negates some of the environmental benefits. Advances in electrolysis, where renewable electricity splits water into hydrogen and oxygen, are crucial. Furthermore, the high volumetric energy density of hydrogen poses storage challenges, which require breakthroughs in compression, liquefaction, and solid-state storage technologies. Addressing these challenges is crucial to unlocking the full potential of hydrogen as a clean and sustainable energy carrier [6].

I.2.4 Wind Energy

Transfer the kinetic energy of the wind into mechanical power in a manner that electricity is produced. Wind's kinetic energy is the source of wind energy, which is a renewable source of energy. Wind turbines, which transfer the kinetic energy of the wind into mechanical power and, in turn, electricity, are employed to harness it. With the world moving towards cleaner and greener sources of energy, wind power has emerged as a major source. Because wind power does not deplete itself over time, it is renewable. In contrast to non-renewable resources, the use of wind power leaves very little footprint on the environment. As it releases no air pollutants or greenhouse gases at all throughout the whole process of generating power, wind power is a clean form of energy that has climate change mitigation impacts. In addition, wind power can improve energy security and resilience by limiting the reliance on fossil fuels [7] [8].

I.3 Photovoltaic PV

I.3.1 Photovoltaic (PV) cells

In addition to traditional power sources for electric vehicles, such as batteries and fuel cells, there are several alternative options available. These include solar photovoltaic systems.

Photovoltaic (PV) cells, commonly known as solar cells, are devices that convert sunlight directly into electricity. The process, called the 'photovoltaic effect,' involves quantum-mechanical interactions between sunlight and electrons in the cell's semiconductor material, generating electric current. This electricity can be stored in batteries, used directly to power Direct Current (DC) equipment, or converted to Alternating Current (AC) via an inverter for use like grid power.

Solar panels are just one component of a complete photovoltaic (PV) solar system. The core of the system is the solar modules, often referred to as the power generators. Additionally, mounting structures are essential to secure and position the PV modules toward the sun. For PV systems that need to operate during nighttime or periods of poor weather, energy storage is necessary, requiring batteries to store electricity. The performance of a PV module depends on sunlight intensity and cell temperature, so components like charge regulators are needed to condition the direct current (DC) output and deliver it to batteries, the grid, or the load for smooth system operation. In cases where alternating current (AC) is required, DC/AC inverters are integrated into the PV system. These additional components, along with others, make up the balance of system (BOS). Finally, the household appliances and equipment powered by the PV system, such as radios, TVs, and lights, are collectively referred to as the electrical load. Together, these elements form a fully functional PV system [9].

I.3.1.1 Short History of Photovoltaic

Photovoltaic (PV) have an interesting historical trajectory. Starting in the 1950s, early PV cells were developed primarily for satellite applications, characterized by high costs and low efficiencies. The 1970s saw advancements that reduced costs and increased efficiencies, making terrestrial applications viable. During this period, PV cells began to be used in remote areas for telecommunication links, isolated household power supplies, and water pumping. By the 1980s, PV technology continued to improve, with its reliability and low maintenance making it a preferred choice for remote applications over options such as diesel generators and windmills.

The 1990s to 2000s marked a period where PV technology became more affordable and efficient, leading to increased urban use. One of the fastest-growing markets for PV technology during this time was grid-connected systems installed on buildings. From the 2010s to the present, PV technology has continued to advance significantly, with marked improvements in efficiency and cost reductions. Solar energy has become a mainstream renewable energy source, with PV system adoption growing rapidly worldwide.

Throughout its history, photovoltaic has evolved from a niche technology designed for space applications into a widespread and essential component of the global renewable energy landscape [10].

I.3.1.2 Solar cells work

PV cells are constructed from semiconductor materials like silicon, which behave as insulators at low temperatures but act as conductors when exposed to heat or energy. These semiconductors are fundamental to the electronics industry and are utilized in devices such as microprocessors, including those in personal computers. The "photovoltaic effect" is a unique phenomenon where an electric current is generated when the semiconductor material is illuminated by light. For example, when photons of light strike silicon, their energy is transferred to the negatively charged electrons in the silicon, enabling them to break free from their atoms. This process creates free electrons and leaves behind "holes," or positively charged spaces. Typically, these free electrons would lose energy as heat and recombine with the silicon atoms. Therefore, to harness this light-induced current, a mechanism is required to guide the free electrons and establish a continuous flow of electricity.

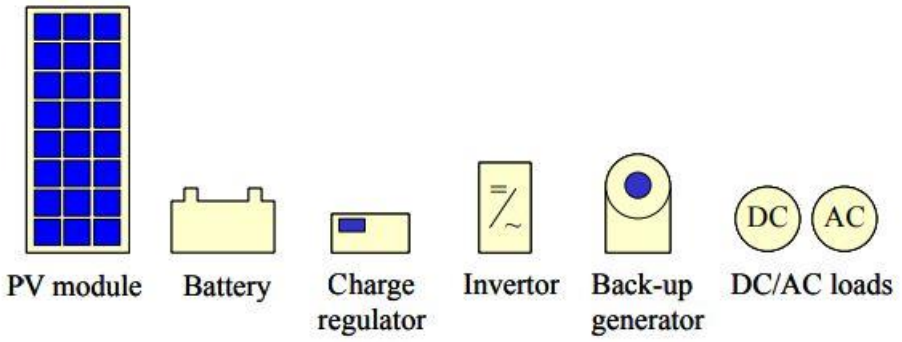

Figure 1.2: The components of a PV system.

I.3.2 Solar PV technology

Photovoltaic (PV) technology refers to the use of materials and devices that convert sunlight into electrical energy. A single PV device is called a cell, which is typically small and generates around 1 to 2 watts of power. These cells are constructed from various semiconductor materials and are usually thinner than four human hairs. To ensure durability and longevity in outdoor conditions, the cells are encased between protective layers of glass and/or plastics.

A solar cell operates in three key steps: First, photons from sunlight strike the solar panel and are absorbed by semiconducting materials like silicon. This energy knocks electrons (which are negatively charged) free from their atoms, enabling them to flow through the material and generate electricity. Because of the unique structure of solar cells, electrons are restricted to moving in only one direction. A collection of solar cells then transforms solar energy into a practical amount of direct current (DC) electricity.

I.3.2.1 Key Elements of a Solar Panel

- Glass Cover: Offers protection against environmental factors like weather and debris.
- Anti-Reflective Coating: A layer applied to minimize light reflection, ensuring more light is absorbed by the panel.

- Top Negative Contact: Acts as the negative terminal (similar to a battery's negative post).
- N-Type Layer: A semiconductor layer treated with phosphorus to create an excess of electrons.
- P-Type Layer: A semiconductor layer treated with boron to create an excess of positively charged "holes."
- Bottom Positive Contact: Serves as the positive terminal (similar to a battery's positive post) [11].

I.3.2.2 PV modules

A solar cell serves as the fundamental building block of a photovoltaic (PV) system. While a single cell generates direct current (DC) and typically delivers 1 to 2 watts of power insufficient for most applications its output depends on size and material. For example, a standard 10 cm × 10 cm crystalline silicon solar cell produces approximately 1.5 peak watts (Wp), with an open-circuit voltage (Voc) of around 0.6 volts and a short-circuit current (Isc) of about 3.5 amps. To meet practical energy requirements, multiple solar cells are wired together in series or parallel configurations, creating a PV module capable of higher voltage, current, and power output.

There are two methods of using solar panels, either onboard or off board the vehicle. Clearly even if the whole of a car plan area were covered with cells only a very limited amount of power would be obtained. For example, a car of plan area 5m2 would produce a maximum of around 375W at the panel output, and an average of around 188W, giving 1.88kWh of energy over a 10hour day, equivalent to the energy stored in around 50kg of lead acid batteries. This energy could be stored in a battery and used to power the vehicle for short commuter and shopping trips [12].

I.3.2.3 Types of photovoltaic cells

Photovoltaic (PV) cells can be produced using diverse manufacturing techniques and materials, yet they share a common purpose: capturing sunlight and transforming it into usable electrical energy. While silicon a semiconductor remains the most widely used material in solar panel production, other substances are also employed. A single solar panel requires multiple interconnected PV cells to function effectively, and a collection of panels forms a photovoltaic array, which scales up energy generation capacity.

I.3.2.3.1 Monocrystalline Silicon Cell

The earliest widely produced solar cells utilized monocrystalline silicon, a highly purified form of silicon. The manufacturing process begins by extracting a seed crystal from molten silicon, forming a cylindrical ingot with a uniform crystal structure. This ingot is sliced into thin wafers, polished, and chemically treated (doped) to establish a p-n junction. Subsequent steps include applying an anti-reflective coating and attaching front and rear electrical contacts. The finished cells are then assembled and connected with others to create a complete solar panel. While monocrystalline silicon cells boast high efficiency, their complex, labor-intensive production process makes them costlier compared to polycrystalline silicon or thin-film alternatives.

Figure 1.3: Monocrystalline Silicon Cell.

I.3.2.3.2 : Polycrystalline Silicon Cell

Unlike monocrystalline solar cells, which possess a single uniform crystal structure, polycrystalline (or multicrystalline) cells are composed of numerous small, randomly oriented crystalline grains. Traditional manufacturing involves casting a cubic ingot from molten silicon, followed by slicing and processing. Alternatively, the Edge-Defined Film-Fed Growth (EFG) technique draws a thin ribbon of polycrystalline silicon directly from molten material. While generally more cost-effective than monocrystalline options, polycrystalline silicon PV cells exhibit slightly lower efficiency. Despite this, they remain a dominant force in the global solar market, accounting for approximately 70% of global PV production as of 2023.

I.3.2.3.3 Thin Film Cells

Thin-film solar cells, like amorphous silicon (a-Si), offer cost advantages due to reduced material usage and simpler production. However, their efficiency is lower than crystalline cells due to the disordered structure of the silicon. Additionally, a-Si cells exhibit a notable initial performance decline before stabilizing.

I.3.2.4 Solar PV systems and applications

Solar photovoltaic (PV) systems find applications in both off-grid and grid-connected settings. Key applications include: off-grid domestic use for households lacking grid access; off-grid power for telecommunications, water pumping, and navigation; grid-connected distributed systems integrated into residential, commercial, and public buildings; and large-scale grid-connected power plants. While grid-connected systems historically dominated the market (representing over 99% in 2009), off-grid applications, often operating without subsidies, are experiencing significant growth globally. System sizes vary: residential systems typically range up to 20 kW, commercial installations for businesses, institutions, and retail establishments can reach up to 1 MW, and utility-scale plants exceed 1 MW in capacity.

Solar panels serve multiple purposes in electrical energy applications. When integrated into power grids, they contribute to energy distribution for networks of different scales. In the case of

electric vehicles, their role varies based on their power capacity—they can function as the main propulsion source or as a supplementary energy supply to enhance battery range [13].

I.3.2.5 Hybrid Systems

Due to the inherent variability of solar radiation throughout the year, relying solely on photovoltaic (PV) power necessitates either an oversized solar array or a substantial energy storage system (like large batteries). This significantly increases the system's cost, particularly when high reliability is crucial. To address this, hybrid systems combining PV with other generation technologies, such as fossil fuels (diesel or gas) offer a more practical and cost-effective solution.

In favorable weather conditions, the PV system meets the entire energy demand, with surplus power stored in batteries. During periods of low solar irradiation (nighttime or inclement weather), the batteries initially supply the required power. However, to prevent excessive battery discharge, a backup generator seamlessly transitions to provide electricity while simultaneously recharging the batteries

I.3.2.6 Grid-Connected PV Systems

Grid-connected photovoltaic (PV) systems offer a means to supplement or even displace grid-supplied electricity. PV arrays can be installed independently, on rooftops, or integrated into building structures (roofs, walls, windows, or skylights). Essential components include the PV array, an inverter to convert DC power to AC, and meters to track grid-supplied and PV-generated electricity. Excess PV power can be fed back into the grid, while the grid acts as a backup source when PV generation is insufficient. This grid-tied configuration simplifies system design by eliminating the need for large battery banks. However, in regions with unreliable grid power, such as developing countries, incorporating a battery bank may enhance system reliability and independence [14].

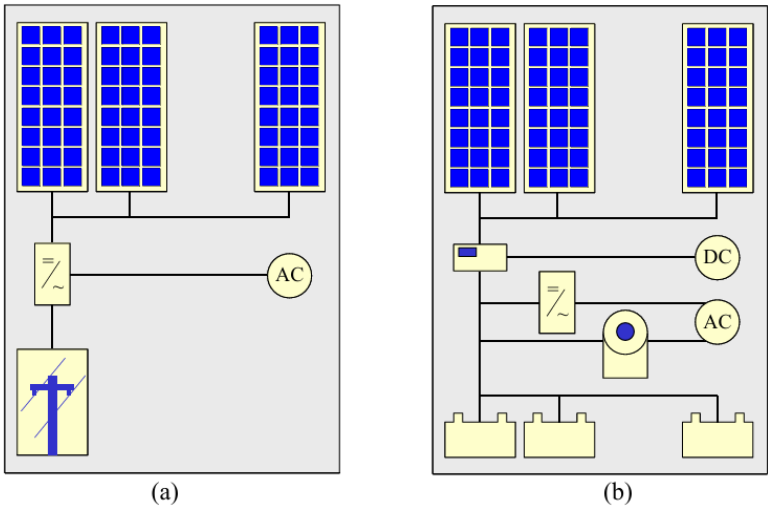

Figure 1.4: Schematic representation of (a) a grid-connected PV system, (b) a hybrid system.

I.3.2.7 Photovoltaic Cell Efficiencies

The primary factor influencing the power output of a PV cell is the amount of sunlight it absorbs. The efficiency of a PV cell in converting sunlight into energy depends on various elements. Some of these are inherent to the cell's material properties, while others are influenced by external environmental conditions, such as temperature and humidity.

I.3.2.7.1 Effect of temperature on PV performance

Solar cells vary under temperature changes. The change in temperature will affect the power output from the cells. The voltage is highly dependent on the temperature and an increase in temperature will decrease the voltage.

I.3.2.7.2 Operating temperature

The efficiency of a PV cell is influenced by its operating temperature, which depends on both the surrounding temperature and the thermal properties of the PV module's housing. Since most PV cells operate at an efficiency of less than 20%, a significant portion of the unused energy is converted into heat. As a result, PV modules often function at temperatures higher than the ambient environment, sometimes reaching up to 50°C above it. This excessive heat can lead to a notable decrease in the power output of the PV system [15].

I.3.2.8 Solar car

In recent years, solar photovoltaic energy has seen significant growth in various sectors, including electricity production, industrial applications, and powering remote locations. With decreasing oil production and increasing efforts to lower harmful emissions, this renewable energy source is becoming essential for embedded systems in transportation, such as cars, airplanes, and boats. However, using solar energy to power electric vehicles comes with challenges. Its low energy density and limited conversion efficiency mean that large surface areas are required to generate sufficient power. Additionally, because solar energy is not consistently available, energy storage solutions like batteries are necessary to ensure a continuous power supply.

The integration of sustainable energy sources, such as solar, wind, Fuel cells, and, into hybrid electric vehicle (HEV) drive systems is a key focus for enhancing energy efficiency and reducing environmental impact. One innovative approach is the use of solar roofs, where the vehicle's roof is equipped with photovoltaic panels that generate electricity. This energy can be utilized to power onboard accessories or recharge the hybrid battery, thereby reducing the reliance on fossil fuels. For instance, the Fisker Karma incorporated a solar roof that provided additional electrical power to support its auxiliary systems, improving overall vehicle efficiency and minimizing the load on the internal combustion engine. Beyond solar energy, emerging technologies like regenerative braking and kinetic energy recovery systems are also being explored to harness mechanical vibrations and motion, further optimizing energy use in HEVs. These advancements not only contribute to lower fuel consumption but also align with global efforts to transition toward cleaner and more sustainable transportation solutions [16].

Figure 1.5: Solar car.

Solar energy is a highly demanded renewable electricity source, helping meet growing energy needs while reducing dependence on fossil fuels and mitigating climate change. The development of advanced materials, particularly nanotechnology, is enhancing the competitiveness of next-generation solar cells.

Monocrystalline silicon cells dominate the market due to their high efficiency, which reached 25% two decades ago and has only slightly improved to 26.6%. As this technology nears its efficiency limit, researchers are exploring alternative materials and production methods. Polycrystalline and amorphous thin-film silicon cells are potential competitors, but their lower efficiency remains a challenge.

I.4 Fuel cells

Fuel cells are electrochemical converters that directly convert chemical energy into electricity. The various types are based on the same fundamental principles but possess four essential elements: electrolyte, anode, cathode, and interconnect. The type of electrolyte used is mainly responsible for dividing them into groups, as it decides such important characteristics as working temperature, warm-up time, fuel sources one can utilize with them, methods of transporting ions, and life expectancy. Fuel cells are commonly used for second-level power generation and depend on pure hydrogen, which needs to be produced with primary energy sources apart from high-temperature forms based on direct liquid fossil fuel. There are many companies in the automobile, electronics, and energy sectors that have developed functional fuel cell systems, yet further development is required to

enhance lifespan and lower the cost. In the discussion of two high-temperature fuel cells (typically solid oxide and molten carbonate), and two low-temperature types (polymer electrolyte and direct methanol), the emphasis falls on their material composition and the attendant electrochemical processes [17].

I.4.1 History of the fuel cell

The invention of the first fuel cell was made by Sir William Robert Grove, an experimental philosopher at the Royal Institution in London in 1839. Since then, he has been known as the "Father of the Fuel Cell", the first mention of a device that would later be known as a fuel cell resulted from his experiments on electrolysis, which involved splitting water into hydrogen and oxygen using electricity. He theorized that it might be possible to reverse the electrolysis process and produce electricity by reacting oxygen and hydrogen. To test this theory, he enclosed two strips of platinum in separate bottles. One contains hydrogen and the other oxygen. The two electrodes started to generate a current and water formed in the gas bottles when these containers were immersed in diluted sulfuric acid. By connecting multiple devices in series, he was able to increase the voltage produced and create what he called a 'gas battery', the precursor to modern fuel cells [18].

The fuel cell was revived in the early 1960s as National Aeronautics and Space Administration NASA, sought ways to generate power for space missions. NASA had already ruled out batteries due to their weight, solar power due to its high cost, and nuclear energy due to its high risk. They were searching for an alternative. The fuel cell arose as a promising solution, leading NASA to award multiple research contracts for the development of this technology. This research led to the development of the first proton exchange membrane, "polymer electrolyte membrane" [19].

These fuel cells, which utilized pure oxygen and pure hydrogen, were compact but costly and not available commercially. NASA's renewed interest in fuel cells, combined with the 1973 energy crisis, spurred further development of this technology. Since that time, ongoing research has advanced fuel cell technology, enabling its successful implementation in a broad range of applications [20].

I.4.2 Basic Principles

It is well established that the fundamental principle of a fuel cell involves the release of energy through a chemical reaction between hydrogen and oxygen. The primary distinction between this process and simply burning the gas is that the energy is produced in the form of an electric current, rather than heat. How is this electric current produced?

To understand this, we need to consider the separate reactions taking place at each electrode. These important details vary for different types of fuel cell, but if we start with a cell based on an acid electrolyte, we shall consider the simplest and the most common type.

At the anode of an acid electrolyte fuel cell the hydrogen gas ionizes, releasing electrons and creating H+ ions (or protons).

At this point, the search for alternative energy sources must continue without concentrating solely on one specific technology, Instead, it should follow a parallel approach, allowing new technologies to compete with one another before any widespread replacement of fossil fuels can occur.

$$2H_2 \rightarrow 4H^+ + 4é \quad (1.1)$$

This reaction releases energy. At the cathode, oxygen reacts with electrons taken from the electrode, and H+ ions from the electrolyte, to form water.

$$O_2 + 4é + 4H^+ \rightarrow 2H_2O \quad (1.2)$$

For both reactions to continue uninterrupted, the electrons generated at the anode must travel through an electrical circuit to the cathode. Additionally, H+ ions need to pass through the electrolyte. An acid, which contains free H+ ions, fulfills this role effectively. Some polymers can also be designed to hold mobile H+ ions, and these materials are known as "proton exchange membranes," since an H+ ion is essentially a proton.

By comparing equations (1.1) and (1.2), it is clear that two hydrogen molecules are required for every oxygen molecule to maintain a balanced system. It is important to note that the electrolyte must permit only H+ ions to pass through, while blocking electrons. If electrons were able to flow through the electrolyte instead of the external circuit, the entire process would fail, as the electrical current would be lost [21].

I.4.3 Types

Fuel cells are most commonly classified by the kind of electrolyte being used. These include proton exchange/polymer electrolyte membrane fuel cells (PEMFCs), direct methanol fuel cells (DMFC), alkaline fuel cells (AFC), phosphoric acid fuel cells (PAFC), molten carbonate fuel cells (MCFC), solid oxide fuel cells (SOFC), which vary widely in their required operating temperature.

Fuel cell type	**Mobile ion**	**Operating temperature ºC**	**Applications and notes**
Alkaline (AFC)	OH^-	50 – 200	Used in space vehicles, e.g. Apollo, Shuttle.
Proton exchange membrane (PEMFC)	H^+	30 – 100	Vehicles and mobile applications, and for lower power CHP systems
Direct methanol (DMFC)	H^+	20 – 90	Suitable for portable electronic systems of low power, running for long times
Phosphoric acid (PAFC)	H^+	~220	Large numbers of 200kW CHP systems in use
Molten carbonate (MCFC)	CO_3^{2-}	~650	Suitable for medium to large scale CHP systems, up to MW capacity

Solid oxide (SOFC)	O^{2-}	500 - 1000	Suitable for all sizes of CHP systems, 2kW to multi-MW

Table 1.1 Data for different types of fuel cell

Six fuel cell types are current, viable contenders for use both now and in the near future. General details on the systems are provided in Table 1.1. All of these categories react differently to different challenges but make use of the unique strength of fuel cells in different ways. Proton Exchange Membrane Fuel Cell (PEMFC) exploits the inherent simplicity of fuel cell technology. Its electrolyte is a solid polymer that supports proton mobility, and its chemistry is identical with acid electrolyte fuel cells. Since it contains a solid nonmoving electrolyte, the PEMFC is essentially simple in configuration. This cell has the optimum prospect for utilization in automobiles and is utilized in most of the most advanced demonstration fuel cell autos so far.

PEM fuel cells are run at relatively low temperatures, and this necessitates the use of sophisticated electrodes and catalysts to counteract the problem of slow reaction rates. The catalyst is platinum, but recent developments have cut the quantity that is needed quite drastically, so the cost of platinum now only represents a small fraction of the total cost of a PEM fuel cell. But the problem of hydrogen supply has still to be resolved, as although these cells need very pure hydrogen, there are various means of supplying it.

One theoretically fascinating solution to the problem of hydrogen supply is utilization of methanol, a liquid fuel produced on a large scale (chemical substance CH_3OH), as a hydrogen replacement. This is performed in Direct Methanol Fuel Cells (DMFCs), in which the qualifying term "direct" is used to signify that methanol is utilized in its liquid state without hydrogen being taken out of it. DMFCs are alas low-power devices, and their use is restricted to those applications where a slow and steady supply of electricity is needed over extended time intervals. Although a demonstration DMFC-powered go-cart has been constructed, the most likely near-term use of such a cell is in portable electronics, a very rapidly growing market.

Although PEM fuel cells were utilized in early manned missions, Apollo missions utilized and Shuttle Orbiter is utilizing the Alkaline Fuel Cell (AFC). The drawback of AFCs' slow reaction rates is mitigated by employing highly porous electrodes with a platinum catalyst and even operating at elevated pressures in some applications. While early alkaline fuel cells were run at around 200°C, they normally run below 100°C. AFCs have been showcased in several demonstration electric vehicles, always as a hybrid with batteries. While easier and less expensive to build than PEMFCs, they possess less power and their electrolyte is also corrosive when it reacts with atmospheric carbon dioxide, so earth-based applications become awkward.

Phosphoric acid fuel cell (PAFC) first entered commercial production and extensive terrestrial use. Numerous 200 kW systems, manufactured by the International Fuel Cells Corporation, have been installed in the USA and Europe, as well as units from Japanese producers. PAFCs are not viable for vehicular use, however, due to their operating temperature of around 220°C and their poor performance when cooled and restarted. Otherwise, they are best suited to applications where power is needed continuously over long durations, for example, industrial or utility-scale power generation.

Each of the fuel cell types solves certain problems but generates others in the process. The SOFC, for instance, works in a range of 600 to 1000°C. Its high temperature allows for high reaction rates to be achieved without utilizing costly catalysts such as platinum and allows for the use of fuels such as natural gas directly or internal reforming within the cell itself. By not requiring a dedicated hydrogen supply, SOFCs reap the inherent simplicity of fuel cells. Despite all of these advantages, SOFCs are costly to manufacture due to the complexity of working with ceramic materials, and ancillary equipment such as air and fuel pre-heaters, complex cooling systems, and startup mechanisms are required to create a viable system. So, SOFCs are not being developed to propel vehicles but rather are being investigated for application in smaller auxiliary power units (APUs) in traditional vehicles, where they can fulfill the increasing electrical load for features such as air conditioning.

In contrast to SOFCs, which are solid at high temperatures, the molten carbonate fuel cell (MCFC) has an always-liquid electrolyte. MCFCs have the special requirement of needing carbon dioxide from the air in order to operate. Their high operating temperature enables efficient reaction through the use of relatively low-cost nickel as a catalyst, which also provides the electrode's electrical base. Like SOFCs, MCFCs can be operated on methane or coal gas (a combination of H_2 and CO), which makes the fuel supply infrastructure simpler. Nevertheless, the electrolyte is a hot, corrosive lithium, potassium, and sodium carbonate mixture that poses great engineering challenges. MCFCs are not viable for vehicles since they work best in large and continuously operating systems, which makes them better suited for stationary power generation.

In summary, while each fuel cell type offers distinct benefits, their limitations dictate their suitability for specific applications, ranging from stationary power generation to auxiliary roles in transportation [21].

I.4.4 PEMFC Components

The main parts of a practical PEMFC are illustrated in Figure 1.6 , the membrane electrode assembly (MEA) consists of the polymer membrane together with the electrodes and gas diffusion layers.

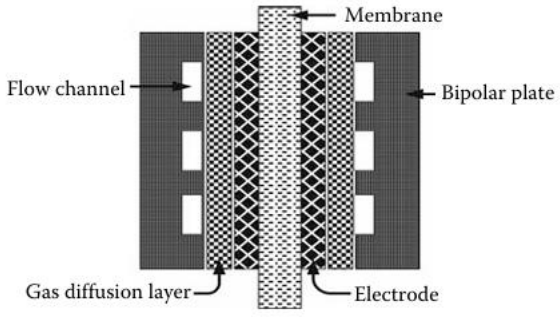

Figure 1.6: The main functional parts of a PEMFC.

Each electrode is composed of a catalyst particle layer, usually platinum on carbon support powder, and is bonded to either the membrane or the gas diffusion layer. The gas diffusion layer, being an electrically conductive porous material such as carbon cloth, permits reactants to diffuse in and out of the Membrane Electrode Assembly (MEA), collects the generated current by making

electrical contact with the outside bipolar plate, and provides a means for water produced at the cathode to leave through the gas channels. Bipolar plates, or flow field plates, distribute the reactant gases uniformly over the electrode surfaces through flow channels of different geometry, collect the produced current, and give mechanical support to the fuel cell. Bipolar plates are typically solid graphite because of its high electrical and thermal conductivity, mechanical strength, and chemical stability [22].

I.4.4.1 Membrane

The electrolyte membrane is the key element of a Proton Exchange Membrane Fuel Cell (PEMFC), which employs a proton-conducting polymer as the electrolyte and derives the name for the fuel cell from there. Polytetrafluoroethylene is the result of polyethylene as raw material, in which hydrogen is replaced by fluorine. The membrane is extremely robust and chemically inert due to the carbon-fluorine bonds. In order to maximize its proton-conducting abilities, sulfonic acid groups (HSO_3) are incorporated ionically, thereby making it capable of attracting H^+ ions into the electrolyte. This patented material, which was developed by DuPont and sold under the brand name Nafion®, has been instrumental in improving PEMFC technology.

I.4.4.2 Bipolar Plates

Bipolar plates, also known as flow field plates, account for the majority of the weight and volume of a PEMFC and are used for distributing reactant gases to the Membrane Electrode Assembly (MEA) via machined flow channels or grooves. The plates provide even distribution of reactants over the electrode surfaces while collecting the electrical current produced by the electrochemical reaction. In order to operate efficiently, bipolar plates need to have high electrical and thermal conductivity, mechanical strength, and chemical stability. Graphite is the present material of choice but is being researched to make it lighter in weight in an effort to increase the power density of the fuel cell. Flow channel geometry differs with each individual fuel cell design and application, and the design plays an important role in the overall PEMFC performance.

I.4.4.3 Heating or Cooling Plates

These plates may be used to either heat the PEMFC or cool it in order to keep its temperature close to the one that yields optimal operating performance. Heating plates typically rely on the use of electricity and ohmic (resistive) heating. Cooling plates are used when air cooling is insufficient; then liquid, such as water, is actively circulated through these plates to cool the stack.

Fuel cells are a highly efficient and environmentally sustainable energy technology with significant potential to transform energy systems across industries. Their ability to generate electricity through electrochemical processes, coupled with zero or low emissions, positions them as a critical component in the global shift toward decarbonization. However, widespread adoption is currently hindered by challenges such as high production costs, limited hydrogen infrastructure, and the need

for sustainable hydrogen sourcing. To capitalize on the benefits of fuel cells, strategic investments in R&D, infrastructure development, and policy support are essential.

I.5 Converters

Converters are essential components in electrical systems today, particularly in view of renewable energy systems, electric vehicles, and smart grids. They enable the electrical power conversion from one form to another, facilitating efficient energy utilization and system integration of various technologies. In this review, a discussion on the types of converters, their applications, as well as their challenges, is presented.

I.5.1 Definition

converter is a circuit or device that converts the current, voltage, or frequency of electric energy to match particular load requirements. It does so by controlled switching of semiconductor devices (e.g., MOSFETs, IGBTs) and energy storage devices (e.g., inductors, capacitors). Converters are generally categorized according to their input/output configurations [23].

I.5.2 Types

Power converters are classified into four categories: direct current-to-direct current (DC-DC), direct current-to-alternating current (DC-AC), alternating current-to-direct current (AC-DC), and alternating current-to-alternating current (AC-AC). DC-DC converter boosts the voltage of the fuel cell stack in FCVs to supply a stabilized power source to the DC-AC converter, which powers the traction motor. Furthermore, there is a need for a high-voltage DC-DC converter in automotive systems to supply high-voltage loads.

I.5.2.1 DC-DC Converters

DC-DC converters are electronic circuits that convert a direct current (DC) voltage from one level to another, essential for powering devices with varying voltage requirements. Used in power supplies, battery chargers, renewable energy systems, and portable electronics. Modern designs often employ synchronous rectification (replacing diodes with MOSFETs) for higher efficiency.

Types:

- Step-down (Buck) Converter.
- Step-up (Boost) Converter.
- Buck-Boost Converter.
- Cuk Converter.
- SEPIC Converter.
- Zeta Converter.

I.5.2.2 DC-AC Converters

DC-AC converters, known as **inverters**, transform direct current (DC) into alternating current (AC). They are critical for powering AC devices from DC sources like batteries, solar panels, or EVs. Inverters bridge the gap between DC energy sources (batteries, solar) and the AC-powered world, with topologies ranging from simple square-wave circuits to sophisticated grid-interactive systems.

Types:

- Voltage Source Inverters (VSI).
- Current Source Inverters (CSI).
- Single-phase vs. Three-phase Inverters.

I.5.2.3 AC-DC Converters

AC-DC converters, also called rectifiers, convert alternating current (AC) to direct current (DC). They are fundamental in power supplies, battery charging, and electronic devices. AC-DC converters bridge the gap between grid/mains AC power and the DC needs of modern electronics, with topologies ranging from simple diode bridges to sophisticated SMPS designs.

Types:

- Uncontrolled Rectifiers (Diode Bridges).
- Phase-Controlled Rectifiers (Thyristor-Based).
- PWM Rectifiers.

I.5.2.4 AC-AC Converters

AC-AC converters modify alternating current (AC) voltage or frequency to meet specific load requirements. Unlike DC-DC converters, they operate on AC input and output, making them essential for applications like motor speed control, lighting systems, and grid-tied renewable energy. Modern AC-AC converters often use advanced semiconductor devices (e.g., SiC MOSFETs) and digital control (DSPs) to improve efficiency and dynamic response.

Types:

- Cycloconverters.
- Matrix Converters.

Power converters play a pivotal role in modern energy systems, particularly in fuel cell vehicles (FCVs) and renewable energy applications. The four primary converter types DC-DC, DC-AC, AC-DC, and AC-AC enable efficient energy management by adapting voltage and current to meet system requirements. In FCVs, DC-DC converters are indispensable for boosting fuel cell stack voltage to power high-voltage traction systems, while multi-stage unidirectional DC-DC converters address the growing demand for high-gain voltage conversion in hybrid vehicles and electric

propulsion systems. These converters also enhance compatibility with renewable energy sources, battery storage, and industrial motor drives.

I.6 Battery

Battery storage is very convenient in solar, fuel cells, wind, and other types of renewable generation schemes where the source of energy is intermittent. It is charged during the time that the source supplies energy. It can be utilized when the source is not available. The characteristics of operation vary extensively depending on application. In-depth specifications are being prepared and such characteristics as high energy efficiency, low self-discharge, cheap, extended cycle and calendar life, and low maintenance requirements are paramount.

The selection of the appropriate battery for such use is a complete analysis of the battery's charging and discharging requirements, such as the load, the solar or alternate energy output and profile, the operating temperature, and charger and other system component efficiency [24].

I.6.1 Types and characteristics of rechargeable batteries

The major characteristics of rechargeable batteries are that charge and discharge, or the transformation of electric energy into chemical energy and vice versa, need to occur nearly in the reverse direction, need to be energy efficient, and need to entail minimal physical changes that can limit cycle life. Chemical reaction, which may result in degradation of the cell components, death, or loss of energy, should not occur, and the cell should possess the characteristic features one would anticipate from a battery such as high specific energy, low resistance, and good performance over a broad temperature range. Such requirements limit the number of materials that can be utilized successfully in a rechargeable battery system.

Rechargeable batteries are critical in electric vehicles (EVs) and renewable energy systems, with each type possessing distinctive characteristics for specific uses. The following is a concise overview of the main types of rechargeable batteries used in EVs, their key features, and application to EV battery systems using renewable energy.

I.6.1.1 Lithium-Ion (Li-Ion) Batteries

Lithium-ion batteries are now used in most portable consumer devices such as cell phones and laptops because of their high energy per unit mass and volume relative to other electrical energy storage systems. They also have high power-to-weight ratio, high energy efficiency, good performance at high temperature, long life, and low self-discharge. Most components of lithium-ion batteries are recyclable, even though material recovery remains costly for the industry. Most of today's all-electric and PHEVs use lithium-ion batteries, though the exact chemistry is usually different from that used in batteries for consumer electronics. Research and development still reduce their relatively high price, extend their useful life, use less cobalt, and enhance safety with respect to various fault conditions.

Chemistry Variants:

- Lithium Nickel Manganese Cobalt Oxide (NMC),
- Lithium Iron Phosphate (LFP),
- Lithium Nickel Cobalt Aluminum Oxide (NCA).

Figure 1.7: Lithium-Ion Battery

I.6.1.1.1 Characteristics:

- Energy Density: High (150–250 Wh/kg), enabling longer driving ranges (e.g., 300+ miles for some EVs).
- Power Density: Good, which enables quick acceleration and charging.
- Cycle Life: 1,000–2,000 cycles (LFP up to 3,000), depending on chemistry.
- Cost: Moderate, with LFP less energy-dense but lower cost.
- Safety: NMC/NCA contain thermal runaway risks; LFP is less hazardous but heavier.
- Charging Speed: Able to charge quickly (e.g., 80% in 20–30 minutes for some models).
- Application in EVs: Common in EVs (e.g., Tesla uses NCA, BYD uses LFP) due to high energy density and efficiency.
- Application with Renewables: High efficiency (90–95%) makes them a good option to store renewable power in EV batteries or BESS for grid balancing.

I.6.1.2 Nickel-Metal Hydride (NiMH) Batteries

Nickel-metal hydride batteries, which are being utilized every day in computer and medical equipment, deliver reasonable specific energy and power capability. Nickel-metal hydride batteries offer a much higher life cycle than lead-acid batteries and are safe and abuse-tolerant. Nickel-metal hydride batteries have been used to a great extent in HEVs. The main issues with nickel-metal hydride batteries are their high cost, high self-discharge rate, heat generation at high temperatures, and the need to manage hydrogen loss

Chemistry: Metal hydride anode, nickel-based cathode.

I.6.1.2.1 Characteristics:

- Energy Density: Moderate (60–120 Wh/kg), less than Li-ion.
- Power Density: Good, suitable for hybrid vehicles.

- Cycle Life: 500–1,000 cycles.
- Cost: Less than Li-ion but less cost-effective for EVs.
- Safety: Safe compared to Li-ion, with minimal thermal runaway.
- Charging Speed: Less suitable for fast charging compared to Li-ion.
- Application in EVs: Used in hybrid vehicles (e.g., Toyota Prius) but largely substituted by Li-ion in full EVs.
- Relativity to Renewables: Not as effective in renewable energy storage due to lower energy density and efficiency (70–85%).

I.6.1.3 Lead-Acid Batteries

High power lead-acid batteries are possible to build and are inexpensive, safe, recyclable, and dependable. Their low specific energy, poor cold-temperature behavior, and limited calendar and lifecycle are a drawback to their application. High-power advanced lead-acid batteries are in the process of being built, but they are used only in commercially available electric vehicles for ancillary loads. They are used for stop-start applications in internal combustion engine-powered vehicles to eliminate idling at standstill and reduce fuel consumption

Chemistry: Sulfuric acid electrolyte with lead plates.

I.6.1.3.1 Characteristics:

- Energy Density: Low (30–50 Wh/kg), limits range.
- Power Density: Medium, suitable for low-power devices.
- Cycle Life: 200–500 cycles, short life.
- Cost: Very low, lowest cost.
- Safety: Safe but dense and prone to sulfation during over-discharging.
- Speed of Charging: Reduces, not suitable for high-rate charging.
- Application in EVs: Applied in some vintage EVs and low-speed EVs (such as golf carts), not in high-performance EVs.
- Relevance to Renewables: Extremely limited use in renewable storage due to low efficiency (70–80%) and short life.

Battery Type	Energy Density (Wh/kg)	Cycle Life	Cost	Safety	Charging Speed	EV Application	Renewable Integration
Lithium-Ion (NMC/LFP)	150–250	1,000–3,000	Moderate	Moderate/High	Fast	Full EVs (e.g., Tesla, BYD)	High (BESS, V2G)
NiMH	60–120	500–1,000	Low	High	Slow	Hybrids (e.g., Prius)	Moderate
Lead-Acid	30–50	200–500	Very Low	High	Slow	Low-speed EVs	Low

Table 1.2: Comparison Table.

- Energy Density: Determines EV range. Li-ion leads, but solid-state shows potential for improvement.
- Cycle Life: Determines battery life. LFP and sodium-ion are best for long-term use.
- Cost: LFP and sodium-ion are cheap, critical for mass EV adoption.
- Safety: LFP, sodium-ion, and solid-state are safer, reducing fire risks.
- Charging Speed: Li-ion and solid-state support fast charging, aligning with renewable energy peaks (e.g., solar during midday).
- Environmental Impact: High-resource-intensive production of Li-ion, although there are recycling efforts and sodium-ion advancements to reduce impacts.
- Renewable Integration: High-performance batteries (solid-state, Li-ion) and long cycle battery life (LFP, sodium-ion) have the best capacity for renewable storage and V2G system operation.

I.6.2 Battery Capacity, Energy and Voltage

It is necessary to know battery capacity, energy, and voltage in evaluating rechargeable batteries for application in electric vehicles (EVs) and their relevance to renewable energy systems.

I.6.2.1 Battery Capacity

Battery capacity refers to the amount of electrical charge a battery contains, typically measured in terms of ampere-hours (Ah) or milliampere-hours (mAh) for smaller batteries. For EVs, capacity is measured in kilowatt-hours (kWh) since it measures usable energy, which incorporates charge and voltage.

I.6.2.2 Energy

Energy is the work capacity of a battery, in watt-hours (Wh) or kilowatt-hours (kWh) for electric vehicles. It is calculated as:

$$\text{Energy (Wh)} = \text{Capacity (Ah)} \times \text{Voltage (V)}$$

For example, a 100 Ah battery at 400 V provides 40,000 Wh (40 kWh).

High energy density batteries (Li-ion, solid-state, etc.) are best for the effective storage of intermittent renewable energy (solar, wind) with minimal energy loss in battery energy storage systems (BESS).

I.6.2.3 Voltage

Voltage is the potential difference across a battery expressed in volts (V). Voltage represents the driving force behind electric current. The voltage of the battery depends upon the chemistry and cell arrangement (series/parallel).

Every battery chemistry has a nominal cell voltage. EV battery packs arrange cells in series to achieve higher voltages (e.g., 400 V or 800 V systems) [25].

I.6.3 Battery Chargers

Battery chargers supply electric power to charge EV batteries, converting AC (from the grid or alternative sources of energy) to DC for the battery. They are designed to optimize charging rate, efficiency, and battery life while offering safety [26].

Signifiant types are :

I.6.3.1 On-Board Chargers (OBCs)

Integrated into the EV, to charge AC from power stations or alternative energy sources (e.g., solar panels) to DC for the battery. OBCs can be programmed for smart charging, aligning with renewable energy peaks (e.g., solar at midday).

I.6.3.2 Off-Board Chargers (DC Fast Chargers)

External chargers (e.g., public stations) that supply high-power DC to the battery directly, bypassing the OBC.

I.6.4 Renewable Integration:

Chargers combined with BESS store excess solar/wind energy for EV charging, reducing fossil fuel dependence. Smart charging and V2G peak hour charging using renewables enhances sustainability (e.g., Italian peak-hour renewable-EV optimization models) [27].

Renewable energy-powered EV battery systems are an environment-friendly option for reducing GHG emissions and ensuring grid stability. With direct charging, BESS, and smart technologies like V2G, EVs can make use of renewables to the best effect, and practical uses as reflected through case studies from Italy, China, Denmark, and others are made evident. Despite there being challenges, joint research and policy efforts are paving the way for a cleaner, more integrated energy future.

I.7 Electric motor drive

Electric motor machines that transform electrical energy into mechanical energy are key elements of electric vehicles (EVs). Several motors are utilized in EVs, such as DC, induction, switched reluctance, and permanent magnet brushless motors, which possess diverse characteristics influencing efficiency, weight, cost, and performance. Different manufacturers have varying motor selections with various considerations, such as power needs, efficiency, power density, reliability, and size. Increased environmental awareness and limitations of non-renewable fuels have propelled innovations in more efficient EVs. As the EV industry continues to improve, it is more critical than ever to comprehend the reasoning behind motor selection. Current work involves the evaluation of current motors and studies on new designs like permanent magnet hybrid, spoke, and inset motors to offer better EV powertrains [28] [29].

I.7.1 Development of NEV Traction Motors

NEVs' traction motors are primarily direct current motors (DCMs), induction motors (IMs), permanent magnet motors (PMMs), and switched reluctance motors (SRMs). PMMs are further divided into permanent magnet DC motors (PMDCMs), permanent magnet synchronous motors (PMSMs), permanent magnet brushless DC motors (PM-BLDCMs), and permanent magnet hybrid excitation motors (PM-HEMs) . In order to decrease the reliance on permanent magnet materials, excitation synchronous motors are also used in automobiles.

I.7.2 Types of electrical motor drivers

Electric vehicles (EVs) require special motor drives, and several of them are being considered for their optimum performance. Some of the well-known ones include switched reluctance motors (SRM), induction motors (IM), permanent magnet brushless DC motors (PMBLDC), and brushed

DC motors. These motors possess various characteristics such as efficiency, cost, weight, and reliability that make them more or less appropriate for EV applications. Though some research indicates that SRMs are the best option because of their light weight, high reliability, and fault tolerance, others contend that axial flux PMBLDCs are the best. PMBLDCs have high efficiency and power density, and IMs have good controllability and low price. The choice of a suitable motor drive for EVs depends on several parameters such as performance, price, and special vehicle design limitations [30].

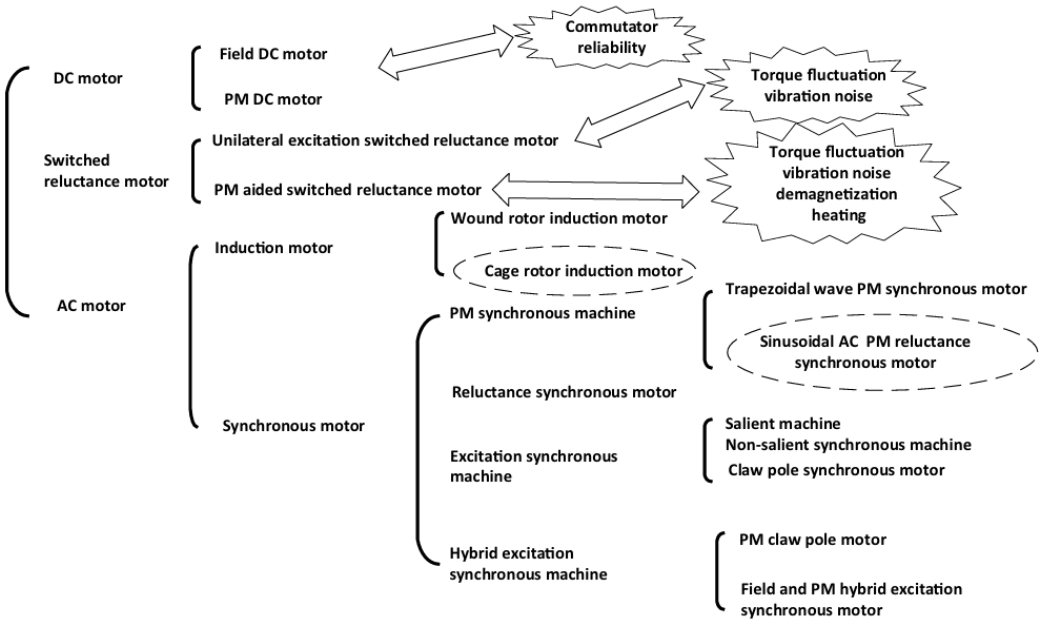

Figure 1.8: Traction motors of NEVs.

I.7.2.1 DC Motors

The initial electric vehicles (EVs) employed DC motor drives nearly exclusively due to the direct compatibility of DC motors with the battery-powered systems utilized in such vehicles. DC motor technology was not only available during this period but was also in the process of undergoing significant advancements, leading to its gradual optimization and refinement. DC motors were favored due to their simplicity, ease of control, and ability to provide high starting torque, which was necessary for early EV applications. The motors did have some drawbacks, such as the need for frequent maintenance due to brush wear and lower efficiency than modern options.

In DC motors, the stator is provided with permanent magnets (PMs) or electromagnets to generate the magnetic field, and the armature is wound on the rotor. This design ensures that torque and speed can be easily controlled, making DC motor drives extremely suitable for electric vehicle (EV) drives. Their torque-speed characteristic, which provides high torque at low speeds and lower torque at higher speeds, is ideally suited to the needs of EV applications. Of all DC motors, series-wound DC motors are the most appealing option. In such motors, field and armature circuits are connected in series, which produces a characteristic torque-speed profile delivering high starting torque ideal for acceleration from a standstill as well as declining torque as speed increases.

I.7.2.2 Induction Motor:

Induction Motors (IMs) are characterized by their three-phase AC (Alternating Current) stator windings and short-circuited copper windings (or cast aluminum bars) on the rotor, forming a so-called squirrel-cage rotor. Unlike brush and commutator machines, which are often avoided due to their extremely high maintenance requirements, squirrel-cage IMs are favored everywhere because of their simplicity, ruggedness, low price, and reliability. These features have made them an industry standard in industrial drives and a prime contender for electric vehicle (EV) drive systems.

Squirrel-cage IMs are particularly valued for their good field-weakening performance, that is, they can deal with a wide operating speed range in an efficient manner. With more advanced control strategies like vector control, it is feasible to separate the magnetic field and torque so the torque and speed can be controlled tightly like DC motor drives. The capability to extend the operating area of the motor beyond its base speed makes this drive applicable for use in high-speed EV drives. In efficiency, IMs perform well at high speed and low torque since there are reduced copper and core losses. They are less efficient at low speed and high torque since rotor losses are greater.

Detailed reviews of EV motor drives and expert surveys have all collectively identified induction motors as a very attractive choice for EV propulsion due to their low cost, high reliability, and well-established manufacturing and power converter technologies. Good examples of EVs powered by induction motors are the Chevrolet Silverado, Daimler Chrysler Durango, BMW X5, and Renault Kangoo. Despite their advantages, IMs have certain drawbacks, such as lower efficiency, poor power factor, and less-than-ideal inverter utilization. These drawbacks may restrict their usage in high-speed EV drives and big motor drives where higher efficiency and power density are crucial. [31].

I.7.2.3 Permanent Magnet Motor

I.7.2.3.1 Permanent magnet direct current motor

When the field windings and magnetic poles of conventional DC motors (DCMs) are replaced with permanent magnets (PMs), the result is a permanent magnet DC motor (PM-DCM). PM-DCMs offer significant advantages, including higher power density and improved efficiency, as the use of permanent magnets eliminates the need for field windings, reducing energy losses. However, these motors still rely on a commutator and brush system, which introduces drawbacks such as increased maintenance requirements, limited lifespan, and torque fluctuations due to mechanical wear and electrical arcing. These issues remain critical challenges for their adoption in electric vehicle (EV) applications, where reliability, durability, and smooth operation are essential.

I.7.2.3.2 Permanent magnet synchronous motor:

In Permanent Magnet Synchronous Motors (PMSMs), the stator, which features three-phase windings, is similar to that of induction motors (IMs) or traditional synchronous motors. However, instead of using excitation windings, PMSMs utilize permanent magnets (PMs) to generate the magnetic field. Based on the placement of these magnets, PMSMs are categorized into two main types: surface-mounted PMSMs (SPMs), where the magnets are mounted on the rotor's surface, and interior permanent magnet motors (IPMs), where the magnets are embedded within the rotor.

IPMs, in particular, are highly regarded for their advanced design features, including high reluctance torque, improved efficiency, high power factor, reduced heat generation, compact structure, and low noise levels. These characteristics make IPMs particularly well-suited for demanding applications such as electric vehicle (EV) traction systems. With advancements in power electronics and control strategies, IPMs have emerged as the dominant choice for traction motors, offering superior performance and reliability.

Additionally, IPMs benefit from a fully enclosed structure, which eliminates the need for maintenance and reduces wind friction losses and wind noise. This makes them ideal for applications where durability, quiet operation, and energy efficiency are critical. The combination of these features has solidified IPMs as a leading technology in modern motor design, particularly in the rapidly growing EV market, where high performance and low maintenance are essential.

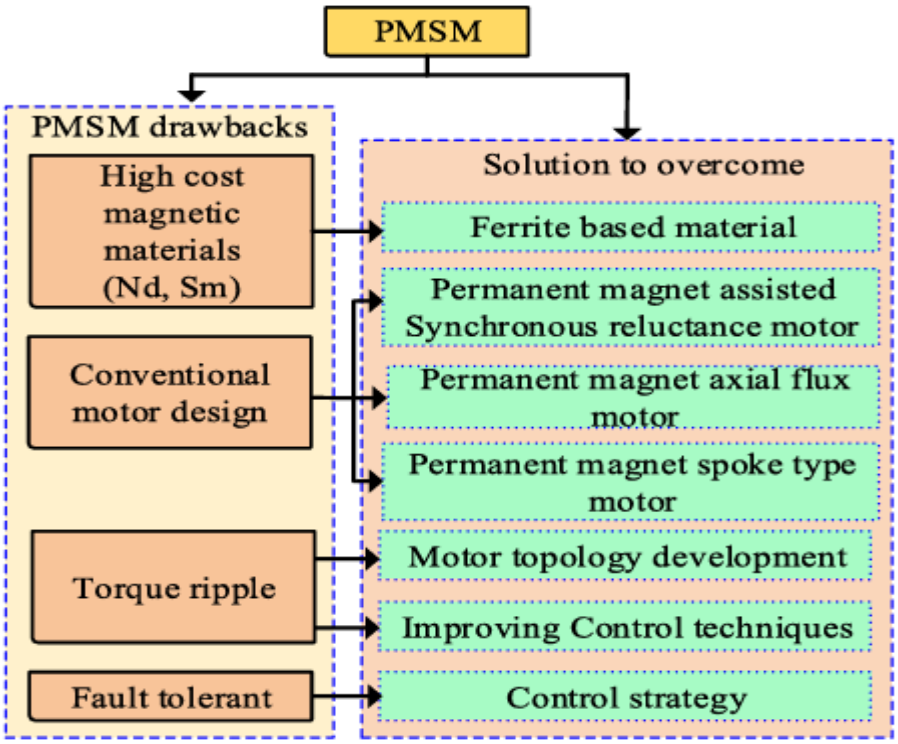

Figure 1.9: PMSM limitation in EVs.

I.7.2.3.3 Permanent magnet brushless DC motor

The Permanent Magnet Brushless DC Motor (PM-BLDCM) is structurally and theoretically a specialized type of Permanent Magnet Synchronous Motor (PMSM). However, it differs in key aspects: its stator windings are typically concentrated rather than distributed, and the stator current waveform is trapezoidal instead of sinusoidal, as seen in surface-mounted PMSMs (SPMs). Unlike traditional DC motors, PM-BLDCMs do not require a commutator-brush system, which eliminates mechanical wear and reduces maintenance needs.

I.7.2.3.4 Permanent magnet hybrid excitation motor

By incorporating excitation windings into a Permanent Magnet Synchronous Motor (PMSM), the motor evolves into a Hybrid Excited Motor (PM-HEM), combining the benefits of both permanent magnets and electromagnetic excitation. This hybrid design offers several advantages, including minimal flux leakage, high air-gap flux density, enhanced power density, and excellent torque-speed characteristics, making it well-suited for high-performance applications.

However, the integration of two excitation sources—permanent magnets and electromagnetic windings—introduces greater complexity in both the motor's topology and control strategies. The need to manage and coordinate these separate excitation systems adds to the design and operational challenges. Despite these complexities, PM-HEMs represent a promising advancement in motor technology, particularly for applications requiring high efficiency, power density, and precise control, such as electric vehicles and advanced industrial systems. Ongoing research aims to simplify their design and improve control algorithms to fully harness their potential [32].

Index	DCM	IM	IPM	SRM
Efficiency	●	●●	●●●	●
Speed	●	●●●	●●	●●●
Size	●	●●	●●●	●●
Reliability	●	●●	●●●	●●●
Control simplicity	●●●	●●	●	●●
Performance	●	●●	●●●	●●

Table 1.3: Comparison of NEV traction motors.

I.7.3 Development of the PMSM Technology

The future of traction motor technologies for New Energy Vehicles (NEVs) is centered on achieving high efficiency, high-speed operation, high power density, low vibration and noise, improved electromagnetic compatibility (EMC), and cost reduction. These factors are critical to meeting the growing demands of the automotive industry for more sustainable and high-performance electric vehicles (EVs).

For instance, the EV Development 2025 Roadmap outlined by the U.S. Department of Energy sets ambitious targets for EV motors, including an efficiency of 97%, a power density of 50 kW/L, and a cost reduction to 3.3 $/kW. Similarly, China's "Energy-saving and New Energy Vehicle Technology Roadmap 2.0" aims for a specific power (power-to-mass ratio) of 5.0 kW/kg, a power density (power-to-volume ratio) of 35 kW/L, and a peak efficiency of 97% by 2025. These goals highlight the global push toward more advanced and cost-effective motor technologies.

To meet these targets, global NEV traction motor suppliers and research institutions are intensifying their efforts to innovate and optimize both the innovation chain and the supply chain. This includes advancements in materials science, such as the development of high-performance rare-

earth-free magnets, high-temperature superconductors, and advanced cooling systems to enhance thermal management. Additionally, improvements in manufacturing processes, power electronics, and control algorithms are being pursued to boost motor performance and reduce production costs.

Collaboration across industries is also playing a key role, with partnerships between automakers, motor manufacturers, and material suppliers driving the development of next-generation traction motors. These efforts are not only focused on achieving the technical benchmarks but also on ensuring scalability and affordability to support the widespread adoption of NEVs. As a result, the future of traction motors is poised to deliver significant advancements in efficiency, performance, and sustainability, paving the way for a cleaner and more energy-efficient transportation ecosystem.

I.7.3.1 High-Speed Motor Technology

A motor's size is directly related to the torque it needs to produce. Since power is the product of torque and speed, for a given power output, increasing the motor's operating speed reduces the required torque. This, in turn, allows for a smaller and lighter motor, effectively increasing its power density. For instance, the Tesla Model 3 uses a traction motor operating at 17,900 rpm, and China's NEV Technology Roadmap 2.0 aims to achieve motor speeds of 25,000 rpm in new energy vehicles by 2035.

I.7.4 Motor Control Technologies

Variable Voltage-Variable Frequency (VVVF) control offers significant performance advantages over other PMSM control methods. It surpasses the simpler, open-loop Constant Volts-per-Hertz (V/F) control, which relies on steady-state motor models. VVVF also outperforms the more complex closed-loop Field-Oriented Control (FOC) and Direct Torque Control (DTC), both of which are based on dynamic motor models. A comparison of these three control methods is summarize in Table 1.4.

Control technology	Structural complex-ity	Robustness to parameters pertur-bation	Starting performance	Torque ripple	Speed range
V/F control	Simple	Low	Rough	High	Narrow
FOC	Complex	High	Smoothly	High	Wide
DTC	Complex	High	Smoothly	Relatively high	Wide

Table 1.4: Performance comparison of the three motor control technologies.

I.7.5 Electric Motor Drive Faults

Three main groups of faults in PMSM motor drives are categorized as electrical, three main groups of faults in PMSM motor drives are categorized as electrical, mechanical and sensor faults. These faults may occur in the motor part or the inverter part. Figure 1.10 shows a diagram of various electric motor drive faults. Mechanical and sensor faults. These faults may occur in the motor part or the inverter part. Figure 3 shows a diagram of various electric motor drive faults [33].

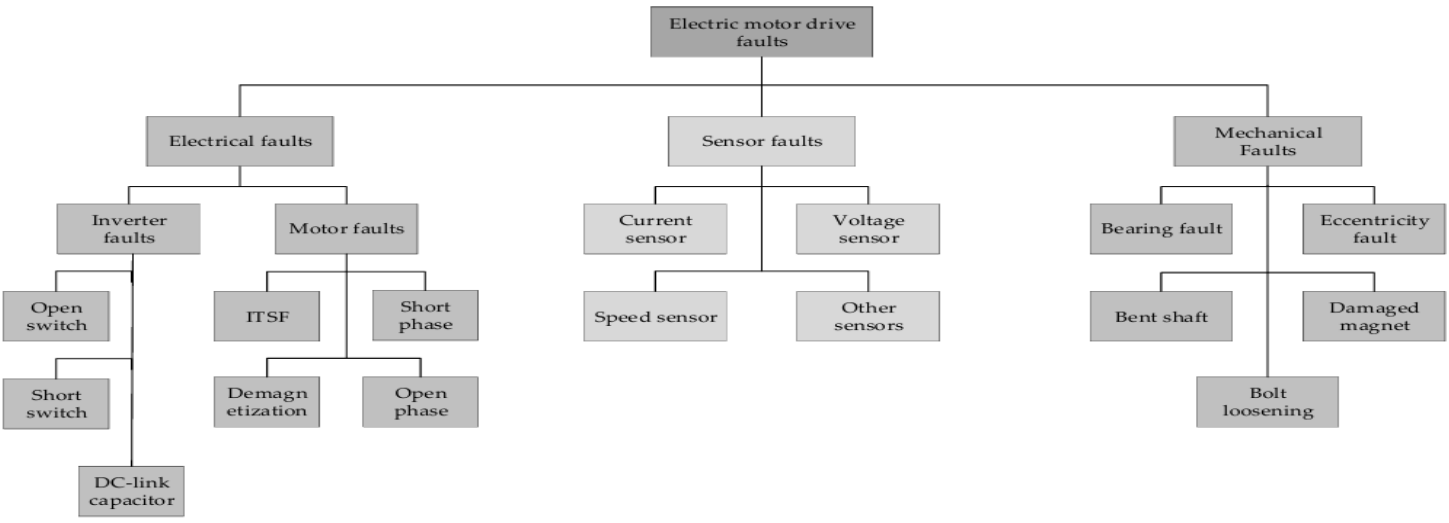

Figure 1.10: Various electric motor drive faults.

I.8 Supercapacitors

I.8.1 Supercapacitors for Electrified Vehicles

Supercapacitors (SCs), also called ultracapacitors, or electrochemical double-layer capacitors (EDLCs), are electrochemical energy storage devices designed for rapid energy storage and release. SCs store energy in the same way that regular capacitors do, by two solid electrodes separated by an electrolyte solution, but with much higher capacitance, holding up to 20 times more energy-storing capacity. SCs provide high power density, fast charge-discharge cycles, and theoretically unlimited cycle lifetimes. They are increasingly applied in industrial and transportation applications as high-power buffers, stand-alone or in conjunction with electrochemical batteries. SCs deliver 100 to 1000 times more power but contain three to thirty times less energy than batteries, perfect for applications where bursts of power but not large reservoirs of stored energy are required. Compared to heavy and stiff traditional capacitors, the new SCs for consumer electronics must be light, thin, flexible, and transparent with unique properties. The three main types of SCs applied in electric vehicles are EDLCs, pseudo capacitors, and hybrid capacitors. The merits and demerits of capacitor energy storage are tabulated and compared in Table 1.5.

Electric Double-Layer Capacitor	Pseudocapacitor	Hybrid Capacitor
High voltage and high power operation	Low-voltage functioning is restricted by electrochemistry and the solvent's solvent decomposition voltage.	Increased cell voltage
Electrode's substance of choice is carbon.	Materials utilized as electrodes are metal oxides and conducting polymers.	Consisting of materials containing either conducting polymers or metal oxides in the carbon
The creation of an electrochemical double layer serves as a charge storage mechanism, non-Faradaic process.	Redox reactions, faradaic process allow the charge to be stored.	Both faradaic and non-faradaic processes store the charge.

Table 1.5: Advantages and disadvantages of electric double-layer capacitors, pseudo capacitors, and hybrid capacitors.

I.8.1.1 Electric Double-Layer Capacitors

The two charged layers that exist at the electrode/electrolyte interfaces are referred to as electric double layers (EDL), and the charge storage capability that results from a potential dependence is attributed to electric double-layer capacitance [34 35 36]. Such SCs are therefore also referred to as electric double-layer capacitors (EDLCs). EDLCs have a much higher capacitance compared to electrostatic capacitors because they utilize high specific surface nanoporous materials as active electrode material.

I.8.1.2 Pseudo capacitors

Pseudo capacitors increase energy density and specific capacitance greater than EDLCs because the charge is stored through electro sorption, oxidation–reduction reactions, and intercalation processes, known as faradaic processes. The pore size and shape of the electrochemical pores in the electrode and the chemical attraction of the materials to the adsorbed ions on the surface of the electrode influence the electrodes' ability for the pseudo capacitance effect. The storage of the charge is increased linearly by the applied voltage.

I.8.1.3 Hybrid Capacitors

More recently, hybrid supercapacitor systems with increased voltages and improved energy density have been created by combining some battery-type electrodes and supercapacitor type electrodes. According to some researchers, "hybrid" supercapacitor systems are really "asymmetric" supercapacitor systems since they are constructed using two disparate supercapacitor type electrodes [34].

I.9 Conclusion

The integration of electric drive systems powered by renewable energy sources marks a pivotal step toward achieving a cleaner and more sustainable energy future. By utilizing energy from sources such as solar power and hydrogen fuel cells, these systems offer an eco-friendly alternative to traditional fossil fuel-based technologies. Nevertheless, several challenges remain, including managing energy intermittency, optimizing efficiency, and overcoming storage limitations, all of which are critical to ensuring a consistent and reliable power supply.

Hybrid energy systems (HES) have gained prominence as an effective solution by integrating multiple renewable energy sources in a manner that mitigates the individual limitations of each. The advancement of power electronics, alongside high-efficiency energy storage solutions and intelligent control strategies, is instrumental in improving the performance, stability, and adaptability of these systems across diverse applications. This holistic approach not only enhances the viability of renewable energy but also supports the transition to a more resilient and sustainable energy infrastructure [37].

Chapter II

Modeling of the association renewable sources Systems-Electric vehicle

II.1 Introduction

Electric vehicles (EVs) represent a transformational shift in the automotive industry, driven by the imperative need to fight climate change, reduce greenhouse gas emissions, and decrease reliance on fossil fuels. Unlike traditional internal combustion engine (ICE) vehicles, EVs are powered by electric drivetrains that use rechargeable battery packs, offering a cleaner alternative for private and commercial transportation [38]. The revival of EVs in the 21st century comes on the back of a long history dating back to the 19th century, with deep advancements in battery technology, power electronics, and energy management systems underpinning their modern adoption [39]. EVs are today recognized as a cornerstone of sustainable transport, contributing to global efforts to decarbonize the transportation sector, which accounts for a significant proportion of energy-related emissions globally [40].

The academic attention to EVs spans disciplines like engineering, environmental science, and economics to factor in their multifaceted effect. Research points to the efficiency of electric power, with electric motors capable of converting a greater proportion of energy into motion than their ICE counterparts, as well as the potential for zero tailpipe emissions with the utilization of renewable energy sources [41]. Even then, areas of high-priority research include battery production cost, infrastructure development in charging points, and range limitation [42]. Current studies identify policy incentives, technological innovation, and consumer behavior as central drivers to encourage the uptake of EVs, positioning them as part of the potential solution to reaching global climate objectives, as outlined in the Paris Agreement [43]. This introduction provides background for an intenser exploration of the EV powertrain, an area of focal academic modeling focus to optimize performance and sustainability.

II.2 Modeling of the electric vehicle propulsion system

The electric vehicle (EV) propulsion system serves as the foundational mechanism that enables sustainable transportation by harnessing electrical energy to power motion [44]. Rather than focusing solely on complex engineering, its significance lies in replacing fossil fuel dependency with a cleaner, more efficient alternative, aligning with global environmental goals [45]. The system integrates a battery pack, typically lithium-ion-based, which stores energy and releases it to drive the vehicle, marking a shift from traditional mechanical complexity to electrical simplicity [46]. An electric motor, often overlooked in its elegance, transforms this energy into rotational force, delivering propulsion with minimal energy waste compared to combustion engines [47]. Supporting this, a power inverter ensures seamless energy conversion, while a basic transmission adapts the motor's output to practical driving needs [48]. Beyond mechanics, the propulsion system embodies a synergy of innovation and control, relying on software to balance efficiency and performance under diverse conditions [49]. Its development reflects a broader commitment to reducing emissions and rethinking mobility, positioning it as a cornerstone of modern automotive evolution [50].

II.2.1 Dynamic model of an electric vehicle

II.2.1.1 Rolling resistance force

The rolling resistance is primarily due to the friction of the tyre of the vehicle on the road. There is also a friction contribution from bearings and the gear system. The rolling resistance is approximately a constant value, and hardly depends on vehicle speed. It is a function of the weight of the vehicle. The equation is:

$$F_{rr} = \mu_{rr}.\mathrm{mg} \tag{2.1}$$

Where μ_{rr} is the coefficient of rolling resistance. The main factors controlling μrr are the type of tyre and the tyre pressure. The value of μ_{rr} can reasonably readily be found by pulling a vehicle at a steady very low speed, and measuring the force required.

Typical values of μ_{rr} are 0.015 for a radial ply tyre, down to about 0.005 for tyres developed especially for electric vehicles [21].

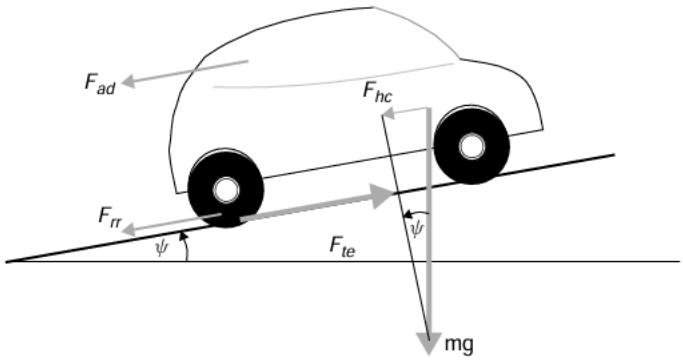

Figure 2.1: The forces acting on a vehicle moving along a slope.

II.2.1.2 Aerodynamic drag

This part of the force is due to the friction of the vehicle body moving through the air. The equation is:

$$F_{ad} = \frac{1}{2}\rho A C_d V^2 \tag{2.2}$$

where ρ is the density of the air, A is the frontal area, and V is the velocity. C_d is a constant called the drag coefficient.

Drag coefficient C_d can be reduced by good car design. A typical value for a saloon car is 0.3, but some electric vehicle designs have achieved values as low as 0.19. There is greater opportunity for reducing C_d in electric vehicle design because there is more flexibility in the location of the major

components, and there is less need for cooling air ducting. However, some vehicles, will inevitably have much larger values, and C_d figures of around 0.7 are more typical in such cases.

The density of air does of course vary with temperature, altitude and humidity. However, a value of $1.25\ Kg.m^{-3}$ is a reasonable value to use in most cases. Provided that SI units are used (m^2 for A, $m.s^{-1}$ for V) then the value of F_{ad} will be given in Newtons [21].

II.2.1.3 Hill climbing force

The force that is needed to move the vehicle up a hill is simplest to find. It is simply the part of the weight of the car in the direction of the slope. Through simple resolution of forces, we have that:

$$F_{hc} = mg.\sin(\psi) \tag{2.3}$$

where m is the vehicle mass (in kilograms), g is the gravitational acceleration, and ψ is the angle of the incline (in radians or degrees, with $\sin(\psi)$ converting the slope to a force component) [51].

II.2.1.4 Acceleration force

If the velocity of the vehicle is changing, then clearly a force will need to be applied in addition to the forces. This force shown in Figure 2.1 will provide the linear acceleration of the vehicle, and is given by the well-known equation derived from Newton's second law:

$$F_{la} = ma \tag{2.4}$$

However, to have a better idea of the force which needs to accelerate the vehicle we should also consider the force needed to make the rotating parts turn faster. We need to consider rotational acceleration as well as linear acceleration. The main issue here is the electric motor, not necessarily because of its particularly high moment of inertia, but because of its higher angular speeds [21].

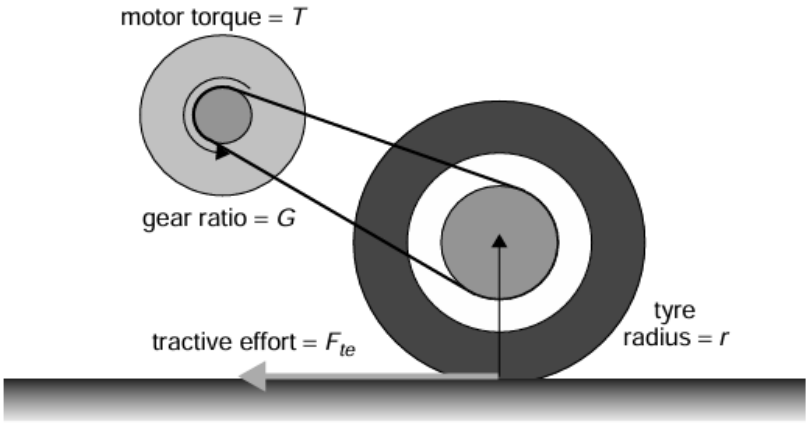

Figure 2.2: A simple arrangement for connecting a motor to a drive wheel

Referring to Figure 2.2, clearly the axle torque $= F_{te}.r$, where r is the radius of the tyre, and F_{te} is the tractive effort delivered by the powertrain. If G is the gear ratio of the system connecting the motor to the axle, and T is the motor torque, then we can say that:

$$T = \frac{F_{te}\, r}{G}$$

$$F_{te} = \frac{G.T}{r} \tag{2.5}$$

We will use this equation again when we develop final equations for vehicle performance. We should also note that:

$$axle\ angular\ speed = \frac{v}{r}\ rad.s^{-1}$$

So, motor angular speed:

$$\omega = G\frac{v}{r}\ rad.s^{-1} \tag{2.6}$$

Similarly, motor angular acceleration:

$$\dot{\omega} = G\frac{v}{r}\ rad.s^{-2}$$

The torque required for this angular acceleration is:

$$T = IG\frac{a}{r}$$

where I is the moment of inertia of the rotor of the motor.

The force at the wheels needed to provide the angular acceleration ($F\omega a$) is found by combining this equation with equation (2.5), giving:

$$F_{\omega a} = \frac{G}{r}\ IG\frac{a}{r} = I\frac{G^2}{r^2}a \tag{2.7}$$

We must note that in these simple equations we have assumed that the gear system is 100% efficient, it doesn't create any losses. Since the system will generally be very simple, the efficiency will generally be very high. But it will never be 100%, and thus we must refine the equation by incorporating the gear system efficiency η_g. The force required will be a little higher, so equation (2.7) can be refined to:

$$F_{\omega a} = I\frac{G^2}{\eta_g\, r^2}a \tag{2.8}$$

II.2.1.5 Total tractive effort

The total tractive effort is the sum of all these forces:

$$F_{te} = F_{\omega a} + F_{la} + F_{hc} + F_{ad} + F_{rr} \quad (2.9)$$

Where:

- F_{rr} is the rolling resistance force, given by equation (2.1).
- F_{ad} is the aerodynamic drag, given by equation (2.2).
- F_{hc} is the hill climbing force, given by equation (2.3).
- F_{la} is the force required to give linear acceleration given by equation (2.4).
- $F_{\omega a}$ is the force required to give angular acceleration to the rotating motor, given by equation (2.8).

F_{la} and $F_{\omega a}$ will be negative if the vehicle is slowing down, and that F_{hc} will be negative if it is going downhill [21].

II.3 Double Stator Machine

II.3.1 Description

The three-phase double-stator asynchronous machine DSASM is a system with two fixed stators shifted by an angle α = 30° with respect to each other and a rotor capable of moving in between them. Figure 2.3.

Each stator of the double-stator asynchronous machine consists of three identical windings with p pole pairs whose axes are displaced from each other with an electrical angle of 2π/3. The windings are placed in the slots cut on the magnetic circuit.

The two stator windings are powered by a balanced three-phase current system that creates a rotating magnetic field in the air gap.

The speed of rotation of this rotating magnetic field is proportional to the number of pole pairs of the machine and the angular frequency of stator currents as given:

$$\Omega_s = \frac{\omega_s}{P}$$

The rotor is designed to have three windings with the same number of poles as the stator [52].

This is supposed to be the assumption that rotor's electrical arrangement is squirrel-cage rotor (aluminum conductive bars within ferromagnetic laminations). So, the machines are cost-effective, robust, easy-to-use, and almost maintenance-free. When the rotor rotates at a rotor speed Ω different from Ω_s, a kind of three-phase electromotive force system happens in the rotor cage with three rotor currents. So, stator-induced effects on the induced rotor currents account in the development of an electromagnetic torque on the rotor so that the difference in speeds decreases.

The ratio $g = \frac{\Omega_s - \Omega}{\Omega_s}$: is called the rotor slip relative to the stator's rotating field [53].

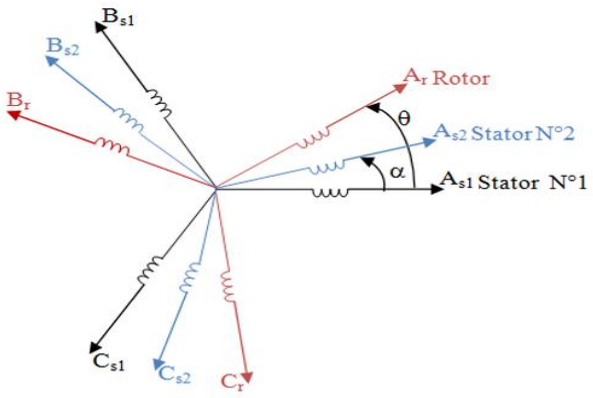

Figure 2.3: Representation of the DSASM windings.

We denote the quantity of the first stator as index s_1 and the quantity of the second stator as index s_2. Phases of the first stator are A_{s1}, B_{s1}, C_{s1} and of the second stator are A_{s2}, B_{s2}, C_{s2}, and of the rotor are A_r, B_r, C_r. The displacement angle between the two stators is α. θ_1 is the position of the rotor (phase A_r) in relation to the stator 1 (phase A_{s1}). The position of the rotor in relation to the stator 2 is denoted as θ_2[54]; the angles are as per the following equations:

$$\theta_1 = \Omega_m t + \theta_0$$

$$\theta_2 = \theta_1 - \alpha$$

With:

- Ω_m [rad/s]: the mechanical speed of the rotor.
- θ_0: The position of the rotor relative to stator 1.

II.3.2 Operating principle of the DSASM

The three-phase currents of frequency f_s supplying winding 1 of the stator of the machine give rise to a rotating field at synchronous speed N_s, such that:

$$N_s = \frac{f_s}{p} \left[\frac{tr}{s}\right]$$

With: p the number of pairs of poles.

The identical three-phase currents but displaced with an angle α exciting winding 2 of the same stator also generate another rotating field with the same speed N_s . These two rotating fields of the two stator windings will cause current in the conductors of the rotor, thereby creating electromotive forces which will drive the rotation of the rotor at the speed N [tr/s] lower than the synchronous speed (N < N_s). Stator actions on the rotor caused currents are the creation of an electromagnetic torque on the rotor in such a way that the speed difference is reduced to a minimum. It is stated that these two fields are slipping relative to the rotor, and this relationship is given as:

$$g = \frac{N_s - N}{N_s}$$

II.3.3 Modeling of the DSASM

II.3.3.1 Natural model of the DSASM

By using the simplifying assumptions mentioned previously, along with the notation of vectors of voltages, currents, and fluxes, one can specify those particular vectors for stator voltages, currents, and fluxes:

$$\text{stator}(1): \begin{cases} [V_{s1}] = [v_{as1} v_{bs1} v_{cs1}]^T \\ [I_{s1}] = [i_{as1} i_{bs1} i_{cs1}]^T \\ [\phi_{s1}] = [\phi_{as1} \phi_{bs1} \phi_{cs1}]^T \end{cases} \quad (2.10)$$

$$\text{stator}(2): \begin{cases} [V_{s2}] = [v_{as2} v_{bs2} v_{cs2}]^T \\ [I_{s2}] = [i_{as2} i_{bs2} i_{cs2}]^T \\ [\phi_{s2}] = [\phi_{as2} \phi_{bs2} \phi_{cs2}]^T \end{cases} \quad (2.11)$$

$$\text{rotor}: \begin{cases} [V_r] = [v_{ar} v_{br} v_{cr}]^T \\ [I_r] = [i_{ar} i_{br} ic_r]^T \\ [\phi_r] = [\phi_{ar} \phi_{br} \phi_r]^T \end{cases} \quad (2.12)$$

II.3.3.2 Equations of tensions

The combination of Hom's law and Lentz's law allows us to write the following relationships:

$$[V_{s1}] = [R_{s1}][I_{s1}] + \frac{d}{dt}[\phi_{s1}] \quad (2.13)$$

$$[V_{s2}] = [R_{s2}][I_{s2}] + \frac{d}{dt}[\phi_{s2}] \quad (2.14)$$

$$[V_r] = [R_r][I_r] + \frac{d}{dt}[\phi_r] \quad (2.15)$$

II.3.3.3 Equations of flux

The stator and rotor fluxes as a function of the currents, intrinsic inductances, and mutual inductances are expressed by the following equations:

$$[\phi_{s1}] = [L_{s1,s1}][I_{s1}] + [M_{s1,s2}][I_{s2}] + [L_{s1,r}][I_r] \quad (2.16)$$

$$[\phi_{s2}] = [L_{s2,s1}][I_{s1}] + [M_{s2,s2}][I_{s2}] + [L_{s2,r}][I_r] \quad (2.17)$$

$$[\phi_r] = [L_{r,s1}][I_{s1}] + [M_{r,s2}][I_{s2}] + [L_{r,r}][I_r] \quad (2.18)$$

$[R_{s1}]$; $[R_{s2}]$; $[R_r]$: the matrices of stator resistances (stator 1 and 2) and rotor resistances respectively:

$$\begin{cases} [R_{s1}] = R_{s1}\ [ID]_{3.3} \\ [R_{s2}] = R_{s2}\ [ID]_{3.3} \\ [R_r] = R_r\ [ID]_{3.3} \end{cases} \quad (2.19)$$

With:

- $[ID]_{3.3}$: The identity matrix of order 3.
- R_{s1} : The resistance of a phase of the first stator.
- R_{s2} : The resistance of a phase of the second stator.
- R_r : The resistance of a phase of the rotor.

The submatrices of the inductances in equations (2.16), (2.17) and (2.19) are expressed as follows:

$$[L_{s1,s1}] = \begin{bmatrix} (L_{s1} + L_{ms}) & -\frac{1}{2}L_{ms} & -\frac{1}{2}L_{ms} \\ -\frac{1}{2}L_{ms} & (L_{s1} + L_{ms}) & -\frac{1}{2}L_{ms} \\ -\frac{1}{2}L_{ms} & -\frac{1}{2}L_{ms} & (L_{s1} + L_{ms}) \end{bmatrix} \quad (2.20)$$

$$[L_{s2,s2}] = \begin{bmatrix} (L_{s2} + L_{ms}) & -\frac{1}{2}L_{ms} & -\frac{1}{2}L_{ms} \\ -\frac{1}{2}L_{ms} & (L_{s2} + L_{ms}) & -\frac{1}{2}L_{ms} \\ -\frac{1}{2}L_{ms} & -\frac{1}{2}L_{ms} & (L_{s2} + L_{ms}) \end{bmatrix} \quad (2.21)$$

$$[L_{r,r}] = \begin{bmatrix} (L_r + L_{mr}) & -\frac{1}{2}L_{ms} & -\frac{1}{2}L_{ms} \\ -\frac{1}{2}L_{ms} & (L_r + L_{mr}) & -\frac{1}{2}L_{ms} \\ -\frac{1}{2}L_{ms} & -\frac{1}{2}L_{ms} & (L_r + L_{mr}) \end{bmatrix} \quad (2.22)$$

$$[M_{s1,s2}] = \begin{bmatrix} L_{ms}\cos(\alpha) & L_{ms}\cos(\alpha + \frac{2\pi}{3}) & L_{ms}\cos(\alpha + \frac{4\pi}{3}) \\ L_{ms}\cos(\alpha + \frac{4\pi}{3}) & L_{ms}\cos(\alpha) & L_{ms}\cos(\alpha + \frac{2\pi}{3}) \\ L_{ms}\cos(\alpha + \frac{2\pi}{3}) & L_{ms}\cos(\alpha + \frac{4\pi}{3}) & L_{ms}\cos(\alpha) \end{bmatrix} \quad (2.23)$$

$$[M_{s1,r}] = \begin{bmatrix} M_{sr}\cos(\theta_m) & M_{sr}\cos(\theta_m + \frac{2\pi}{3}) & M_{sr}\cos(\theta_m + \frac{4\pi}{3}) \\ M_{sr}\cos(\theta_m + \frac{4\pi}{3}) & M_{sr}\cos(\theta_m) & M_{sr}\cos(\theta_m + \frac{2\pi}{3}) \\ M_{sr}\cos(\theta_m + \frac{2\pi}{3}) & M_{sr}\cos(\theta_m + \frac{4\pi}{3}) & M_{sr}\cos(\theta_m) \end{bmatrix} \quad (2.24)$$

$$[M_{s2,r}] = \begin{bmatrix} M_{sr}\cos(\theta_2) & M_{sr}\cos(\theta_2 + \frac{2\pi}{3}) & M_{sr}\cos(\theta_2 + \frac{4\pi}{3}) \\ M_{sr}\cos(\theta_2 + \frac{4\pi}{3}) & M_{sr}\cos(\theta_2) & M_{sr}\cos(\theta_2 + \frac{2\pi}{3}) \\ M_{sr}\cos(\theta_2 + \frac{2\pi}{3}) & M_{sr}\cos(\theta_2 + \frac{4\pi}{3}) & M_{sr}\cos(\theta_2) \end{bmatrix} \quad (2.25)$$

$$[M_{s2,r}] = [M_{s1,s2}]^T; [M_{r,s1}] = [M_{s1,r}]^T; [M_{r,s2}] = [M_{s2,r}]^T$$

With:

- L_{s1}: The self-inductance of the 1st stator.
- L_{s2}: The self-inductance of the 2nd stator.
- L_r: The self-inductance of one phase of the rotor.
- L_{ms}: The maximum value of the coefficients of stator mutual inductance.
- L_{mr}: The maximum value of the coefficients of rotor mutual inductance.
- M_{sr}: The maximum value of the coefficients of mutual inductance between a stator and the rotor.

II.3.3.4 Mechanical equation

The fundamental equation of rotor rotation is described by the following two relations:

$$(C_{em} - C_r - K_f . \Omega_m) = J \frac{d\Omega_m}{dt} \quad (2.26)$$

$$\frac{d\theta_m}{dt} = \Omega_m \quad (2.27)$$

With:

- J: the moment of inertia of the machine.
- C_{em}: The electromagnetic torque.
- C_r: The resisting torque (torque of the load).
- K_f: The coefficient of friction.

II.3.3.5 Magnetic energy

It can be calculated from the expression below:

$$\omega_{mag} = \frac{1}{2}([I_{s1}]^T[\phi_{s1}] + [I_{s2}]^T[\phi_{s2}] + [I_r]^T[\phi_r]) \quad (2.28)$$

Electromagnetic couple

The electromagnetic torque can be defined only in terms of the partial derivation, that is, the electromagnetic stored energy with respect to the geometrical rotation angle of the rotor.

$$C_{em} = \frac{d\omega_{mag}}{d\theta_m} = p\frac{d\omega_{mag}}{d\theta_e} \quad (2.29)$$

With:

- p: number of pairs of poles.
- θ_m: mechanical angle.
- θ_e: electrical angle.

The electromagnetic torque is given by the following expression:

$$C_{em} = [\frac{p}{2}]([I_{s1}]\frac{d}{d\phi_r}[L_{s1,r}][I_r]^t + [I_{s2}]\frac{d}{d\phi_r}[L_{s2,r}][I_r]^t) \quad (2.30)$$

The equations (2.10), (2.11), (2.12), (2.13), (2.14), (2.15), (2.26), (2.27) and (2.29) form the complete electromagnetic model of the DSASM in the real system, taking into account the aforementioned simplifying assumptions [53].

II.4 PV system modeling

A solar cell is a fundamental converter of photon energy to green and clean electricity if the converter device is interfaced in parallel and series way then PV module is created. For creating PV arrays more such modules are interconnected in parallel and series configuration which are susceptible to generate clean and green electricity. A solar cell may be referred as a section an electric circuit. It possesses a p–n junction which is known as a diode, a photocurrent generator which is a generation of current from light and resistors two where one is connected in series and one other one is parallel which described the Joule effect and recombination losses. Then the above combination is known as a single diode solar cell model [54].

Modeling, simulation and analysis of solar PV generator is essential pre-mounting phase at any installation site of PV system, which helps in understanding the real behavior and characteristics in real climatic conditions of that place.

II.4.1 Ideal photovoltaic cell

A photovoltaic cell can be simply described as an ideal current source that produces a current I proportional to the incident light power, in parallel with a diode that corresponds to the p-n transition area of the PV cell. If a resistive load is connected to the terminals of the photovoltaic generator, it only absorbs the current I such that:

$$I = I_{ph} - I_D$$

For an ideal PV cell, the voltage across the resistor is equal to the voltage across the diode:

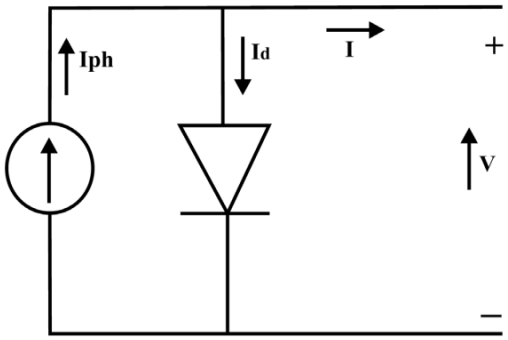

Figure 2.4: Simplified equivalent circuit of PV panel.

As the diode is a non-linear device, the characteristic (I-V) is represented by the relation.

$$I_D = I_S[\exp\left(\frac{V_D}{V_T}\right) - 1]$$

With:

I_S: Diode reverse saturation current given by:

$$I_S = KT^3A = e^{-\frac{Eg}{KT}}$$

- $V_T = KT/q$: Thermal potential.
- q: Electron charge (1 .602×10 C).
- K: Boltzmann constant (1.381×10 J/k).
- Eg: bandgap energy (for crystalline silicon, it is equal to 1.12 eV).

The equivalent current flow is:

$$I = I_{ph} - I[\exp\left(\frac{V_D}{V_T}\right) - 1]$$

This model remains theoretical and does not reflect the behavior of a photovoltaic cell under real-life conditions. However, it remains valid under certain assumptions (no voltage loss, leakage current, etc.). There are other models, still theoretical, but which give a more accurate picture of photovoltaic cell behavior [55].

II.4.2 Mathematical Model of Photovoltaic Cells

II.4.2.1 Single-Diode Model

got an analytical equation for extracting the parameters of the solar cell single-diode model from experimental data. Figure 2.5: shows the perfect photovoltaic cell circuit having a diode (D), a shunt resistance (RSH) and a series resistance (RS). The shunt resistance and the diode are parallel to the current source. The current source known as photocurrent (IPV) is generated when the cell is exposed to sunlight. IPV is linearly altered with different solar irradiation and fixed cell temperature. ID is the current that is flowed over the parallel diode. ISH is the shunt current flown due to RSH presence.

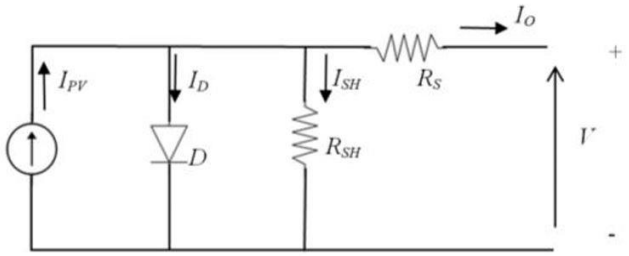

Figure 2.5: Single-Diode Model.

The equation for the output current I_0 is given by:

$$I_0 = I_{PV} - I_D - I_{SH} \tag{2.31}$$

$$I_{PV} = I_{SC}\left(\frac{R_S}{R_{SH}}\right) + I_{RC}\left(exp\frac{I_{SC}R_S}{aV_T} - 1\right)$$

$$I_D = I_{RC}\left[\exp\left(\frac{V + IR_S}{aV_T}\right) - 1\right]$$

$$I_{SH} = \frac{V + IR_S}{R_{SH}}$$

With $V_T = \frac{KT}{q}$

The definition of I_D is the Shockley diode equation, I_{RC} is the reverse saturation current of the diode.

T Tis the ambient temperature and a is the diode ideal constant.

Equation (2.31) will be:

$$I_0 = I_{sc}\left(1 + \frac{R_S}{R_{SH}}\right) + I_{RC}\left(exp\frac{I_{scR_S}}{aV_T} - 1\right) - I_{RC}\left[\exp\left(\frac{V+R_S}{aV_T}\right) - 1\right] - \frac{V+IR_S}{R_{SH}} \quad (2.32)$$

II.4.2.2 Double Diode Model

Two-diode model for photovoltaic (PV) cells is increasingly being accepted as an able alternative for PV simulation. It possesses an additional advantage over other models in the form of its ability to predict I-V behavior under very large values of solar irradiance (G) and temperature (T). Being the double-diode model, it considers the joint action of the carriers and hence proves to be a more accurate version than the single-diode model [56].

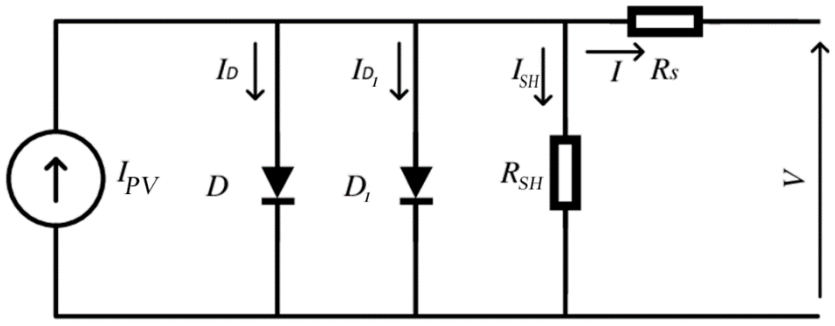

Figure 2.6: Double Diode Model

The equation for the output current I_0 in this double diode model given by;

$$I_0 = I_{PV} - I_D - I_{D1} - I_{SH}$$

$$I_D = I_{RC1}\left[\exp\left(\frac{V+IR_S}{a_1V_T}\right) - 1\right] \quad \text{and} \quad I_{D1} = I_{RC2}\left[\exp\left(\frac{V+IR_S}{a_2V_T}\right) - 1\right]$$

a_1 and a_2 represent ideality factor for diodes D and $D1$; I_{RC1} and I_{RC2} are the reverse saturation current of the diodes.

Equation (2.32) becomes:

$$I_0 = I_{sc}\left(1+\frac{R_S}{R_{SH}}\right) + I_{RC}\left(exp\frac{I_{sc}R_S}{aV_T}-1\right) - I_{RC1}\left[\exp\left(\frac{V+IR_S}{a_1V_T}\right)-1\right] - I_{RC2}\left[\exp\left(\frac{V+IR_S}{a_2V_T}\right)-1\right] - \frac{V+IR_S}{R_{SH}} \quad (2.33)$$

II.4.3 The Current-Voltage (I-V) and Power-Voltage (P-V) Characteristics Curve

Current-Voltage $(I-V)$ and Power-Voltage $(P-V)$ characteristic curves are generally used to describe the performance of output current I_0 and output power P which are produced by PV panel. Generally, the curve represents the combinations of current, voltage and power at which the string could be operated or 'loaded' if the solar irradiance and cell temperature could be held constant. The curve of $(I-V)$ and $(P-V)$ characteristics for PV cell show a detailed description of its solar energy conversion ability and efficiency. This curve is determining the device's output performance and solar efficiency. I_{sc} Is the maximum current that the cell can provide and it occurs when the cells are short-circuited. V_{OC} Is the maximum voltage that exists between the cells' terminals and is obtained when there is no load connected across them. I_{MPP} And V_{MPP} are being produced by the cell. It is called as P_{MAX} is product of I_{MPP} and V_{MPP}. Whereas I_{SC}, V_{OC}, I_{MPP}, V_{MPP} and P_{MAX} are given by the manufacturer. Figure 2.7 described the plotting point of I_{SC}, V_{OC}, I_{MPP}, V_{MPP} and P_{MAX}.

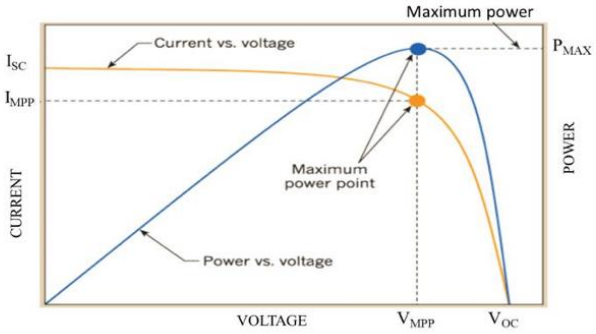

Figure 2.7: A typical current, voltage and power curve

II.4.4 Proposed Mathematical Model

This study took into account a single-diode model of PV cells. PV cells are connected in series to form PV modules in practice, and PV modules are arranged in series or parallel to form PV arrays. Through this connection, greater electricity is produced based on the load requirement. The performance of an individual PV module directly influences the overall efficiency and output of the PV array. The mathematical model is important because it has the ability to predict the PV cells behavior and performance by considering the plausible factors. In this study, the factors affecting the performance of the PV module are G and T [57] [58].

These factors will be influencing I_{PV}, I_{RC}, R_s, R_{SH} and a. The others factor should be considered is fitted parameter given by manufacturer. An accurate estimation of performance for PV module is the main goal by minimal in making the assumption. The previous study agreed that I_{RC} as represent the characteristics of a component that caused the accuracy of T. Thus, the estimation of I_{RC} must be considered with the environmental and working condition for having more accurate solution.

II.4.4.1 Calculation of I_{PV} (Single-Diode Model)

The single-diode model has been widely used to describe PV cell behavior as it offers the best balance between accuracy and simplicity. The equivalent circuit is comprised of a current source, a diode, and resistors employed to represent losses.

$$I = I_{PH} - I_D - I_{SH}$$

With:

- I_{PH}: Photocurrent (proportional to irradiance).
- I_D: Diode current, modeled using the Shockley equation.
- I_{SH}: Shunt current.

$$I_{SH} = \frac{V_D}{R_{SH}} = \frac{V + R_S I}{R_{SH}}$$

$$I = I_{PH} - I_S \left[\exp\left(\frac{V+R_S I}{aV_T}\right) - 1\right] - \frac{V+R_S I}{R_{SH}} \quad (2.34)$$

Where:

- I_S: Reverse saturation current of the diode.
- V: Output voltage.
- a: Diode ideality factor (typically 1–2).
- V_T: Thermal voltage,
- R_S: Series resistance.
- R_{SH}: Shunt resistance.

The short-circuit current I_{CC} represents the maximum current generated by the cell. It is produced when it is subjected to a short circuit $V = 0$. Since $R_S << R_{SH}$, we can assume that equation:

$I_{PH} = I_{CC}$ (2.34) becomes

$$I = I_{CC} - I_S \left[\exp\left(\frac{V+R_S I}{aRV_T}\right) - 1\right] - \frac{V+R_S I}{R_{SH}} \quad (2.35)$$

II.4.4.2 Calculation of I_S

Open-circuit voltage V_{CO} calculated when current is zero; as follows:

$$V_{CO} = aV_T \ln\left(1 + \frac{I_{CC}}{I_S}\right)$$

$I_{CC} \gg I_S$ it is also possible to calculate V_{CO} using the following relationship:

$$V_{CO} = aV_T \ln\left(\frac{I_{CC}}{I_S}\right)$$

Therefore, the reverse saturation current of the diode I_S is given by:

$$I_S = I_{CC}/[e^{\frac{V_{CO}}{aV_T}} - 1]$$

II.4.4.3 Calculation of series resistance in the point V_{CO}

The differentiation of equation (2.35), gives:

$$DI = 0 - I_S(\frac{dV + R_S dI}{aV_T})e^{\frac{(V+IR_S)}{aV_T}}$$

The result:

$$R_S = -\frac{dV}{dI} - \frac{aV_t}{I_S e^{\frac{(V+IR_S)}{aV_t}}} \quad (2.36)$$

In open circuit the voltage is $V = V_{CO}$ and equation (2.36) becomes:

$$R_S = -\frac{dV}{dI}\Big|V_{co} - aV_t/(I_S e^{\frac{V_{co}}{aV_t}})$$

Where:

$\frac{dV}{dI}\Big|V_{co}$ is the slope of the I(V) curve at point $V = V_{CO}$ (calculate from the I(V) curve in the module data sheet, then divide by the number of cells in series) [59].

The equations obtained so far are valid for a single mode of operation in terms of illuminance and temperature. To generalize the modeling for changing illuminances and temperatures, we use the model that shifts the reference curve to new locations.

The new value of the short-circuit current I for a given irradiation G and temperature T is then calculated according to the following equation [60]:

$$I_{cc}(G,T) = I_{ccr}\frac{G}{1000}\left[1 + a\left(T - T_{ref}\right)\right]$$

With:

- I_{ccr} : Short-circuit current measured under 1000W/m irradiation.
- a : Coefficient of variation of current versus temperature (a=0.65e-3).
- T_{ref} : Reference temperature, 298K (25°C).

The diode saturation current is also a function of temperature. Its value at temperature T is provided by equation (2.37).

$$I_s(T) = I_{sr}(\frac{T}{T_{ref}})^{\frac{3}{a}}e^{\left(\frac{-qE_g}{ak}\right)\left(\frac{1}{T}-\frac{1}{T_{ref}}\right)} \quad (2.37)$$

With:

- I_{sr} The reference inverse saturation current is given by the following equation:

$$I_{sr} = I_{ccr}/[e^{\frac{V_{CO}}{aV_{T_{ref}}}} - 1]$$

- V_{CO}: Open circuit voltage a T_{ref}.
- a : Diode ideality constant.

The ideality coefficient needs to be estimated and has a value ranging from 1 to 2. It is 1 for an ideal diode. The value for the I-V characteristic of the datasheet is 1.62.

II.4.5 Construction of a photovoltaic panel

A photovoltaic panel or module is realized by interconnecting an array of PV cells in series and/or parallel. The current output of the PV module and voltage at the module terminals are described by the following equations:

$$I_{module} = N_P * I_{cells}$$

$$I_{CCmodule} = N_P * I_{CCcells}$$

$$V_{module} = N_S * V_{cells}$$

$$V_{COmodule} = N_S * I_{COcells}$$

Number of cells in series (N_S): Determines the total voltage.

Number of parallel strings (N_P): Determines the total current [61].

II.5 Battery modelling

II.5.1 The simple electric battery model

The simple electrical model includes a fem E_0 modeling the battery's open-circuit voltage capacitor modelling the battery's internal capacity C_b and an internal resistance resistor (R_s).

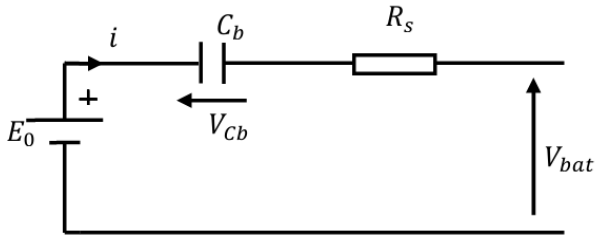

Figure 2.8: R-C battery model.

$$V_{bat} = E_0 - R_s * i - V_{cb}$$

The battery serves as the power source of the EV, and its type of critical importance in determining the EV system performance. There are different types of battery technologies, such as Lithium ion, Lead acid, Nickel metal hydride, etc. But the Lithium a lithium-ion (li-ion) battery is the most suitable option for EV usage since to its superior features, compared to the other types of batteries. These are high cell voltage, high energy density, low self-discharge rate and long cycle life [62]. In EV applications, the battery pack provides the power needed by the electric motor for

acceleration and also affects its operating performance as the EV range. The li-ion battery mathematical model that is utilized in this study is explained by using the following two equations.

The discharging model (i^*greater than0)

$$(V_{batt}) = f_1(it\ , i^*, i) = E_0 - Ri - \frac{K \times Q}{Q - it} \times i^* - \frac{K \times Q}{Q - it} \times it + A \times \exp(-B \times it) \quad (2.38)$$

The charging model (i^*<0)

$$(V_{batt}) = f_2(it\ , i^*, i) = E_0 - Ri - \frac{K \times Q}{it - 0.1 \times Q} \times i^* - \frac{K \times Q}{Q - it} \times it + A \times \exp(-B \times it) \quad (2.39)$$

Where following notations have been used:

- V_{batt} Battery voltage (V).
- E_0 Battery constant voltage (V).
- K Polarization constant or polarization-resistance (Ohm).
- i^* Dynamics of the low frequency current (A).
- i Battery current (A).
- R Resistance internal.
- it Actual battery charge $(Ah)^{-1}$.
- Q Maximum battery capacity (Ah).
- A Exponential voltage (V).
- B Exponential capacity $(Ah)^{-1}$.

The capacity of the battery is a basic characteristic of the performance of the EV, along with; the total energy that the battery must provide to the load is called the State of Charge (SoC), and it relies on the charging and discharge cycles of the battery pack.

The available energy in the battery pack can be calculated by:

$$Energy = Energy - Ebatt * i * T \quad (2.40)$$

Where; the first part of the right side of (2.40) represents previous value of the battery energy and the second part represents the consumed or recovered energy depends on battery current, and E_{batt} represent battery voltage and obtained from (2.38) or (2.39) above based on charging or discharging mode and the state of charge of the battery can be obtained by [63]:

$$SoC = \frac{Energy}{Full - Energy}$$

II.6 Fuel cell modeling

II.6.1 Description

The fundamental configuration of a PEM fuel cell can be described as two electrodes (cathode and anode) that are separated by a solid membrane acting as an electrolyte (Figure 2.16). Hydrogen fuel flows through a network of channels to the anode, where it dissociates into protons that move through the membrane to the cathode and electrons that are attracted as electrical current by an

external circuit between the two electrodes. The oxidant (air) travels through an identical array of channels to the cathode where oxygen combines with the electrons in the external circuit and the protons that flow through the membrane, thus producing water. The chemical reactions occurring at the anode and cathode electrode of a PEM fuel cell are as follows:

Anode reaction: $2H_2 \rightarrow 4H^+ + 4e^-$

Cathode reaction: $O_2 + 4H^+ + 4e^- \rightarrow 2H_2O$

Total cell reaction: $2H_2 + O_2 \rightarrow 2H_2O + electricity + heat$

The products of this process are water, DC electricity and heat [64].

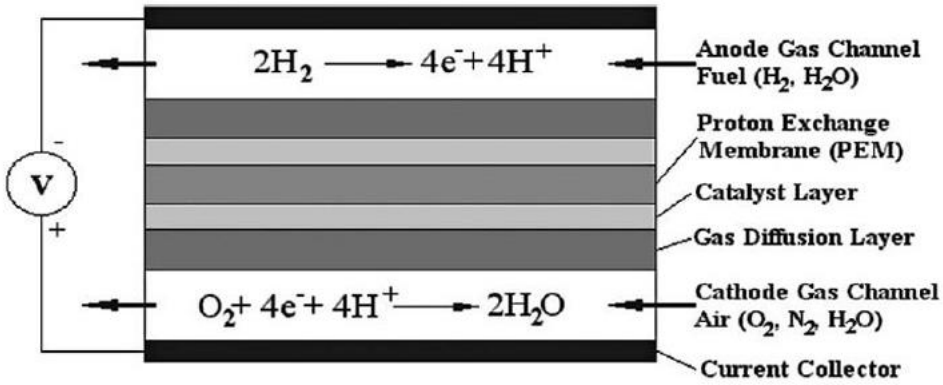

figure 2.9: Schematic of a single typical proton exchange membrane fuel cells PEMFC.

II.6.2 Mathematical modeling

This part presents a mathematical model for a Proton Exchange Membrane (PEM) fuel cell, covering the electrochemical performance and key loss mechanisms.

II.6.2.1 Open Circuit Voltage

The open circuit voltage (OCV) of a PEM fuel cell is computed by employing the Nernst equation, which considers the temperature-corrected thermodynamic potential and partial pressures of the reactants [65].

Nesrt equation:

$$E_{Nerst} = E_0 + \frac{R \cdot T}{2F} Ln\left(\frac{P_{H_2} \cdot P_{O_2}^{0.5}}{P_{H_2O}}\right)$$

With:

- E_0 : Standard cell potential (1.229 V at 25°C)
- R: Universal gas constante (8.314 J/mol·K).
- T: Temperature (K).
- F: Faraday's constant (96485 C/mol).
- P_{H_2} , P_{O_2} , P_{H_2O} : Partial pressures of hydrogen, oxygen, and water vapor (atm).

II.6.2.2 Cell Voltage

The actual cell voltage is reduced from the Nernst voltage due to various losses: activation, ohmic, and concentration losses [66].

Equation:

$$V_{cell} = E_{Nerst} - \eta_{act} - \eta_{ohm} - \eta_{conc}$$

With:

- V_{cell} : Actual cell voltage (V).
- η_{act} : Activation overpotential (V).
- η_{ohm} : Ohmic overpotential (V).
- η_{conc} : Concentration overpotential (V).

II.6.2.3 Activation Overpotential

Activation losses arise from the energy required to initiate electrochemical reactions, modeled using the Tafel equation [67].

Equation:

$$\eta_{act} = A \cdot \ln(\frac{i}{i_0})$$

$$A = \frac{RT}{\alpha nF}$$

With:

- A: Tafel slope.
- α: Charge transfer coefficient (typically 0.5 for PEMFCs).
- n: Number of electrons transferred (2 for oxygen reduction).
- i: Current density (A/cm²).
- i_0: Exchange current density (A/cm², typically 10^{-4} to 10^{-8} for oxygen reduction).

II.6.2.4 Ohmic Overpotential

Ohmic losses result from resistance to ion flow in the electrolyte and electron flow in the electrodes and interconnects [68].

Equation:

$$\eta_{ohmic} = i \cdot R_{ohmic}$$

With:

- R_{ohmic} : Total ohmic resistance (Ω·cm²), including contributions from membrane, electrodes, and contacts.

II.6.2.5 Concentration Overpotential

Concentration losses occur due to mass transport limitations of reactants to the electrode surface, particularly at high current densities [69].

Equation:

$$\eta_{conc} = -\frac{RT}{nF} \cdot \ln(1 - \frac{i}{i_{lim}})$$

With:

- i_{lim}: Limiting current density (A/cm²), where reactant concentration at the electrode approaches zero.

II.6.2.6 Power Density

The power density of the fuel cell is calculated as the product of cell voltage and current density [70].

Equation:

$P = V_{cell} \cdot i$

With:

- P: Power density (W/cm²)

II.7 SUPERCAPACITOR MODELING

II.7.1 Modeling of the Supercapacitor

The equivalent circuit schematic, which was used for the conventional capacitor, can be equally applied to the supercapacitor. Figure 2.10 shows the schematic circuit diagram representing the first-order model for a supercapacitor as stated in [71].

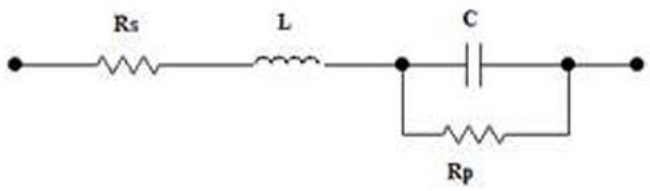

Figure 2.10: The first order circuit model of a supercapacitor.

Four ideal components of the circuit shown in Figure 1 are: capacitance C, series resistor RS, parallel resistor Rp and series inductance L. During charging and discharging, series resistance which is also called the equivalent series resistance (ESR) contributes to energy loss. Leakage current resistance, which is the parallel resistance Rp, also takes energy loss due to capacitor self-discharge. In practical capacitors Rp is typically much larger than Rs therefore Rp can be neglected especially in high-power applications.

A supercapacitor can be modeled at a cell level with the help of certain standard circuit components as depicted in figure one whereas the elementary structure of a supercapacitor based on the double layer capacitor technology consists of two activated porous carbon-based electrodes. The porous structure of the material makes it get surface area closer to two thousand square-meters per gram. The measured capacitance of activated carbon shows a non-linear relationship with their surface area, primarily due to the porous material used to form the electrodes yielding a dispersed resistance and capacitance so that their electrical response can be modeled by the transmission line model seen in figure 2.11, which provides a more exact depiction of the equivalent circuit of the supercapacitor [72]. Therefore, the theoretical model of supercapacitor could be addressed by a transmission line with the voltage-dependent distributed capacitance.

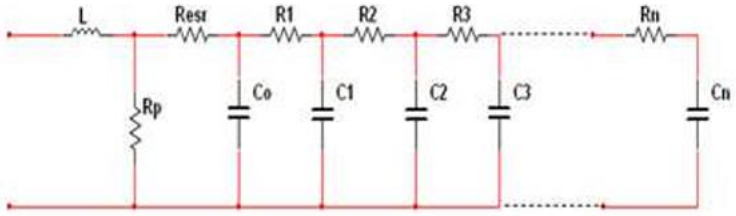

Figure 2.11: Exact equivalent circuit of the supercapacitor.

However, the simplified equivalent circuit of supercapacitor cell employed in this study is presented in figure 3.11 with other RC's slow branch circuits neglected. The traditional equivalent circuit model presented in figure 2.12 is the simplest among the supercapacitor models and can appropriately spell out the capacitor's performance in slow discharge processes (of a few seconds). This model circuit is used to describe the terminal behavior of the supercapacitor.

The total capacitance of the supercapacitor cell is a variable of supercapacitor voltage with value expressible in the form of constant capacitor and variable capacitor depending linearly on the cell voltage ($Vcell$). Thus, the equivalent capacitance is expressed by:

$$C_{cell} = C_o + kV_c \tag{2.41}$$

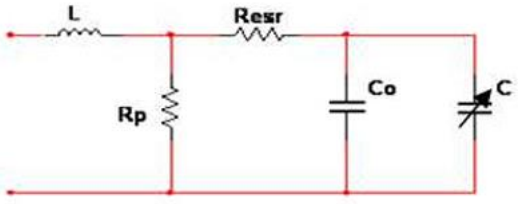

Figure 2.12 Simplified equivalent circuit of the supercapacitor.

We applying Kirchhoff's voltage law that says the total voltages in close loop must be zero, when charging a supercapacitor, will have this equation:

$$(R_{line} + R_{ESR})i + \frac{1}{C_{total}} \int idt = V_T \quad (2.42)$$

This equation can be converted into a differential equation in terms of charge (q) as:

$$(R_{line} + R_{ESR}) \frac{dq}{dt} + \frac{1}{C_{total}} q = V_T$$

While $q = CV$

Thus, it can be expressed in terms of the voltage of the supercapacitor (VC):

$$(R_{line} + R_{ESR})(C_0 + 2kV_c) \frac{dV_c(t)}{dt} + V_c(t) = V_T$$

Or

$$\frac{dV_c}{dt} = \frac{V_T - V_c}{(R_{line} + R_{ESR})(C_0 + 2kV_c)} \quad (2.43)$$

Determining the voltage required to overcome the internal resistance:

$$R_{ESR} i(t) + \frac{1}{C_{total}} \int i(t)dt = v_t \quad (2.44)$$

At instant of switching $t = 0^+$:

$$R_{ESR} i(t) - \frac{1}{C_{total}} \int i(t)dt = V_0$$

Multiply by C_{total} and take a derivative:

$$C_{total} R_{ESR} \frac{di(t)}{dt} - i(t) = 0$$

Multiply by R_{ESR} and note that $V_r(t) = Ri(t)$:

$$C_{total} R_{ESR} \frac{dV_r(t)}{dt} - V_r(t) = 0 \quad (2.45)$$

And the solution if equation 2.45 is:

$$V_r(t) = ke^{\frac{1}{C_{total} R_{ESR}} t} \quad (2.46)$$

Therefore, the voltage at the supercapacitor's terminals is:

$$V_t(t) = V_r(t) + V_c(t) \tag{2.47}$$

Equation of discharging a supercapacitor is:

$$\frac{dV_c}{dt} = \frac{-(V_c)}{(R_{line}+R_{ESR})(C_0+2kV_c)} \tag{2.48}$$

Terminal voltage of the supercapacitor in discharging is:

$$V_t(t) = V_c(t) + V_r(t) \tag{2.49}$$

II.7.2 Modeling for Energy Efficiency of the Supercapacitor

One of the main parameters of a supercapacitor is its series resistance. Internal losses occur due to this resistance. Many manufacturers have succeeded in reducing the value of this resistance, but it still results in an energy efficiency lower than one, which leads to a decrease in available power. The energy efficiency of the supercapacitor must be considered, especially when sizing a supercapacitive bank. The method of charging or discharging supercapacitors will affect their performance. Therefore, it is crucial to assess the energy efficiency of supercapacitors at varying levels of operating voltages before they are used in a specific application. This will serve as the foundation for developing power electronics that will regulate the current and voltage for charging and discharging, thereby optimizing the performance of supercapacitors [73].

The effectiveness of energy usage is significantly influenced by the internal series resistance (R) and capacitance (C) values. Experimental results have established a connection between efficiency and discharging time [74].

$$\eta_{eff} = e^{\frac{-2\,C_{total}\,R_{ESR}}{t_{dch}}} \tag{2.50}$$

The time required for discharging can be represented as a ratio of voltage discharge, which can be obtained from the equivalent circuit of the supercapacitor that is connected to the load, as illustrated in figure 2.17.

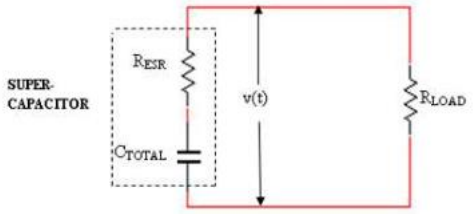

Figure 2.13: Equivalent circuit of discharging the supercapacitor.

The voltage v(t) can be calculated using the equation of a parallel RC circuit, given the initial condition that $V(0) = V_0$. The $V_c(t)$ of the circuit mentioned above can then be computed and expressed as:

$$V_c(t) = V_0 e^{-t/R_T C_{total}} \tag{2.51}$$

And

$$V(t) = V_c(t) + V_{R_{ESR}}(t)$$

So that:

$$V(t) = V_0(1 + \frac{R_{ESR}}{R_T})e^{-t/R_T C_{total}} \tag{2.52}$$

The voltage discharge ratio can be expressed as:

$$d = \frac{V(t)}{V_0} = (1 + \frac{R_{ESR}}{R_T})e^{-t/R_T C_{total}} \tag{2.53}$$

And solving for the discharge time from equation 2.53:

$$t_{dt} = -(R_{ESR} + R_{load})C_{total} \ln\left[\frac{(R_{ESR}+R_{load})d}{2R_{ESR}+R_{load}}\right] \tag{2.54}$$

Where $R_{load}$is determined by voltage (v) because the current (i) during discharging was maintained as constant.

II.8 Conclusion

The modeling of integrated renewable energy systems and electric vehicles, which includes components such as double stator motors, fuel cells, photovoltaic (PV) systems, batteries, and supercapacitors, showcases the complexity and interconnection of sustainable energy solutions. These models facilitate optimized energy management, efficient power distribution, and enhanced performance of vehicles while utilizing renewable resources. By combining these technologies, the system achieves better efficiency, lower environmental impact, and a dependable energy supply, setting the stage for innovative, environmentally-friendly transportation solutions.

Chapter III
Control of the electric drive system

III.1 Introduction

For all vehicles, range and performance prediction is important. Computers allow us to do this quite easily. Above all else, computer-based methods allow us to change quite quickly the parameters of the vehicle, such as the motor power, the size and type of battery, weight, and so on, and see how the changes affect the range and performance. For all vehicles, range and performance prediction is important. Computers can easily make this possible. Most importantly, computer-based methods allow us to easily test parameters of the vehicle, such as motor power, battery size, supercapacitor and type, weight, etc., and see the effect of the change on the performance and range.

The FC-SC-Battery system is more reliable than a single power system because it combines the high energy density of batteries with the high-power density of supercapacitors. However, it is more expensive. Additionally, there is a FC-PV-Battery system that is also somewhat more reliable than a single power system, but it has limitations due to a low dynamic response. Despite restrictions in output surface area for vehicles, it requires a high-gain converter to boost the low output voltage of the photovoltaic source connected to the DC link. We have typical electric vehicle system [75] in figure 3.1:

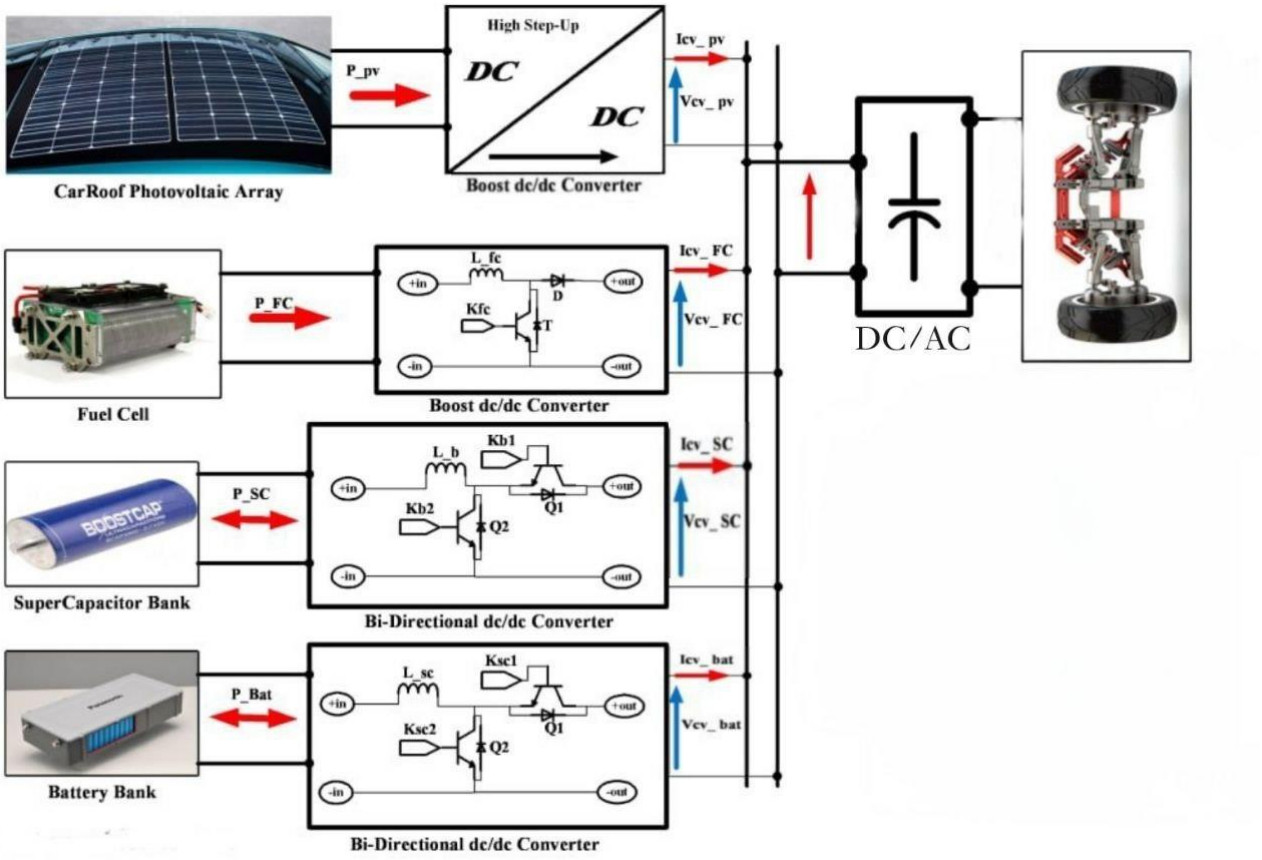

Figure 3.1: Typical electric vehicle system.

III.2 Perturb and Observe (P&O) MPPT algorithm for PV array

By analyzing Figure 3.2, it can be concluded that a positive variation in the PV voltage V_{PV}, leading to an increase in power P_{PV}, signifies that the operating point is situated to the left of the Maximum Power Point (MPP). Conversely, if an increase in V_{PV} results in a decrease in P_{PV}, the operating point is located to the right of the MPP. The same reasoning applies when considering a decrease in voltage. Based on these observations of the $P_{PV} - V_{PV}$ characteristic, it is thus possible to determine the relative position of the operating point with respect to the MPP, and to adjust it accordingly by means of an appropriate control strategy [76].

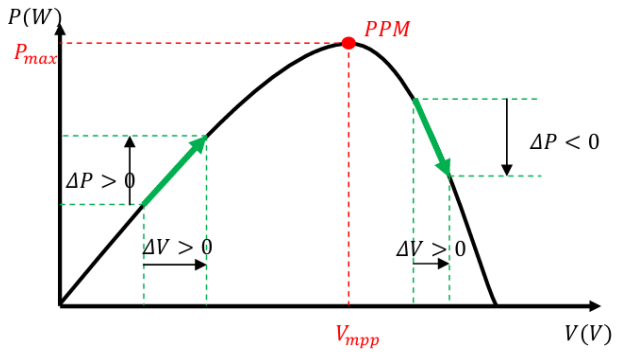

Figure 3.2 Positioning the operating point following the sign of ΔP and ΔV on the power characteristic.

Among the various Maximum Power Point Tracking (MPPT) techniques, the Perturb and Observe (P&O) algorithm is the most commonly employed in practice, as reported by numerous authors [77–78]. This algorithm constitutes an iterative method founded on the aforementioned principle, aiming to track the MPP by successively perturbing the operating point of the PV generator and observing the corresponding variations in power. The MPP is attained when the derivative $dP_{PV}/dV_{PV} = 0$. An illustration of the basic flowchart of the P&O algorithm is presented in Figure.3.3.

In doing this, the PV generator operating voltage is perturbed by a slight increase ΔV_{PV}, and the resulting change, ΔP_{PV}, in power is noted. If ΔP_{PV} is positive, then the perturbation of the operating voltage must be maintained in the same direction as the increase. However, if it is negative, the operating point of the system moves in the opposite direction relative to the MPP, and the operating voltage must be adjusted in the opposite direction of the increment. The conventional block diagram of the P&O method is shown in Figure 3.4.(a).

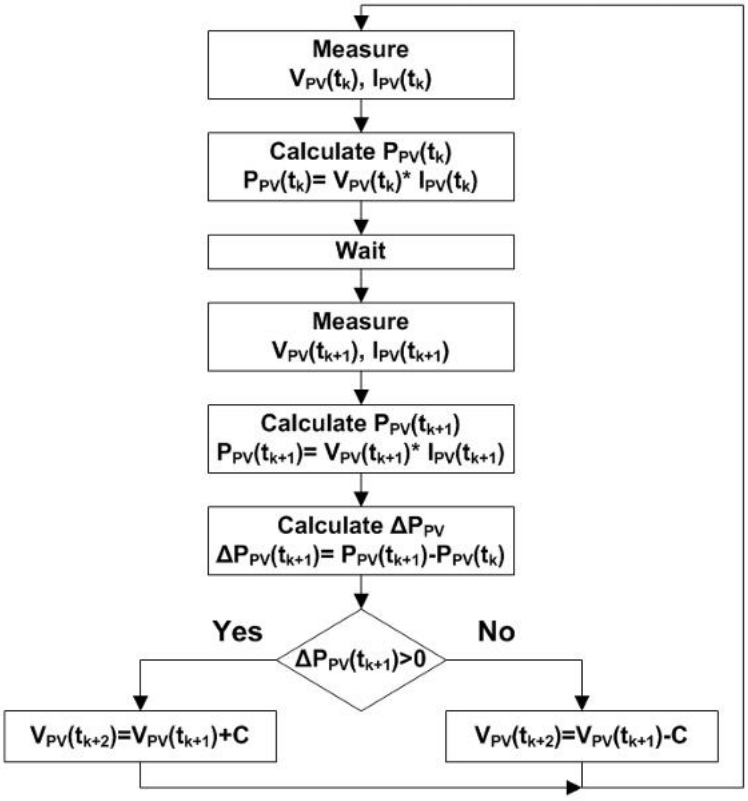

Figure 3.3: Conventional P&O algorithm owchart.

The advantages of this method are that a previous knowledge of PV generator characteristics is not required and it is relatively a simple method.

It is reported that P&O techniques possess certain drawbacks [79-80]. For fixed perturbation steps, steady-state oscillations are proportional to the step value. More step value causes more oscillation. Unfortunately, less step value results in sluggish response. So, the famous trade-off problem between quicker response and steady-state oscillations is inherent. Also, the value of the perturbation step is not universal; hence, MPPT with a fixed step is system dependent [81-82]. In order to obtain better performance, a variable perturbation step is utilized. Early approaches use a variable perturbation values depending on the output power. Although not adaptive in the strict sense, these approaches have better behavior than their fixed perturbation counterparts [83]. Other approaches propose real adaptive adaptations, but are beset by an overwhelming computational burden as a consequence of aggressive derivatives and need initial user-dependent constants for perturbation step adaptation. Therefore, modified approaches of P&O are formulated depending on the controlled variable output of MPPT block and the step value generation.

Several attempts have been proposed to improve the performance of the modified P&O using adaptive perturbation step. The main task is to find the best value of the perturbation step in order to have the fastest tracking time with less oscillation. Based on some publication survey [84-85-86-87], authors de ne the step size as:

$$d(k) = d(k-1) \pm \frac{|\Delta P/\Delta d|}{|P/d|} \tag{3.1}$$

$$d(k) = d(k-1) \pm \frac{M|\Delta P|}{d(k-1)} \tag{3.2}$$

$$d(k) = d(k-1) + M\frac{dP}{dV} \tag{3.3}$$

Despite of good performance, these techniques suffer several demerits, such as high computational load versus accuracy trade-off and predefined constants dependency. Modified P&O with adaptive perturbation step block diagram is shown in Figure.3.3.

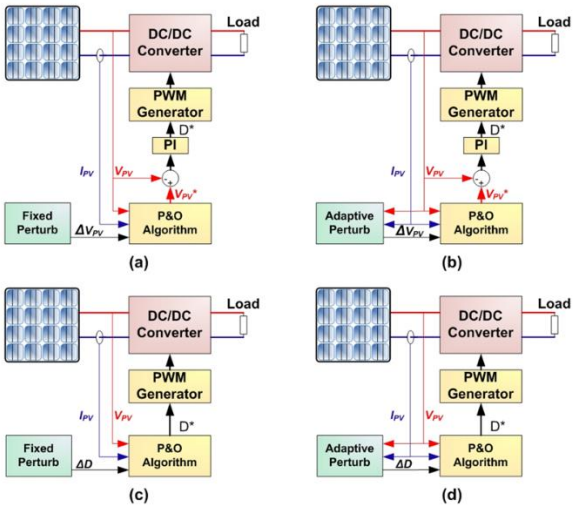

Figure 3.4: Various P&O block diagram topology. (a) Conventional P&O with fixed perturbation step. (b) Conventional P&O with adaptive perturbation step. (c) Modi ed P&O with fixed perturbation step. (d) Modi ed P&O with adaptive perturbation step.

The MPPT algorithm used to get the maximum available PV power controls the DC/DC buck converter. The MPPT is based on the P&O algorithm that was described. Maximum power is the result of tracking the optimum voltage and current due to the variation of the input impedance of the buck converter. The current can be varied depending on the load requirements. Converter is modeled taking into consideration the inductors resistance, the capacitors (ESR) and the MOSFET On resistance.

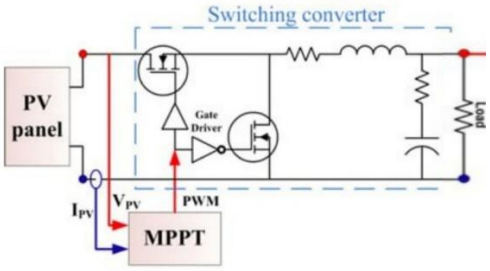

Figure 3.5: Block diagram.

the P&O method is nowadays trendy due to its ease of implementation, but it suffers from some problems with oscillations around the PPM that it generates at steady state since the searching procedure of the PPM must be repeated periodically, Forcing the system to continuously oscillate around the MPP once reached. The oscillations can be minimized by taking the perturbation variable value small. However, a low incremental value slows down the PPM search, so there is a trade-off between precision and speed, and this command is difficult to optimize [76].

III.3 DTC control

The basics of Direct Torque Control (DTC) involve the direct command to open or close the inverter switches on the basis of values of stator flux and torque that have already been calculated beforehand. The changes in the states of the switches are pinned down to the changes in the electromagnetic states of the motor. They are no more controlled from the voltage and frequency setpoints assigned to a pulse width modulation inverter by close control [88].

III.3.1 principle of the DTC command

Control involves the direct manipulation of electromagnetic torque and stator flux through direct determination of the control sequence to be applied on the switches of a voltage inverter. This decision relies on utilizing hysteresis regulators, which are utilized to control the system state, i.e., stator flux amplitude and electromagnetic torque, in a way that keeps the two variables inside specified error limits; the two regulator outputs and the position indication where the flux vector was determining the control (or truth) table that was being used to drive the inverter. The second (two-level inverter) makes it possible, if needed, to realize seven different positions in the phase plane for the eight voltage vector sequences on the inverter output. The direct torque control of the classical torque of a double stator asynchronous machine can be illustrated by the figure 3.6 below. Figure 3.6 illustrates the flux and torque estimators, and also the hysteresis regulators of torque and flux. The position of the flux vector is calculated from its complex components in the αβ plane. The flux regulator is two-level and the torque regulator is three-level as originally proposed by Takahashi [89].

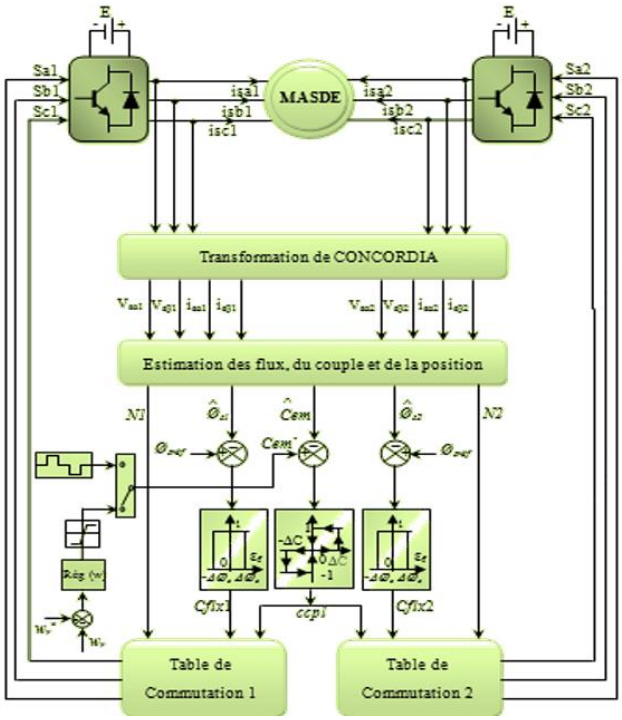

Figure 3.6 General structure of the DTC.

Direct torque control generally has excellent dynamic characteristics, and it is generally defined by [90]:

- A machine shows very fast dynamic response and implementation differs greatly from stream-oriented commands in that it does not involve coordinate transformation (Park) in the rotating axis.
- It ranks among the simple control strategies with low computational costs.
- Variable flow operation does not affect the torque setting, since the decoupling of the control variables is naturally ensured by direct control.

Modifications of rotor parameters of the machine do not affect the control in its simple version; in addition, the estimation of stator flux depends only on the stator resistance (this is via open-loop integration of the stator electromotive force).

III.3.2 Control of stator flux and torque

III.3.2.1 Stator flux control

We place ourselves in a fixed reference frame αβ linked to the stator of the machine. The stator flux can be calculated using this equation:

$$\overrightarrow{V_s} = R_s\overrightarrow{I_s} + \frac{d\overrightarrow{\phi_s}}{dt} \Longrightarrow \overrightarrow{\phi_s} = \overrightarrow{\phi_{s0}} + \int_0^t \left(\overrightarrow{V_s} - R_s\overrightarrow{I_s}\right)dt \qquad (3.4)$$

If we neglect the voltage drop due to resistance, equation (3.4) becomes:

$$\overrightarrow{\phi_s}(k+1) \approx \overrightarrow{\phi_s}(k) + \overrightarrow{V_s}T_e \Longrightarrow \Delta\overrightarrow{\phi_s} \approx \overrightarrow{V_s}T_e \quad (3.5)$$

With:

- $\overrightarrow{\phi_s}(k)$: stator current vector at the current sampling step.
- $\overrightarrow{\phi_s}(k+1)$: stator current vector at the next sampling step.
- $\Delta\overrightarrow{\phi_s} = \overrightarrow{\phi_s}(k+1) - \overrightarrow{\phi_s}(k)$: stator flux variation vector.
- T_e : sampling period.

From relation (3.5), the rotational speed of the flow is equal to applied tension. Tensor application along current vectors directly modify the amplitude of such vectors, while the application of tension vectors in quadrature with the flow alters the flow's phase and causes acceleration or deceleration of the flow vector.

It is found that the end of the stator flux vector describes, from its initial state, a line parallel to the applied tension vector Figure 3.7 [90].

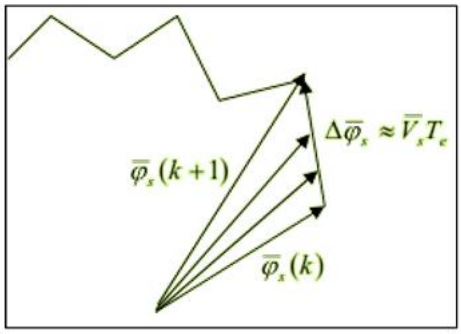

Figure 3.7 Evolution of the flux vector in the αβ plane.

III.3.2.2 Torque control

The electromagnetic couple can be determined by the vector product of the two stator and rotor fluxes.

$$C_{em} = K\left(\overrightarrow{\Phi_s} \wedge \overrightarrow{\Phi_r}\right) = K\|\overrightarrow{\Phi_s}\|\|\overrightarrow{\Phi_r}\| \sin(\gamma) \quad (3.6)$$

The angle γ is the phase shift between the two flows.

The stator flux is the sum of the rotor flux and the total leakage flux.

The dynamics of these two components are not the same [90] [91]:

- The leakage flow has a rapid dynamic due to voltage variations, as the leakage inductances are low.
- The rotor flux, dependent on the magnetizing inductance, has a slower dynamic, about ten times slower with reference to the dispersion coefficient σ, whose average value is around 0,1.

Therefore, it may be assumed that between two switches, the rotor flux remains constant; on the other hand, the stator flux is directly affected by leakage flux.

So, the torque depends only on the product $\|\overrightarrow{\Phi_s}\| \ sin(\gamma)$ .Since the amplitude of the stator flux varies very little, the variation of the torque can be achieved by varying the angle γ .

III.3.3 Direct Torque Control (DTC) Strategy

The direct command of the torque is based on the following algorithm [89][90]:

- The time domain is divided into periods of duration T_e (T_e≤50µs).
- We measure the currents and line voltages at every stroke of the clock.
- We reconstruct the components of the static flow vector.
- The couple is estimated using the following relationship:

$$C_{em} = p(\phi_{\alpha s1} I_{\beta s1} + \phi_{\alpha s2} I_{\beta s2} - \phi_{\beta s1} I_{\alpha s1} + \phi_{\beta s2} I_{\alpha s2})$$

- We will present a logic to determine the tension vector to apply to the machine in what follows.

III.3.4 Estimators

III.3.4.1 Estimation of the stator current

The estimation of the flow can be carried out from the measurements of the stator currents and voltage of the machine [90][91].
From the equation:

$$\begin{cases} \overrightarrow{\phi_{s1}} = \int_0^t (\overrightarrow{V_{s1}} - R_{s1}\overrightarrow{I_{s1}})dt \\ \overrightarrow{\phi_{s2}} = \int_0^t (\overrightarrow{V_{s2}} - R_{s2}\overrightarrow{I_{s2}})dt \end{cases} \quad (3.7)$$

We obtain the components α and β of the vector $\overrightarrow{\phi_s}$:

$$\begin{cases} \overrightarrow{\phi_{\alpha s1}} = \int_0^t (\overrightarrow{V_{\alpha s1}} - R_{\alpha s1}\overrightarrow{I_{\alpha s1}})dt \\ \overrightarrow{\phi_{\alpha s2}} = \int_0^t (\overrightarrow{V_{\alpha s2}} - R_{\alpha s2}\overrightarrow{I_{\alpha s2}})dt \end{cases} \quad (3.8)$$

$$\begin{cases} \overrightarrow{\phi_{\beta s1}} = \int_0^t (\overrightarrow{V_{\beta s1}} - R_{\beta s1}\overrightarrow{I_{\beta s1}})dt \\ \overrightarrow{\phi_{\beta s2}} = \int_0^t (\overrightarrow{V_{\beta s2}} - R_{\beta s2}\overrightarrow{I_{\beta s2}})dt \end{cases} \quad (3.9)$$

The voltages ($V_{\alpha s1}, V_{\beta s1}, V_{\alpha s2}, V_{\beta s2}$) are obtained from the commands (S_{a1}, S_{b1}, S_{c1}), (S_{a2}, S_{b2}, S_{c2}), and from the measurement of the supply voltage V_{dc} by applying the Concordia transformation.

$$\begin{cases} \overrightarrow{V_{s1}} = V_{\alpha s1} + jV_{\beta s1} \\ V_{\alpha s1} = \sqrt{\frac{2}{3}} V_{\mathrm{dc}}(S_{a1} - \frac{1}{2}(S_{b1} - S_{c1})) \\ V_{\beta s1} = \frac{1}{\sqrt{2}} V_{\mathrm{dc}}(S_{b1} - S_{c1}) \end{cases} \quad (3.10)$$

$$\begin{cases} \overrightarrow{V_{s2}} = V_{\alpha s2} + jV_{\beta s2} \\ V_{\alpha s2} = \sqrt{\frac{2}{3}} V_{\mathrm{dc}}(S_{a2} - \frac{1}{2}(S_{b2} - S_{c2})) \\ V_{\beta s2} = \frac{1}{\sqrt{2}} V_{\mathrm{dc}}(S_{b2} - S_{c2}) \end{cases} \quad (3.11)$$

Similarly, the currents ($I_{\alpha s1}$, $I_{\beta s1}$, $I_{\alpha s2}$, $I_{\beta s2}$) are obtained from the measurement of the real currents (Is_{a1}, Is_{b1}, Is_{c1} , Is_{a2}, Is_{b2}, Is_{c2}) by applying the Concordia transformation:

$$\begin{cases} \vec{I}_{s1} = I_{\alpha s1} + jI_{\beta s1} \\ I_{\alpha s1} = \sqrt{\frac{2}{3}} I_{as1} \\ I_{\beta s1} = \frac{1}{\sqrt{2}}(I_{bs1} - I_{cs1}) \end{cases} \quad (3.12)$$

$$\begin{cases} \vec{I}_{s1} = I_{\alpha s1} + jI_{\beta s1} \\ I_{\alpha s1} = \sqrt{\frac{2}{3}} I_{as1} \\ I_{\beta s1} = \frac{1}{\sqrt{2}}(I_{bs1} - I_{cs1}) \end{cases} \quad (3.13)$$

The stator flux module is written as:

$$\begin{cases} \phi_{s1} = \sqrt{\Phi_{\alpha s1}^2 + \Phi_{\beta s1}^2} \\ \phi_{s2} = \sqrt{\Phi_{\alpha s2}^2 + \Phi_{\beta s2}^2} \end{cases} \quad (3.14)$$

The zone N_i in which the vector $\overrightarrow{\phi_s}$ is located is determined by the calculation of the phase of this vector:

$$\begin{cases} \angle\phi_{s1} = arctg \frac{\Phi_{\alpha s1}}{\Phi_{\beta s1}} \\ \angle\phi_{s2} = arctg \frac{\Phi_{\alpha s2}}{\Phi_{\beta s2}} \end{cases} \quad (3.15)$$

III.3.4.2 Estimation of the electromagnetic couple

The couple can be estimated from the following relation [90] [91]:

$$C_{em} = \frac{3}{2}p(\widehat{\Phi}_{\alpha s1}I_{\beta s1} + \widehat{\Phi}_{\alpha s2}I_{\beta s2} - \widehat{\Phi}_{\beta s1}I_{\alpha s1} + \widehat{\Phi}_{\beta s2}I_{\alpha s2}) \quad (3.16)$$

III.3.5 Correctors

III.3.5.1 Flow corrector

The goal of this correction is to keep the amplitude of stator flux within a band and therefore its end within a circular crown as shown in figure 3.7 [90].

$$\begin{cases} If\ \Delta\Phi_s > \varepsilon_\phi\ \ So\ \ K_\phi = 1 \\ If\ 0 \le \Delta\Phi_s \le \varepsilon_\phi\ \ and\ \ \frac{d\Delta\Phi_s}{dt} > 0\ \ So\ \ K_\phi = 0 \\ If\ 0 \le \Delta\Phi_s \le \varepsilon_\phi\ \ and\ \ \frac{d\Delta\Phi_s}{dt} < 0\ \ So\ \ K_\phi = 1 \\ If\ \Delta\Phi_s < -\varepsilon_\phi\ \ So\ \ K_\phi = 1 \end{cases}$$

- $K_\phi = 0$: meaning that it's necessary to reduce the flow.
- $K_\phi = 1$: indicate that it's necessary to increase the flow.

This two-level hysteresis regulator is perfectly suitable for achieving good dynamic performance.\

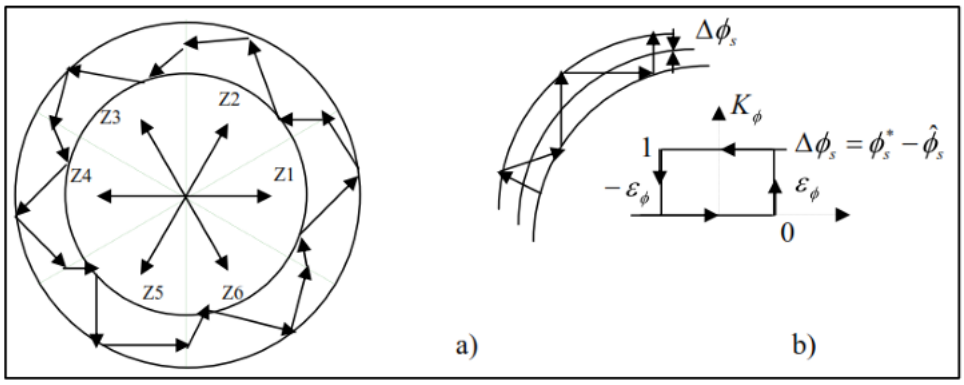

Figure 3.8: a) Selection of voltages Vi to control the flow.
b) Two-level hysteresis comparator for flow control.

III.3.5.2 Couple corrector

The torque controller aims to keep the torque within its hysteresis band and thus impose the amplitude of the torque fluctuations.

Takahashi proposed a three-level hysteresis compensator to control the torque in the four operating quadrants without intervening on the structure. This compensator allows the machine to be controlled in both directions of rotation with either positive or negative torque [92].

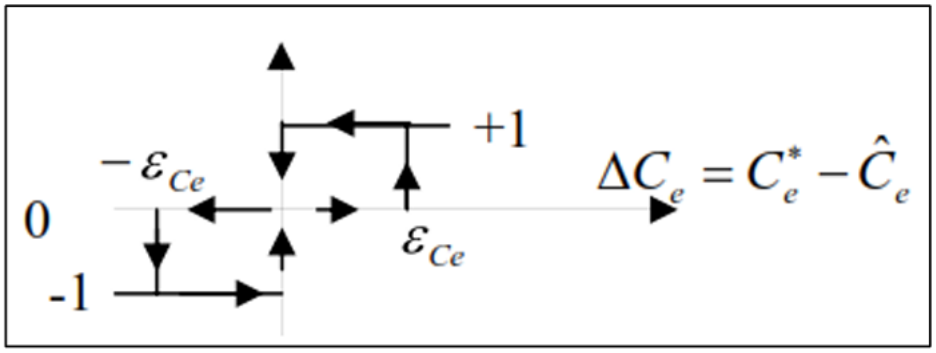

Figure 3.9: Three-level hysteresis comparator for torque adjustment.

This comparator is modeled by the following algorithm:

$$\begin{cases} If\ \Delta C_e > \varepsilon_{Ce} & So\ K_c = 1 \\ If\ 0 \le \Delta C_e \le \varepsilon_{Ce} \quad and \quad \frac{d\Delta C_e}{dt} > 0 & So\ K_c = 0 \\ If\ 0 \le \Delta C_e \le \varepsilon_{Ce} \quad and \quad \frac{d\Delta C_e}{dt} < 0 & o\ K_c = 1 \\ If\ \Delta C_e < -\varepsilon_{Ce} & So\ K_c = -1 \\ If\ 0 \ge \Delta C_e \ge -\varepsilon_{Ce} \ and \ \frac{d\Delta C_e}{dt} > 0 & So\ K_c = 0 \\ If\ 0 \ge \Delta C_e \ge -\varepsilon_{Ce} \ and \ \frac{d\Delta C_e}{dt} < 0 & So\ K_c = -1 \end{cases}$$

- $K_c = 1$: Means that the couple is below the lower limit of the band and therefore it needs to be increased.
- $K_c = -1$: Means that the couple is above the upper limit of the band and needs to be reduced.
- $K_c = 0$: Means that the couple is inside the band and therefore needs to be kept there.

III.4 Simulation results

In this section, the simulation results are tested by using different renewable sources, such as the PV system, battery source, fuel cell, and supper-capacitor, together with the dynamic model of vehicle load. To prove the studies in this part, some simulations have been carried out.

III.4.1 PV

The PV power generation branch characteristics are analyzed. Figs 3.10 and 3.11 show the irradiation profile with MPPT controller and the PV power under different irradiances. It verifies that the PV power generation branch can readily perform the MPPT and achieve the maximum output power at a given irradiance.

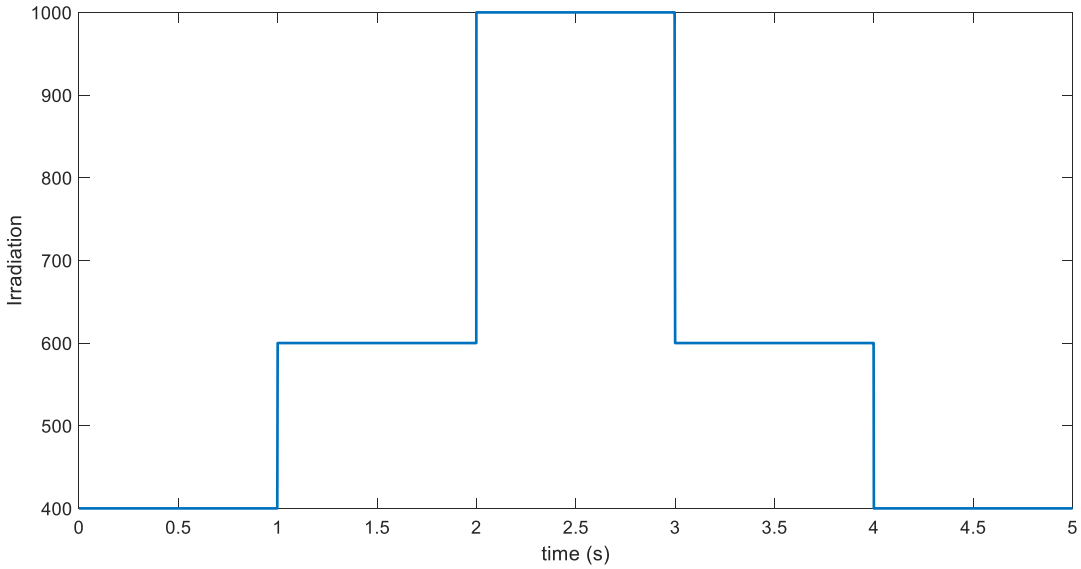

Figure 3.10: Irradiation profile of PV system.

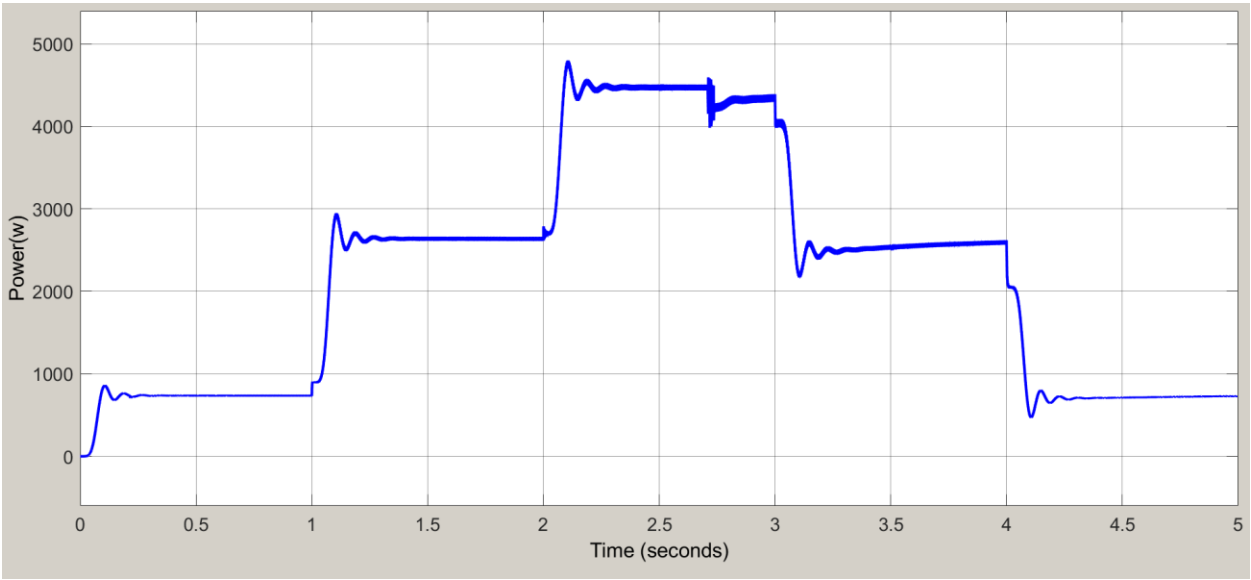

Figure 3.11: PV power.

III.4.2 Fuel cell

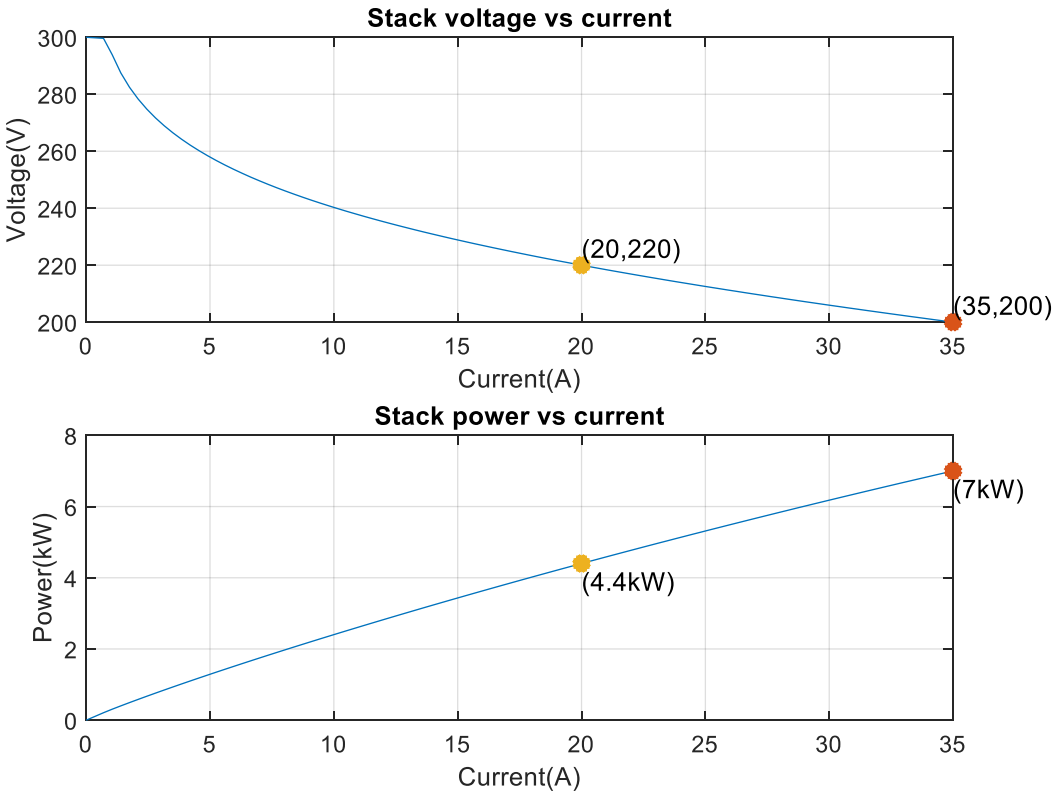

Figure 3.12: diagram of stack voltage vs current and stack power vs current.

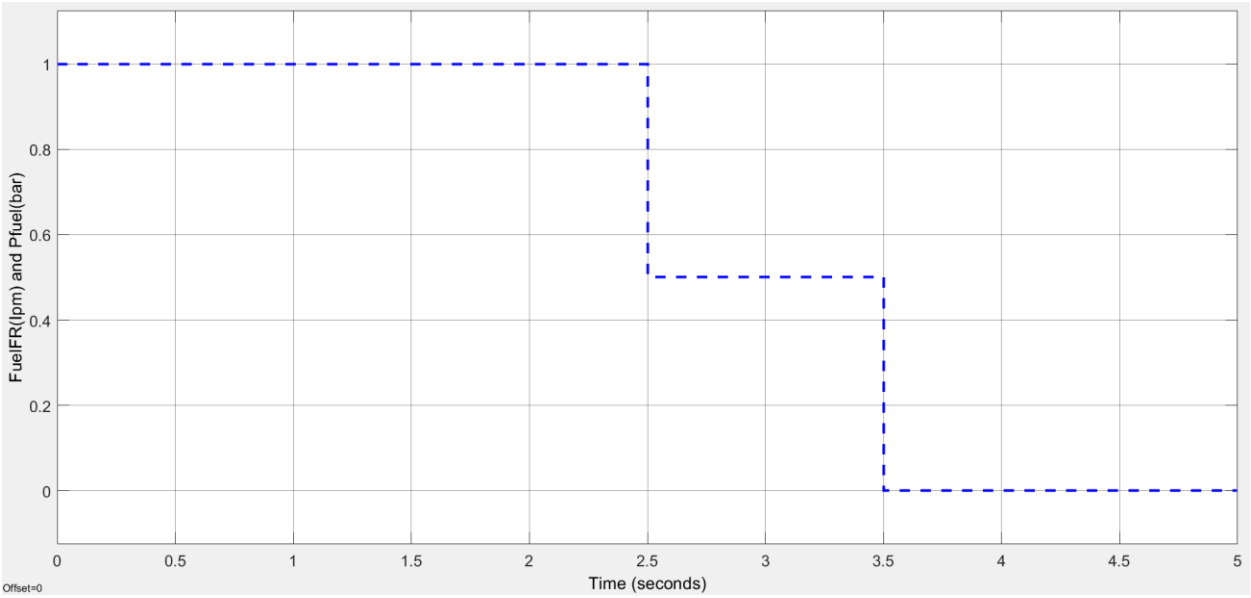

Figure 3.13: Profile of Fuel flow rate and Fuel supply pressure.

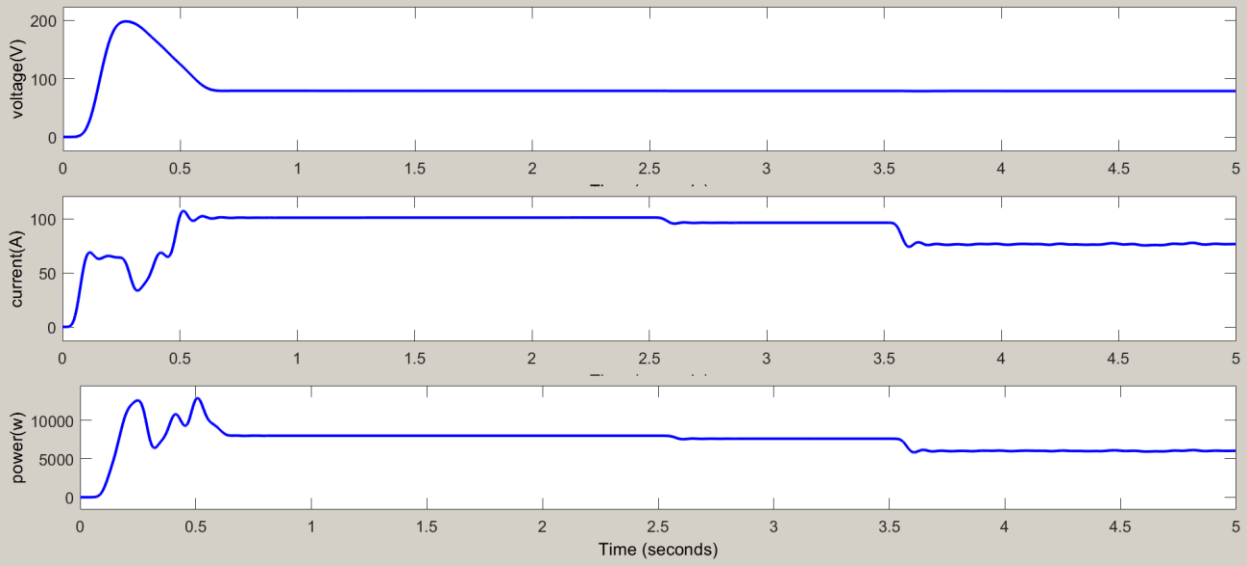

Figure 2.14: Voltage, current, power, and SOC of the fuel cell.

III.4.3 Battery

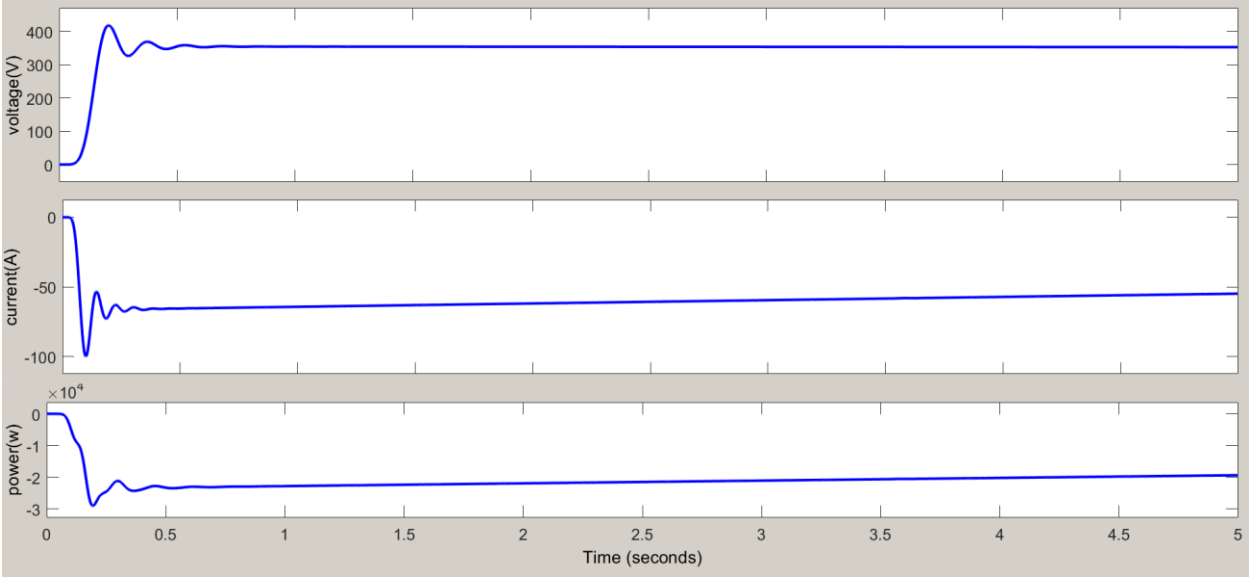

Figure 3.15: Voltage, current and power of the battery source.

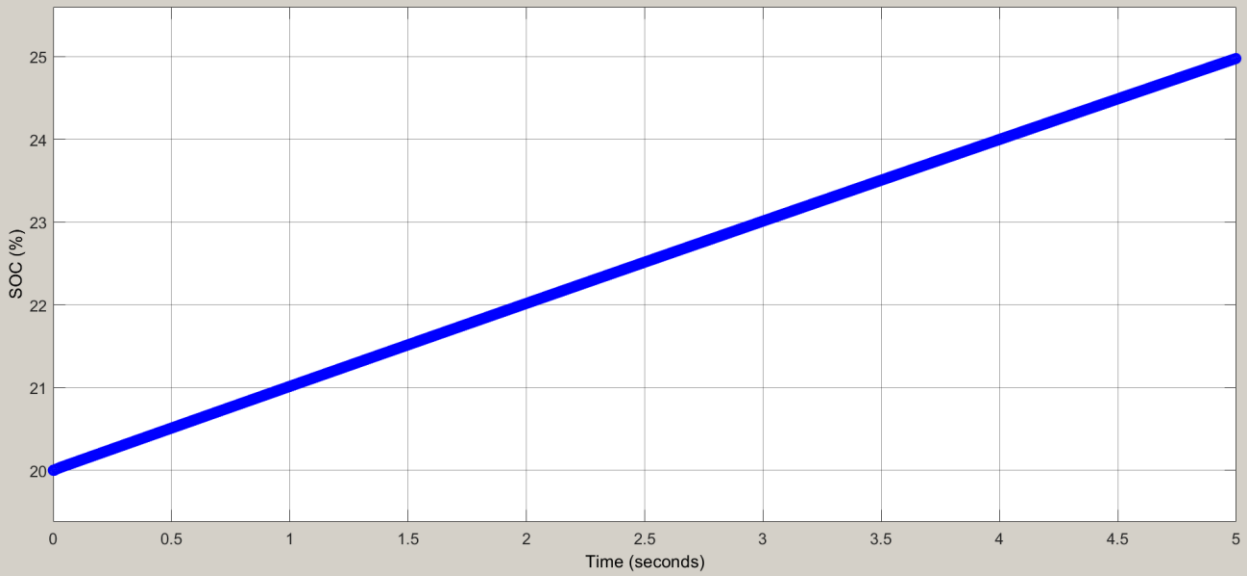

Figure 3.16: SOC of the battery source.

III.4.4 Motor

Figures 3.19 - 3.20 show the stator flux trajectory, rotor speed, and torque for the DSIM system. When we are extracted the maximum power from the PV, it is needs to be transferred to the DSIM. The speed of the latter is controlled by DTC through PWM inverter. As long as the power is function of the speed and torque, a function relating the PV power and the rotor speed can be derived if the motor losses are ignored. In steady state operation and upon neglecting friction losses, the motor torque will be the same as the EV torque which is given by Figure 3.20.

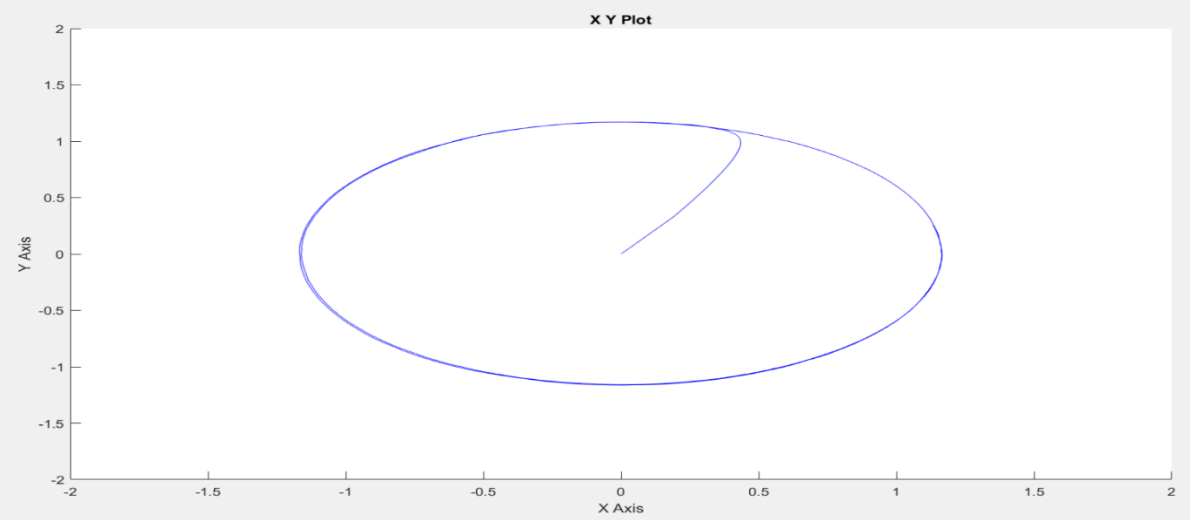

Figure 3.17: Stator flux trajectory.

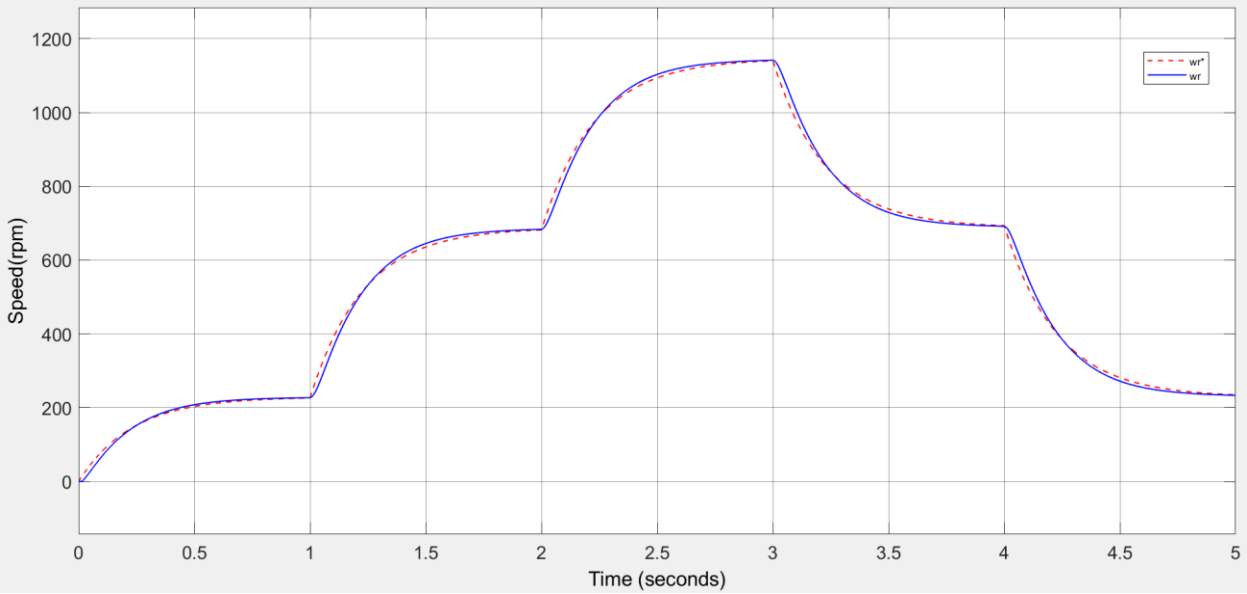

Figure 3.18: Rotor speed of DSIM.

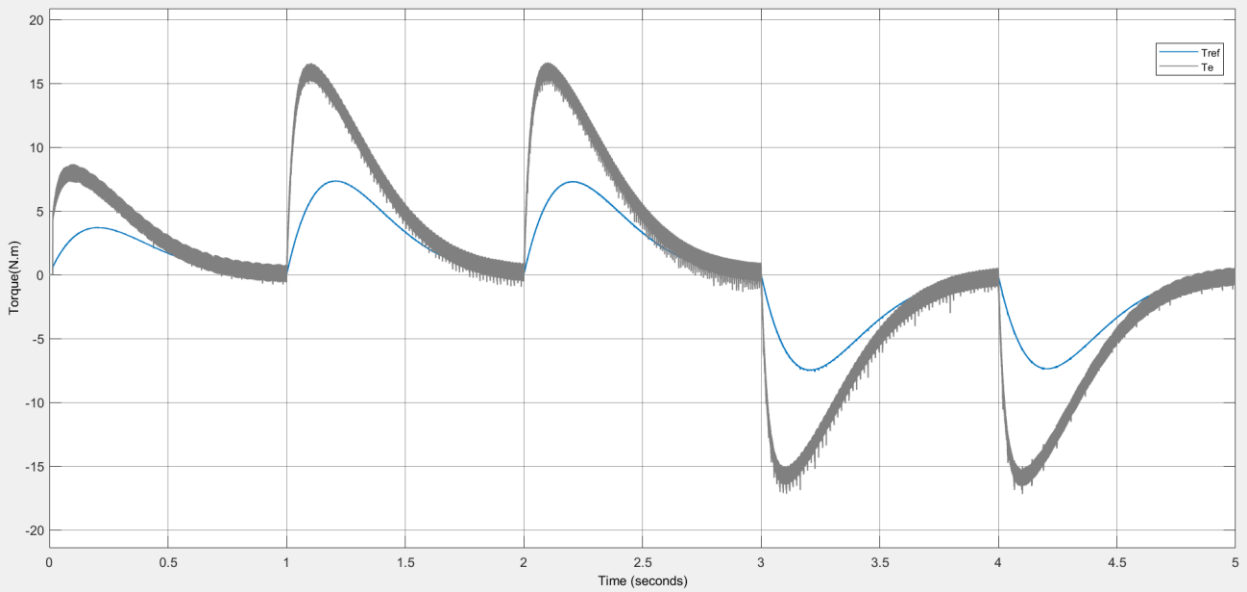

Figure 3.19: DSIM torque and load torque.

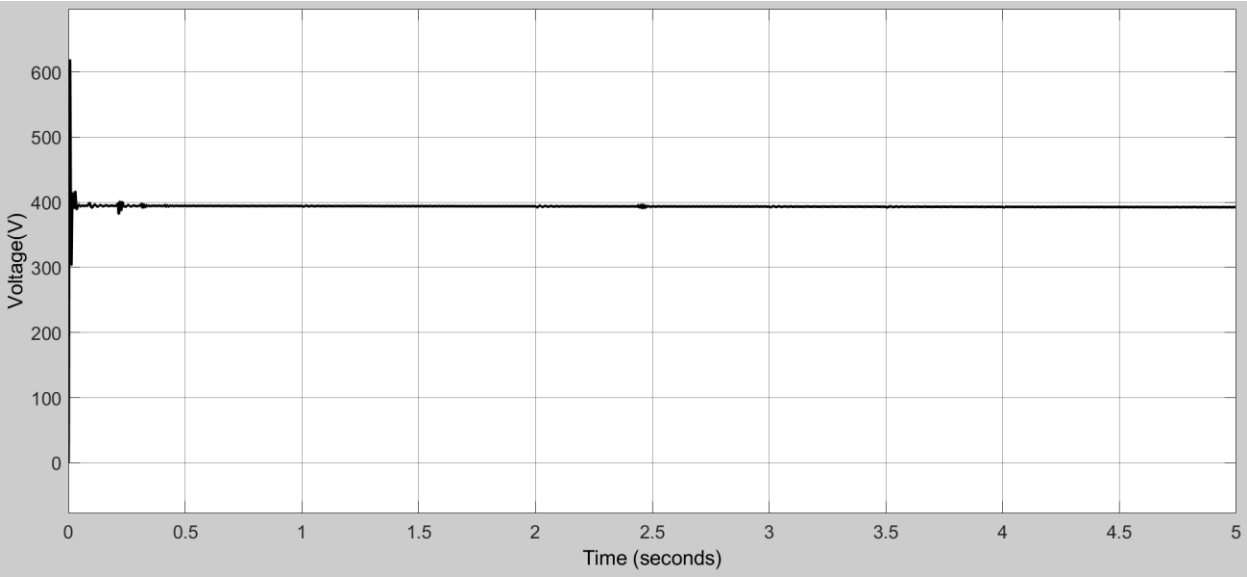

Figure 3.20: DC bus voltage.

III.4.5 Conclusion

According to the chapter, the emphasis is on employing advanced techniques to enhance the performance of electric vehicles. These strategies demonstrate potential in increasing vehicle efficiency and reliability, although there are trade-offs involved, such as higher expenses for certain systems and issues with response speed. The integration of different components seems critical for attaining improved outcomes, with the data indicating substantial possibilities for future progress in electric vehicle technology.

General Conclusion

General Conclusion

The progress of electrical drives powered by renewable energy sources, especially electric vehicles (EVs) that use photovoltaic (PV) panels, fuel cells, batteries, and supercapacitors, is a major step forward in achieving sustainable transportation and caring for the environment. These systems utilize clean energy to operate vehicles, greatly diminishing the hazardous emissions and air pollutants linked to conventional fossil fuel transportation, which negatively affect global ecosystems and public health. PV panels collect solar energy to facilitate vehicle operation, while fuel cells deliver efficient, zero-emission power. Batteries provide dependable energy storage and prolong driving range, and supercapacitors offer high power density for quick charging and discharging, making the combination perfect for compact, city-oriented EVs designed for effective mobility in densely populated regions. By integrating with renewable energy grids, these sophisticated electrical drives present a feasible way to decarbonize transportation, aiding global initiatives to fight climate change and nurture cleaner urban atmospheres.

Significant challenges, however, hinder the widespread adoption of electric vehicles (EVs) powered by photovoltaic (PV) panels, fuel cells, batteries, and supercapacitors. The high costs associated with renewable technologies and the reliance on certain non-renewable components limit their economic competitiveness. Furthermore, the lack of extensive infrastructure, such as hydrogen refueling stations, robust energy grids, and efficient charging networks presents logistical barriers, particularly in areas with underdeveloped energy systems. Technological limitations, including the variability of solar power, the lifespan of energy storage systems, and the energy density of batteries and supercapacitors, further complicate large-scale deployment. Overcoming these challenges will necessitate ongoing investment in research and development, as well as supportive policy measures like subsidies, incentives, and public-private partnerships to enhance the integration of renewable energy in the transportation sector. Collaboration among governments, industries, and researchers is crucial to make these systems a viable and competitive alternative.

Looking forward, the future of electric drives powered by renewable sources has the potential to change global transportation into a sustainable, low-carbon system. Innovations in lightweight materials, high-performance energy storage, power electronics, and smart energy management are set to improve the efficiency, cost-effectiveness, and accessibility of electric vehicles (EVs), particularly for urban mobility uses. Comprehensive policy frameworks that support the adoption of renewable resources and infrastructure development will be essential for achieving this vision. By building on the fundamental promise of electric vehicles and incorporating advanced renewable technologies such as photovoltaic (PV) systems, fuel cells, batteries, and supercapacitors, these sophisticated electric drives can facilitate the transition towards a cleaner and more sustainable energy future, aligning environmental goals with social advancement and marking the beginning of a new era in environmentally friendly transportation.

APPENDIX

Irradiation (W/m²)	Power Output (W)	Effective Power (W, 90% efficiency)	Energy (kWh)	Charging Time (h, for 2.76 kWh)	Range Contribution (km/day)
1000	414	460	2.30	6	55.56
800	331.2	368	1.84	7.5	44.44
500	207	230	1.15	12	27.78
300	124.2	138	0.69	20	16.67
100	41.4	46	0.23	60	5.56

Table 1: PV Panel Performance.

Parameter	**Value**
Pn	4.5kw
Rs, Rr	3.72
Ls1, Ls2	0.022
Lr	0.006
Lm	0.3672
J	0.062

Table 2: Parameter of DSIM

Description	**Value**
Voltage at 0A and 1A	[65 , 63]
Nominal operating point	[133.3 , 45]
Maximum operating point	[225 , 37]
Number of cells	65
Nominal stack efficiency (%)	55
Operating temperature (Celsius)	65
Nominal Air flow rate (lpm)	300
Nominal supply pressure [Fuel (bar), Air (bar)]	[1 , 1.5]
Nominal composition (%) [H2 O2 H2O(Air)]	[99.95 , 21 , 1]

Table 3: Fuel cell parameter.

Description	Value
Maximum Power (W)	459.9
Open circuit voltage Voc (V)	37.5
Voltage at maximum power point Vmp (V)	30
Temperature coefficient of Voc (%/deg.C)	-0.40
Cells per module (Ncell)	72
Short-circuit current Isc (A)	17.63
Current at maximum power point Imp (A)	15.33
Temperature coefficient of Isc (%/deg.C)	0.087005

Table 4: PV array parameter.

Description	Value
Nominal voltage (V)	300
Rated capacity (Ah)	48
Initial state-of-charge (%)	20

Table 5: Battery parameter.

References

References

[1] Nabil, KARAMI. Control of a Hybrid System Based PEMFC and Photovoltaic Panels. Doctoral thesis, Aix-Marseille University, 2013.

[2] Dhameja, Sandeep. Electric Vehicle Battery Systems. Boston: Butterworth-Heinemann/Elsevier Science, 2002.

[3] D. Mignogna, P. Ceci, C. Cafaro, G. Corazzi, and P. Avino, “Production of Biogas and Biomethane as Renewable Energy Sources: A Review,” Applied Sciences, 2023.

[4] J. Milner et al., “Impact on mortality of pathways to net zero greenhouse gas emissions in England and Wales: a multisectoral modelling study,” The Lancet Planetary Health, 2023.

[5] T. Pavlovic, “Solar energy,” in Green Energy and Technology, 2020.

[6] N. S. Hassan et al., “Recent review and evaluation of green hydrogen production via water electrolysis for a sustainable and clean energy society,” International Journal of Hydrogen Energy, 2024.

[7] P. Breeze, Chapter 11 - wind power, in: Power Generation Technologies, seconded., Newnes, London, 2014.

[8] A. Rashad, S. Kamel, F. Jurado, The basic principles of wind farms, in: Distributed Generation Systems, Butterworth-Heinemann, Oxford.

[9] Chapin DM, Fuller CS, Pearson GL, J. Appl. Phys, 1954.

[10] DietlD,Helmreich,SirtlE,Crystals: Growth, Properties and Applications, 1981.

[11] Goetzberger A, Kleiss G, Reiche K, Nordmann T, Proc. 2nd World Conf. on Photovoltaic Energy Conversion, Vienna, Austria, 1998.

[12] S. Power, “Solar Power.”

[13] Daniel de B. Mesquita, João Lucas de S. Silva, Hugo S. Moreira, Michelle Kitayama, and Marcelo G. Villalva, "A review and analysis of technologies applied in PV modules," Conference Paper, November 2019.

[14] Lund P, Improved standalone PV systems with fuel cells, Proc. 17th Euro pean Photovoltaic Solar Energy Conf., Munich. 2001.

[15] Watt, M.Energy analysis (PhD thesis), University of Murdoch, 1983.

[16] P.O. Babalola and O.E. Atiba. IOP Conf. Ser.: Mater. Sci. Eng. 2021.

[17] Kuang Ken, & Easler, Keith. (Eds.) Fuel Cell Electronics Packaging. Springer Science+Business Media, LLC. 2007.

[18] Thomas, S., & Zalbowitz, M. Fuel cells – Green power. U.S. Department of Energy. 1999.

[19] Cook, B. An introduction to fuel cells and hydrogen technology. Engineering Science and Education Journal. 2002.

[20] Cropper, M., Geiger, S., & Jollie, D. Fuel cells: A survey of current developments. Journal of Power Sources. 2004.

[21] Larminie, J., & Lowry, J. Electric Vehicle Technology Explained (1st ed.). Wiley. 2003.

[22] Gou, B., Na, W. K., & Diong, B. Fuel Cells: Modeling, Control, and Applications. CRC Press. 2010.

[23] Mohan, N., Undeland, T. M., & Robbins, W. P. Power Electronics: Converters, Applications, and Design (3rd ed.). Wiley. 2003

[24] Karami N . Control of a Hybrid System Based PEMFC and Photovoltaic Panels. Aix-Marseille University . PhD Thesis 2013

[25] Aydogan, H. Electric Vehicles and Renewable Energy. Journal of Physics: Conference Series. 2024.

[26] Cavus, M.; Dissanayake, D.; Bell, M. Next Generation of Electric Vehicles: AI-Driven Approaches for Predictive Maintenance and Battery Management. Energies 2025.

[27] Manousakis, N.M.; Karagiannopoulos, P.S.; Tsekouras, G.J.; Kanellos, F.D. Integration of Renewable Energy and Electric Vehicles in Power Systems: A Review. Processes 2023.

[28] Li, Z., Khajepour, A., Song, J.: A comprehensive review of the key technologies for pure electric vehicles. 2019.

[29] Zou, Y., Wei, S., Sun, F., Hu, X., Shiao, Y.: Large-scale deploy ment of electric taxis in Beijing: a real-world analysis. 2016.

[30] Wang, S., Deng, C.: Research on electric motor technologies for electric vehicles. Micro Motor (Servo Technology in Chinese. 2006.

[31] Uglielmi, P.: Comparison of induction and PM synchronous motor drives for EV application including design examples. IEEE Trans. Ind. Appl. 2012.

[32] Zeraoulia, M., Benbouzid, M.E.H., Diallo, D.: Electric motor drive selection issues for HEV propulsion systems: a compara tive study. IEEE Trans. Veh. Technol. 2006.

[33] Moosavi, S. Djerdir, A. Ait-Amirat, Y. Khaburi, D. ANN based fault diagnosis of permanent magnet synchronous motor under stator winding shorted turn. Electr. Power Syst. 2015.

[34] Lemian, D., & Bode, F. Battery-supercapacitor energy storage systems for electrical vehicles: A review. Energies2022.

[35] Bourenane, H., Berkani, A., Negadi, K., Marignetti, F., & Hebri, K. Artificial Neural Networks Based Power Management for a Battery/Supercapacitor and Integrated Photovoltaic Hybrid Storage System for Electric Vehicles. Journal Européen des Systèmes Automatisés, 2023.

[36] Djaballah, Y., Negadi, K., Boudiaf, M., Berkani, A., & Marignetti, F. Power management for a fuel cell/battery and supercapacitor based on artificial neural networks for electric vehicles. Przeglad Elektrotechniczny, 2023.

[37] Ehsani, M., Gao, Y., Longo, S., & Ebrahimi, K. Modern Electric, Hybrid Electric, and Fuel Cell Vehicles (3rd ed.). CRC. 2018.

CHAPTER II

[38] Smith, J., & Taylor, R. Electric vehicles and the transition to sustainable mobility. Journal of Cleaner Production. 2023.

[39] Brown, L. A historical perspective on electric vehicle development: From 19th-century pioneers to modern innovation. Technology and Culture. 2022.

[40] International Energy Agency (IEA). Global transport emissions: Trends and projections. IEA Annual Report. 2024

[41] Zhang, Q., & Li, H. Efficiency analysis of electric propulsion systems in modern EVs. Energies. 2023.

[42] Kumar, P., & Singh, A. Challenges in scaling electric vehicle adoption: Battery costs and infrastructure gaps. Transportation Research Part D. 2025.

[43] Müller, K., & Weber, S. Policy drivers of electric vehicle market growth: A global perspective. Environmental Policy and Governance. 2024.

[44] Evans, T., & Carter, M. Sustainable transportation through electric propulsion: A paradigm shift. Renewable Energy Reviews. 2023.

[45] Patel, R., & Kim, S. Environmental impacts of EV propulsion systems: A global perspective. Journal of Sustainable Mobility. 2024.

[46] Liu, Y., & Chen, H. Battery technology in electric vehicles: Foundations and future trends. Energy Storage Materials. 2025.

[47] Thompson, G. Electric motors in EVs: Efficiency and simplicity redefined. IEEE Transactions on Power Electronics. 2023.

[48] Nguyen, D., & Patel, S. Power conversion and transmission in EV propulsion: Bridging energy to motion. Transportation Engineering. 2024.

[49] Garcia, L., & Zhou, Q. Control systems in electric propulsion: Optimizing performance. Automotive Innovation. 2025

[50] Harper, J., & Singh, R. Electric vehicles and the future of mobility: Propulsion as a catalyst. Environmental Science & Technology. 2023.

[51] Khan, A., & Patel, V. Modeling forces in electric vehicle dynamics: A mathematical and schematic approach. Journal of Automotive Engineering. 2024.

[52] : Salem Abd Erraouf. Commande robuste de la machine asynchrone à double stator. Memory of master, Mouhamed Boudiaf Msila University, 2021.

[53]: Omar BAZINE. Commande Directe du Couple (DTC) d'une Machine Asynchrone à Double Etoile alimentée par un redresseur piloté par DPC (Direct Power Control). Ghardaïa University, 2016.

[54] R.C Campbell « A Circuit-based Photovoltaic Array Model for Power System Studies » 39th North American Power Symposium. NAPS '07. 2007.

[55] Phang et al, J.C.H. Phang, D.S.H. Chan, J.R. Philips.Accurate analytical method for the extraction of solar cell model parameters Electron. Lett. 1984.

[56] J.-P. Charles et al. "Consistency of the double exponential model with the physical mechanisms of conduction for a solar cell under illumination", Journal of Physics D: Applied Physics. 1985.

[57] Shukla A, Khare M &Shukla K N.International Journal of Innovative Research in Science, Engineering and Technology. 2015.

[58] Hu Y & Yao. Elsevier Energy Conversion and Management. 2016.

[59] B. Abdelhalim « Etude et régulation d'un circuit d'extraction de la puissance maximale d'un panneau solaire ». Mémoire de magister de l'université Mentouri de Constantine, mai 2009.

[60] S. AREZKI, M. BOUDOUR « Simulation and Modeling of a Photovoltaic System Adapted by a MPPT control reaction Application on a DSIM ». IEEE International Energy Conference, 2010.

[61] Herizi, O. Gestion des flux d'energie d'une alimentation hybride pile à combustible-panneaux solaire dans un véhicule à traction electrique [Magister thesis, Ecole Militaire Polytechnique]. Ecole Militaire Polytechnique, Bordj El Bahri, Algeria. 2013.

[62] Aktas, M., Awaili, K., Ehsani, M., & Arisoy, A. Direct torque control versus indirect field-oriented control of induction motors for electric vehicle applications. Engineering Science and Technology, an International Journal. 2020.

[63] M. Aktas, K. Awaili, M. Ehsani, and A. Arisoy, "Direct torque control versus indirect field-oriented control of induction motors for electric vehicle applications," Engineering Science and Technology, an International Journal, 2020.

[64] Maher A.R. Sadiq Al-Baghdadi. Modelling of proton exchange membrane fuel cell performance based on semi-empirical equations: Renewable energy. 2005.

[65] Larminie, J., & Dicks, A. Fuel Cell Systems Explained. Wiley. 2003.

[66] Barbir, F. PEM Fuel Cells: Theory and Practice. Academic Press. 2012.

[67] O'Hayre, R., Cha, S. W., Colella, W., & Prinz, F. B. Fuel Cell Fundamentals. Wiley. 2016.

[68] EG&G Technical Services, Inc. Fuel Cell Handbook (7th Edition). U.S. Department of Energy. 2004.

[69] Mann, R. F., Amphlett, J. C., Hooper, M. A. I., Jensen, H. M., Peppley, B. A., & Roberge, P. R. Development and application of a generalised steady-state electrochemical model for a PEM fuel cell. Journal of Power Sources. 2000.

[70] Hoogers, G. Fuel Cell Technology Handbook. CRC Press. 2002.

[71] Philippe Barrade, Alfred Rufer, Current Capability and Power Density of Supercacitors: Considerations on Energy Efficiency, LEI, STI-ISE and EPEL, CH-1015 Lausanne, Switzerland EPE 2003

[72] Youngho Kim, Director of Product Development, Ultracapacitor Technology Power Electronic Circuits, NESSCAP Co. Ltd., Korea.

[73] P. Barrade, Energy Storage and Applications with Supercapacitors, Laboratorie d'Electronique Industrielle, LEI STI-ISE, Ecole Polytechnic Fererale de Lausanne, EPFL CH 1015 Lausanne (Switzerland).

[74] Ambrosio B. Cultura, Ziyad M. Salameh, Performance Evaluation of a Supercapacitor Module for Energy Storage Application, Presented Power and Energy Society General Meeting - Conversion and Delivery of Electrical Energy IEEE, 2008.

CHAPTER III

[75] Majid Valizadeh, Mahyar Shiri, Amirhosein Khosravi Sarvenoee, N. Gowtham, Kareem M. AboRas. A comprehensive scheme for power management of FC/SC/battery, and solar-roof PV source in electric vehicle systems. Scientific Reports, 2024.

[76] C. Cabal, « Optimisation énergétique de l'étage d'adaptation électronique dédié à la conversion photovoltaïque ». Thèse de doctorat, Université de Toulouse, Décembre 2008.

[77] N. Femia, G. Petrone, G. Spagnuolo, and M. Vitelli. Optimization of perturb and observe maximum power point tracking method. IEEE Transactions on Power Electronics, july 2005.

[78] I. Sefa and O. Ozdemir. Experimental study of interleaved mppt converter for pv systems. In Industrial Electronics,IECON. 35th Annual Conference of IEEE, nov. 2009.

[79] S. Jain and V. Agarwal. Comparison of the performance of maximum power point tracking schemes applied to single-stage grid-connected photovoltaic systems. Elec tric Power Applications, IET, sept. 2007.

[80] H.P. Desai and H.K. Patel. Maximum power point algorithm in pv generation: An overview. In International Conference on Power Electronics and Drive Systems, nov. 2007.

[81] O. Wasynczuk. Dynamic behavior of a class of photovoltaic power systems. Power Engineering Review, IEEE, sept. 1983.

[82] Jung-Min Kwon, Bong-Hwan Kwon, and Kwang-Hee Nam. Grid-connected photo voltaic multistring pcs with pv current variation reduction control. IEEE Transac tions on Industrial Electronics, nov. 2009.

[83] H. Patel and V. Agarwal. Mppt scheme for a pv-fed single-phase single-stage grid connected inverter operating in ccm with only one current sensor. IEEE Transac tions on Energy Conversion, , march 2009.

[84] Weidong Xiao and W.G. Dunford. A modi ed adaptive hill climbing mppt method for photovoltaic power systems. In Power Electronics Specialists Conference, 2004.

[85] Mao-Lin Chiang, Chih-Chiang Hua, and Jong-Rong Lin. Direct power control for distributed pv power system. In Proceedings of the Power Conversion Conference, volume 1, 2002.

[86] P.J. Wolfs and L. Tang. A single cell maximum power point tracking converter without a current sensor for high performance vehicle solar arrays. In Power Elec tronics Specialists Conference, june 2005.

[87] A. Pandey, N. Dasgupta, and A.K. Mukerjee. High-performance algorithms for drift avoidance and fast tracking in solar mppt system. IEEE Transactions on Energy Conversion, june 2008.

[88] A. CHEBABHI, N.E. ROUABAH, E. GUERBAI, "Application des techniques de l'intelligence artificielle pour le contrôle direct du couple d'une MAS", Mémoire d'ingéniorat de l'Université Mohamed Boudiaf de M'sila, Algérie, Juin 2009.

[89] K. HASSE, "On the Dynamics' of Speed Control of a Static AC Drive with a Squirrel Cage Induction Machine". PhD dissertation, Tech. Hochsch, Darmstadt, 1969.

[90] CANUDAS DE WIT, "Commande des moteurs asynchrones 1- Modélisation, contrôle vectoriel et DTC", France : Hermès Science Publication, 2000.

[91] Bernard de Fornel « Techniques de l'ingénieur ». D3, 623.

[92] I. TAKAHASHI, T. NOGUCHI. "A new quick response and high efficiency control strategy of induction motor". IEEE Transactions on Industrial Electronics, IE-22, 1986.

ملخص

تستكشف هذه الدراسة تصميم نظام تشغيل كهربائي يعمل بالطاقة المتجددة ونمذجته والتحكم فيه لاستخدامه في السيارات الكهربائية. يدمج النظام الألواح الكهروضوئية وخلايا الوقود والبطاريات والمكثفات الفائقة لإنشاء حل هجين للطاقة يعزز الكفاءة والموثوقية والاستدامة. تبدأ هذه الدراسة بمقدمة عن تقنيات الطاقة المتجددة، مثل الطاقة الشمسية وخلايا وقود الهيدروجين وطاقة الرياح، وكيفية دمجها في أنظمة قيادة السيارات الكهربائية. بالإضافة إلى ذلك، تم تطوير نموذج رياضي مفصل لكل مكون لتحليل سلوك وتفاعلات مصادر الطاقة داخل النظام.

استخدمت خوارزمية الاضطراب والملاحظة التقليدية في الأنظمة الكهروضوئية لتتبع نقطة القدرة القصوى للطاقة الكهربائية من النظام الكهروضوئي إلى غاية نظام التشغيل الكهربائي، مع تحسين سرعة محرك الجر لضمان أقصى انتقال للطاقة الكهربائية إلى السيارة. ولتحقيق هذا الهدف، استخدمت استراتيجية التحكم المباشر في عزم الدوران للتحكم في سرعة المحرك. يُسهّل هذا النهج من التحكم في الحصول على أقصى قدر من الطاقة، ويُمكّن المحرك من العمل بكفاءة عالية في ظل ظروف حمولة متغيرة. تؤكد نتائج المحاكاة فعالية النظام المُطبّق، مُظهرةً أداءً مستقرًا، وتوزيع مُحسّن للطاقة الكهربائية، بالاضافة الى تقليل الاعتماد على الوقود الأحفوري.

الكلمات المفتاحية : التشغيل الكهربائي ; المنبع المتجدد للطاقة ; النقطة القصوى للطاقة الكهربائية; التحكم الباشر في العزم; الماكنة الغير متزامنة ذات جزء ثابت مزدوج

Abstract

This study explores the design, modeling, and control of an electric drive system powered by various renewable energy sources for use in electric vehicles (EVs). The system integrates photovoltaic (PV) systems, fuel cells, batteries, and supercapacitors to create a hybrid energy solution that enhances efficiency, reliability, and sustainability. The study begins with an introduction to renewable energy technologies, including solar, hydrogen fuel cells, and wind power, and examines how these technologies are integrated into EVs drive systems. Additionally, a detailed mathematical model for each component is developed to analyze the behavior and interactions among the energy sources within the system.

The conventional Perturb and Observe (P&O) algorithm is employed to track the maximum power point (MPPT) from the photovoltaic (PV) system to the drive system, while optimizing the rotor speed of the drive motor to ensure maximum power transfer to the vehicle. To achieve this objective, a Direct Torque Control (DTC) strategy is utilized for motor speed control. This control approach facilitates maximum energy harvesting and enables the motor to operate with high efficiency under varying load conditions. The simulation results confirm the effectiveness of the implemented scheme, demonstrating stable performance, enhanced energy management, and a reduction in dependence on fossil fuels.

Keywords: Electric drive, Renewable energy source, MPPT, Direct torque control, Double stator asynchronous machine.

Résumé

Cette étude explore la conception, la modélisation et le contrôle d'un système de propulsion électrique alimenté par diverses sources d'énergie renouvelables destiné aux véhicules électriques (VE). Ce système intègre des systèmes photovoltaïques (PV), des piles à combustible, des batteries et des supercondensateurs pour créer une solution énergétique hybride améliorant l'efficacité, la fiabilité et la durabilité. L'étude débute par une introduction aux technologies des énergies renouvelables, notamment l'énergie solaire, les piles à combustible à hydrogène et l'énergie éolienne, et examine leur intégration aux systèmes de propulsion des VE. De plus, un modèle mathématique détaillé est développé pour chaque composant afin d'analyser le comportement et les interactions entre les sources d'énergie du système.

L'algorithme conventionnel Perturbe et Observe (P&O) est utilisé pour suivre le point de puissance maximale du système photovoltaïque au système d'entraînement, tout en optimisant la vitesse du rotor du moteur d'entraînement afin d'assurer un transfert de puissance maximal au véhicule. Pour atteindre cet objectif, une stratégie de contrôle direct du couple est utilisée pour réguler la vitesse du moteur. Cette approche de contrôle optimise la récupération d'énergie et permet au moteur de fonctionner avec un rendement élevé dans des conditions de charge variables. Les résultats de simulation confirment l'efficacité du système mis en œuvre, démontrant des performances stables, une meilleure gestion de l'énergie et une réduction de la dépendance aux combustibles fossiles.

Mots clés : Entrainement électrique, Source d’énergie renouvelable, MPPT, Commande directe du couple, Machine asynchrone à double stator.